PROPERTIES OF EFFECTIVE PAIR POTENTIALS THAT MAP POLYMER MELTS ONTO LIQUIDS OF SOFT COLLOID CHAINS

by

ANTHONY JOHN CLARK

A DISSERTATION

Presented to the Department of Physics
and the Graduate School of the University of Oregon
in partial fulfillment of the requirements
for the degree of
Doctor of Philosophy

March 2013

DISSERTATION APPROVAL PAGE

Student: Anthony John Clark

Title: Properties of Effective Pair Potentials that Map Polymer Melts onto Liquids of Soft Colloid Chains

This dissertation has been accepted and approved in partial fulfillment of the requirements for the Doctor of Philosophy degree in the Department of Physics by:

Dr. Daniel Steck	Chair
Dr. Marina G. Guenza	Advisor
Dr. John J. Toner	Member
Dr. Richard P. Taylor	Member
Dr. Alan Rempel	Outside Member

and

Kimberly Andrews Espy	Vice President for Research & Innovation/ Dean of the Graduate School

Original approval signatures are on file with the University of Oregon Graduate School.

Degree awarded March 2013

DISSERTATION ABSTRACT

Anthony John Clark

Doctor of Philosophy

Department of Physics

March 2013

Title: Properties of Effective Pair Potentials that Map Polymer Melts onto Liquids of Soft Colloid Chains

The ability to accurately represent polymer melts at various levels of coarse graining is of great interest because of the wide range of time and length scales over which relevant process take place. Schemes for developing effective interaction potentials for coarse-grained representations that incorporate microscopic level system information are generally numerical and thus suffer from issues of transferability because they are state dependent and must be recalculated for different system and thermodynamic parameters. Numerically derived potentials are also known to suffer from representability problems, in that they may preserve structural correlations in the coarse-grained representation but many often fail to preserve thermodynamic averages of the coarse-grained representation. In this dissertation, analytical forms of the structural correlations and effective pair potentials for a family of highly coarse-grained representations of polymer melts are derived. It is shown that these effective potentials, when used in mesoscale simulations of the coarse-grained representation, generate consistent equilibrium structure and thermodynamic averages with low level representations and therefore with physical systems. Furthermore, analysis of the effective pair potential forms shows that a small long range tail feature that scales beyond the physical range of the polymer as the fourth root of the number of monomers making up the coarse-grained unit dominates thermodynamic averages at high levels of coarse graining. Because structural correlations are extremely insensitive to this feature, it can be shown that effective interaction potentials derived from optimization of structural correlations would require unrealistically high precision measurements

of structural correlations to obtain thermodynamically consistent potentials, explaining the problems of numerical coarse-graining schemes.

This dissertation includes previously published and unpublished co-authored material.

CURRICULUM VITAE

NAME OF AUTHOR: Anthony John Clark

GRADUATE AND UNDERGRADUATE SCHOOLS ATTENDED:
University of Oregon, Eugene, OR
University of Puget Sound, Tacoma, WA

DEGREES AWARDED:
Doctor of Philosophy in physics, 2013, University of Oregon
Master of Science in physics, 2007, University of Oregon
Bachelor of Science in physics, 2004, University of Puget Sound

AREAS OF SPECIAL INTEREST:
Soft Condensed Matter, Statistical Mechanics, Complex Fluids

PROFESSIONAL EXPERIENCE:

Research and Teaching Assistant, University of Oregon, 2005-2013

PUBLICATIONS:

J. McCarty, A. J. Clark, I. Y. Lyubimov, and M.G. Guenza. Thermodynamic Consistency between Analytic Integral Equation Theory and Coarse-Grained Molecular Dynamics Simulations of Homopolymer Melts *Macromol.*, **45** 8482 (2012).

A. J. Clark, J. McCarty, I. Y. Lyubimov, and M. G. Guenza. Effective Potentials for Representing Polymers in Melts as interacting soft particles *Phys. Rev. Lett.*, **109** 168301 (2012).

I. Y. Lyubimov, J. McCarty, A. Clark, and M. G. Guenza. Analytical rescaling of polymer dynamics from mesoscale simulations. *J. Chem. Phys.*, **132**, 224903, (2010).

A. J. Clark, and M. G. Guenza. Mapping of Polymer Melts onto Soft-Colloidal Chains. *J. Chem. Phys.*, **132**, 044902, (2010).

ACKNOWLEDGEMENTS

I wish to first acknowledge the contributions of my advisor Marina Guenza for starting this project and giving me the chance to make my contributions to it. Furthermore, I must acknowledge the tremendous amount that I have gained from working with my graduate student colleagues Ivan Lyubimov, Jay McCarty, and Jeremy Copperman through my time here. It would be difficult to imagine a better group of people with whom to work. I would also be remiss not to thank my committee for their time in reading this document and providing engaging questions at my advancement exam and defense.

None of this would work would have been possible without the support of the department of physics, particularly Steve Gregory and Steve Kevan. Financial support was provided by teaching assistantships through the department of physics and through grant National Science Foundation grant number DMR-0804145. Some computing resources were provided through the Xsede project

This work is dedicated to my grandmother Eva Clark

TABLE OF CONTENTS

Chapter Page

LIST OF FIGURES

Figure Page

Figure Page

LIST OF TABLES

Table Page

CHAPTER I

REPRESENTATIONS OF POLYMER SYSTEMS

Polymer melts–high density liquids of long, flexible chain molecules–are of great technological interest, as they are used in many plastics and materials manufacturing applications. Because of the variety of properties that they exhibit on different time and length scales, theoretically characterizing and simulating their properties presents a major challenge. To meet this challenge many different levels of representation have been developed and used for theory and computer simulations. Many descriptions, from the chemically detailed to phenomenological, and from low level representations to highly coarse-grained representations and mean-field descriptions have been developed to explore different aspects of polymer systems.[1–6] In this work, the focus is on highly coarse-grained representations of linear homopolymer melts. Low-level representations that are known to reproduce experimental data very accurately, but are too computationally intensive to be used for numerical simulation over a full range of systems of interest are used as a basis for comparison. Despite the large amount of research that has been done on high-level coarse-grained representations, problematic, unanswered questions have remained as to the ability of the effective pair potentials derived to map polymer melts onto these models to represent consistently the equilibrium thermodynamic properties of the real underlying physical system. The remaining chapters of this document will extend analytical theory to describe static structure of the melt at variable levels of high-level coarse-graining and for the first time characterize the effective pair potentials that can be used to represent the system at these levels of representation in a computer simulation. From these, we demonstrate that coarse-grained potentials based on structural correlations can reproduce equilibrium thermodynamic averages consistent with low-level descriptions and show why the common numerical schemes for coarse-graining are often observed to be unreliable. In this chapter, the basic properties of polymer melts are described, and the types of coarse-grained

representations that are used to describe them are overviewed. The problems of transferability and representability that arise for higher-level coarse-grained representations that will be addressed by the original research in this dissertation then discussed. Finally, a chapter-by-chapter outline of content of the dissertation is given.

I.1. Basic Properties of Polymer Melts

A polymer melt is a liquid comprised of polymers alone, with no solvent component present, that is at sufficiently high density that the distribution of chain configurations follows (Gaussian) random walk statistics. All polymers have repulsive interactions between monomers which prevent monomers on the same chain occupying the same space or crossing through each other. Chain configurations for long polymer chains in good solution therefore follow the statistics of self-avoiding random walks, random walks prohibited from crossing any part of their own path. The positions of any two monomers on the chain have a correlation that does not vanish with an increasing number of intervening chain segments, and thus the probability distribution of finding monomers with a given separation distance does not follow the Gaussian central limit theorem for large chain separations. Since the system is such that it has intrachain correlations that grow in chain separation range with the number of monomers on the chain to arbitrarily large chain lengths, the tools of renormalization group theory are required to obtain the scaling properties of the chain. Specifically, the system can be mapped onto an O(n) ferromagnet model in the limit $n \to 0$,[7] giving a radius of gyration (the root-mean-square distance of monomers from the chain center of mass) that scales with the number of monomers, N, as N^{ν}, with $\nu \approx 0.588$[8] at large N.

In a melt, the presence of surrounding polymers provides forces that "screen" the excluded volume effects that would lead to the non-Gaussian distributions of monomers. While intrachain excluded volume effects push chain configurations (on average) away from the center of mass (cm) of the molecule, in a melt monomers pushed outward in this way will encounter monomers on other chains that will push them (on average) back toward the cm of their chains. The presence of surrounding chains' monomers therefore cancel out the effects of intrachain excluded volume over large length scales. From the preceding argument, melt behavior relies on the geometric interpenetration of polymers, as most monomers must be roughly equally likely to

interact with monomers on their own chain and those on other chains. Therefore the density of monomers must be high enough so that each polymer interpenetrates significantly with many other polymers. Each chain occupies on average a volume $V_{ch} = (4/3)\pi R_g^3 = b^3 N^{3/2}$ (since the radius of gyration for long chain melts can be written $bN^{1/2}$, with b the effective segment size). The average number of polymers in the volume of a single chain, $n_{Rg} \propto \rho_c V_{ch} \propto \rho_m N^{1/2} b^3$ must therefore be large. Assuming that the proportionality constants are of order one, the existence of melt behavior on large length scales in the system requires that $\rho_m >> 1/(N^{1/2}b^3)$.[7]

It can be shown through more detailed theory that this screening effect is not exact on all length scales, and that for very long chain melts there are long range correlations on intermediate sub-molecular length scales. Wittmer et al have shown that there is a correction to ideal Gaussian statistical correlations in polymer melts that scales as $1/\rho_m$.[9–12] This makes intuitive sense in light of the above screening argument, as the same analysis could be applied to subsections of a long chain, for which there would be a higher density threshold to achieve the screening necessary to counteract intramolecular excluded volume. The result would be that some "swelling" on these length scales can occur, despite being screened out over the length scale of the whole molecule. For this work, it will be assumed that all melts described are at high enough monomer densities that these corrections are negligible and that the system exhibits ideal random walk statistics on all length scales.

I.2. Representations of Polymer Melts and Coarse-graining

There is in principle no upper bound to the number of monomers that can comprise an individual polymer, and systems of practical interest are typically comprised of polymers with hundreds or even thousands of individual monomers each. A fully microscopic description treating the time evolution of the dynamics of all the atoms in such a system is far beyond the level of complexity that is approachable with computer simulations. Therefore, any practical representation of polymer melts used must be at least somewhat coarse-grained.

The wide variety of models that have been proposed to represent polymer melts can be broadly classified based on their level of coarse-graining and how chemically realistic they are. The higher the level of coarse graining the less degrees of freedom are included in the model to represent the same system. High and low level coarse-grained models can both be designed

to be more chemically realistic or more phenomenological. Chemically realistic models aim to provide a route to mapping onto a specific system and predict properties in terms of microscopic parameters, whereas phenomenological models generally aim to provide information on general properties and scaling laws for systems of the type but cannot predict the behavior of a system in terms of microscopic parameters. Despite the fact that they cannot be predictive of the exact properties of specific systems, such descriptions still have great value in testing scaling laws in such systems where chemically detailed models are not available or make computer simulations impractical or impossible. Common examples of phenomenological models include the bead and spring model, where each postulated degree of freedom represents a small number of monomers and interactions are modeled via effective Lennard-Jones potentials and attractive bond potentials.[13] Because they are *much* less computationally intensive than realistic atomistic models, they have recently allowed low-level dynamical simulations of the long-time plateau in highly entangled polymer melts for the first time.[14] Other phenomenological models that have been employed to explore scaling properties include those assuming a Gaussian form for intermolecular interactions,[15] and mean-field models such as the Rouse and Reptation theories for describing the scaling behavior of the dynamics of unentangled and highly entangled polymer melts respectively.[16] This dissertation will focus on the more difficult realm of chemically realistic coarse-grained models, which attempt to predict the properties of specific systems in terms of microscopic parameters.

I.2.1. Chemically Realistic Low Level Representations

Because the polymers making up a melt can be comprised of arbitrarily many monomer repeat units, and systems of interest are often made up of chains of hundreds or thousands of monomer repeat units, some level of coarse grained representation is always necessary for practical numerical simulations and theories. Low level coarse-grained models include various types of atomistic representations, wherein individual atoms or small collections of atoms are represented by a single degree of freedom that interacts classically with other atoms or units in the system. The atomistic model focused on here is the family of so called "United Atom" (UA) models. In UA models, hydrocarbon groups on the chain are represented by single interacting point particles (effective atoms). For polyethylene, which is used as the test system throughout

this work, the entire ethylene monomer (CH_2) is represented by a single point particle, which interact with monomers on other molecules via an effective potential of Lennard-Jones form.[17–19]

Representations at this level perform very well against experimental data for structure, thermodynamic, and dynamical properties.[20,21] However, simulations using low-level representations are extremely computationally intensive, both in generating trajectories to reach the time scales of interest, and in equilibrating the systems from a starting configuration to a physically realistic configuration. Only through the development of sophisticated chain breaking algorithms for equilibration has it become possible to reach melt simulations of a few hundred monomers with at least 32 chains and one small simulation of a melt 1000 monomer chains with only 8 molecules,[22,23] whereas the full effects of dynamical entanglements only appear for chains of many hundreds or thousands of monomers.[16]

I.2.2. Chemically Realistic Representations at High Levels of Coarse-graining

The computational expense and difficulty of UA simulations has prompted great interest in trying to represent polymer melts in coarse-grained representations that can capture aspects of the system on long time and length scales not accessible to low-level simulations at the cost of losing short time and length scale information about the system. The focus of this work will be on high-level coarse-grained representations where many monomers are grouped together into each coarse-grained unit. To test the properties and behavior of such highly coarse-grained representations, we will compare structural correlations between center of mass coordinates, which are not directly measurable from experiments, against data from UA simulations.

I.3. Effective Interaction Potentials for Coarse-grained Representations

By far the most widely used approach to deriving coarse-grained chemically realistic potentials from low-level representations is the Iterative Boltzmann Inversion (IBI) algorithm. The IBI approach is starts from atomistic level data on a small system to measure the potential of mean force (pmf). The pmf, $w(r)$, defined by the probability of finding two coarse-grained units separated by distance r, $P(r) = \exp[-w(r)/(k_BT)]$ with k_B Boltzmann's constant and T the temperature is used as an interaction potential for mesoscale (MS) computer simulations in the coarse-grained representation. The probability distribution is measured from this simulation

and used again to calculate the pmf. The difference between this and the starting value is used as a correction to obtain a new potential. This procedure is repeated until a tcf equal to the starting tcf from the atomistic simulation is obtained. The final potential with all iterative corrections is then taken to be the effective pair potential.[24] IBI provides a straightforward way of calculating effective potentials, and since there is a one-to-one theoretical relationship between pair potentials and structural pair correlations,[25] it should in principle obtain the optimal effective potential that represents the coarse-grained system.

Another alternative approach is force-matching, which attempts to map the forces from atomistic descriptions onto collective degrees of freedom. This approach has been theoretically examined by Noid,[26] and applied to a variety of mostly biological macromolecular systems by Voth[27–29]

Relatively few of these numerical coarse-graining schemes have attempted to devise chemically realistic effective potentials for very high levels of coarse-graining, where each degree of freedom represents a large number of monomer units and the effective potentials are extremely soft. Most representations at this level are of the phenomenological nature. Padding and Briels have used Gaussian forms with a single free parameter fit to optimize structure against atomistic simulation data as effective potentials for their soft blob and soft sphere models.[30–33] Likos and collaborators have examined very general properties of systems interacting via such extremely soft potentials without assuming specific forms.[35]

The approach that will be pursued here developed from a liquid state integral equation theory suggested by Krackoviack et al[34] to describe the structure of center-of-mass sites in a polymer liquid, which was implemented numerically for polymers in solution by Louis and collaborators.[36,37] The approach is based upon and extends the analytical theory for structural correlations by Yatsenko et al.[38,39] This approach is based upon liquid state integral equation theory. The following chapter will give a brief summary of the relevant concepts in integral equation theory and a description of the coarse graining method, as well as a summary of the work done previously using this approach in the Guenza group.

I.4. Issues for Coarse-grained Representations

Aside from the fact that nearly all available coarse-graining schemes other than ours require atomistic simulation data as a starting point, there are a number of very fundamental problems that numerical coarse-graining schemes cannot adequately address. Louis has broken these issues down into two categories: transferability and representability.[40] Transferability refers to the fact that systems optimized at one set of thermodynamic conditions and one set of system parameters will not generally be applicable to another, as the effective potentials represent free-energies that are dependent on thermodynamic and system parameters. This problem is inherent to numerically derived effective potentials, but does not effect the validity of the potentials in the state at which they are derived. However, it limits the usefulness of numerically obtained effective interaction potentials, as such potentials at high levels of coarse-graining are generally highly dependent on density, temperature and other system parameters, and thus generally low-level simulations in each new state are required to be performed if systems with different parameters are to be studied.

Representability is a more serious and fundamental concern. It refers to the ability of the effective potentials to represent the actual physical properties of the system. Potentials derived using the simple IBI algorithm described above are well know to produce effective potentials that reproduce the correct structure but yield very different pressures from the atomistic level system when used in simulations. Through numerical trial and error, it has been found that the addition of small linear phenomenological functional forms at large separations to the effective potentials and performing a secondary optimization for the pressure of the system can result in effective soft potentials that yield pressures consistent with atomistic simulations while also maintaining consistent static structure for low-level coarse-grained descriptions.[24]

The main focus of this work will be addressing these fundamental issues of transferability by deriving analytical effective pair potentials for representations of polymer melts at high levels of coarse-graining. To address transferability, analytical theory is used to characterize structural correlations and effective potentials for a range of high-level coarse-grained representations. This also allows for the first time the characterization of the contribution of the effective potentials to the virial equation of state of the system and the relationship of the effective potentials to structural correlations measured in the system in the infinite chain limit. The result is that the

equilibrium thermodynamic averages can be preserved in high-level coarse-grained descriptions with effective pair potentials derived from structural correlations, however the sensitivity of the thermodynamic properties is so high as to make numerical coarse-graining schemes at high levels realistically unfeasible.

I.5. Organization of Dissertation

The problem outlined above of understanding the representability and transferability of highly coarse grained models of polymer melts is addressed in the following chapters. In chapter II, a short background overview of the theoretical tools of integral equation theory used to derive the coarse-grained description is given as well as background on the progress made previously using this approach. The place of this research in the larger collaborative project to develop high-level transferable coarse-grained descriptions of polymer liquids is noted. In chapter III, a general analytical solution for the structural correlations in a class of high-level coarse-grained descriptions representing polymer melts by the center of mass points of large chain subsections is developed. The material in sections one through four of this chapter are adapted from "Mapping of Polymer Melts onto Liquids of Soft-Colloidal Chains," coauthored with my advisor Marina Guenza, who initially suggested the idea for this model and offered assistance through the derivation and in shaping the presentation of the theory in the article. This article was previously published in the Journal of Chemical Physics in 2010. Section five of this chapter will appear in "Theoretical Characterization of Effective Pair Potentials that Map the Structure and Thermodynamics of Polymer Melts onto Soft Colloidal Liquids," coauthored with Jay McCarty, Ivan Lyubimov, and Marina Guenza, which is in preparation and is intended to be submitted soon. The portion appearing in this section is solely the work of Anthony Clark. In chapter IV, effective pair potentials for the coarse-grained representation models are derived and their features are characterized, and in chapter VI the thermodynamic properties resulting from these potentials are examined. Chapters IV and V are based on "Theoretical Characterization of Effective Pair Potentials that Map the Structure and Thermodynamics of Polymer Melts onto Soft Colloidal Liquids" and a short letter, "Thermodynamic Consistency in Variable-Level Coarse Graining of Polymeric Liquids," that has been published in the journal Physical Review Letters

with the same co-authors, both of which are coauthored with Jay McCarty, Ivan Lyubimov, and Marina Guenza

CHAPTER II

INTEGRAL EQUATION THEORY

This chapter gives a brief background of the theoretical tools that provide the basis for the new coarse-grained representations discussed in the following three chapters. In the first section the physical assumptions used are discussed and relevant descriptions are given. In the second section, liquid state integral equation theory and its generalizations are discussed. Finally, in the third section, the fictitious site approach to coarse-grained representation is described and the previous work on coarse-graining using this approach is described.

II.1. Starting Assumptions and Definitions

The liquid state occupies a difficult place in statistical mechanics because it is both comprised of many highly interacting particles, making reference to a tractable weakly interacting system, such as is done for a real gas, impossible, but also lacks the symmetries available in a crystalline solid that allow the reduction of the problem to that of characterizing behavior in a finite unit cell.

The starting assumption that will be used throughout this work is that the potential energy of the system can be decomposed into a sum over the pairwise potential energies of all constituent particles in the system. Although some situations can give rise to non-pairwise effective potentials, such as coarse-grained representations of highly polarizable atoms or molecules and fundamental interactions such as Casimir-Polder forces, this assumption has been tested extensively for liquids in the regime of interest here, where the temperature is high and the interest is in phenmonenon on scales much larger than atomic size, and has been broadly found to hold for such systems. With this assumption, solving the probability distribution is reduced to the determination of the two point density correlation function between constituent particles of the liquid. Furthermore, under the assumption that the liquid is homogeneous and isotropic, the two point correlation becomes independent of starting position and orientation, and reduces to a function of a single variable–the separation distance of the particles. This distribution function is termed the "radial distribution function" (rdf). For a simple liquid, $g(r)$ can be defined by

$$g(r) = \frac{1}{\rho}\left\langle \frac{1}{N}\sum_{\substack{i}}^{n_a}\sum_{\substack{j \\ i\neq j}}^{n_a}\delta(\vec{r}-(\vec{r}_i-\vec{r}_j))\right\rangle \ , \tag{II.1}$$

where ρ is the system average number density and the angle brackets denote an ensemble average

This correlation can be visualized as measuring the fraction of the average system-wide number density found in an infinitesimal spherical shell of radius r, given that one particle is located at the origin. In an infinite uniform liquid, $g(r)$ approaches unity as $r \to \infty$. A bounded function at large r known as the "total correlation function" (tcf) is therefore defined by

$$h(r) = g(r) - 1 \ . \tag{II.2}$$

The tcf measures the fractional deviation from the average system density in an infinitesimal spherical shell of radius r given that there is a particle at the origin.

These functions can be related to, and contain the same information as the static structure factor, defined in reciprocal space as

$$\hat{S}(k) = \langle \rho_k \rho_k' \rangle \ , \tag{II.3}$$

which is the quantity that is directly measured as the power spectrum in scattering experiments. For a simple liquid, the static structure factor is related to the tcf as

$$\hat{S}(k) = 1 + \rho\hat{h}(k) \ , \tag{II.4}$$

where ρ is the number density of particles in the system, and $\hat{h}(k)$ is the Fourier transform of the tcf.[41] Here, and throughout this work, the Fourier transform is defined with a normalization convention such that the three-dimensional Fourier transform of a radially symmetric function $f(r)$ is given by

$$\hat{f}(k) = \frac{4\pi}{k}\int_0^\infty r sin(kr) f(r) dr \ . \tag{II.5}$$

II.2. Integral Equation Formalism

The approach taken to solving the liquid systems of interest in this work is based on integral equation theory. Integral equation theory uses an approach that decomposes the tcf into a sum of contributions from all possible sequences of pairwise interactions among constituent particles, by defining a new unknown "direct correlation function" (dcf), that represents the contribution to the total correlation from one pair of interacting particles. The utility of this approach relies upon relating the dcf to the actual pair potential between pairs of particles through a "closure" approximation. To obtain a tractable theory for molecular liquids, such as the polymers of interest here, this approach has further been extended to obtain tractable descriptions of molecular liquids through the "reference interaction site model" (RISM), which allows further decomposition of contributions to the tcfs between "sites" representing parts of the molecule into intramolecular and intermolecular components.

II.2.1. The Ornstein-Zernike Equation

The Ornstein-Zernike, first proposed by Ornstein and Zernike in 1914,[42] defines the dcf. For a simple (non-molecular), isotropic and homogeneous liquid, the Ornstein-Zernike equation is given in modern notation by

$$h(r) = c(r) + \rho(c * h)(r) \ , \tag{II.6}$$

where the symbol "*" denotes the three dimentional convolution, defined for two radially symetric functions $f_1(r)$ and $f_2(r)$ as

$$(f_1 * f_2)(r) = \int d^3r f_1(r') f_2(|\vec{r} - \vec{r'}|) \ , \tag{II.7}$$

and $c(r)$ is the dcf.

II.2.2. Closure Approximations

The Ornstein-Zernike equation is not a route to solving for the structural correlation functions directly, as it merely defines one unknown function (the tcf) in terms of another (the dcf). Its utility lies in the fact that functional relationships can be found that provide

a good approximation of the relationship between the dcf and pair potential for many cases. The two most commonly applicable closure approximations are the hypernetted-chain (HNC) approximation, and the Percus-Yevick (PY) approximation. Hansen and McDonald formulate these approximations intuitively as two linear functional expansions, the PY a linear expansion of 1-body density distribution and the HNC a linear functional expansion of the logarithm of the 1-body density distribution. The PY approximation effectively comes from treating the change in structure due to small perturbations as exponential (a reasonable approximation for many systems with highly repulsive short range interactions where a small perturbation can incur a large change in structure), while the HNC approximation takes the response to a small perturbation as linear in the perturbing field (appropriate when pair potentials are sufficiently slowly-varying). Written in the notation used here the PY approximation is given by

$$c(r) = \left(1 - e^{\beta V(r)}\right) g(r) \tag{II.8}$$

and the HNC by

$$c(r) = -\beta V(r) + h(r) - ln[h(r) + 1] \ , \tag{II.9}$$

with $V(r)$ the pair potential.[41]

II.2.3. Interaction Site Approximations for Molecular Liquids

The Ornstein-Zernike equation can be formulated with full generality for molecular liquids, but in such a formulation the total and direct correlations become functions of all internal degrees of freedom of the molecule.[41] Solving the full molecular equation for a liquid of macromolocules such as a polymer melt is a hopelessly intractable problem, as there may be hundreds or thousands of degrees of freedom required to describe the configuration of each molecule. To make further progress, the (reference) interaction site model (RISM) is employed. In the RISM, "interaction sites" are chosen to represent atoms or groups of atoms making up the molecule. The molecular direct correlation is then decomposed into intramolecular contributions and contributions from an intermolecular site-site direct correlation. The Molecular Ornstein-Zernike equation is then used to obtain a generalized Ornstein-Zernike equation for the matrix of site-site correlation tcfs in terms of the unknown site-site dcfs and the intramolecular

correlations. For an isotropic and homogeneous system, this once again reduces the problem to a set of equations involving functions of one variable (the separation distance of sites).[43]

II.2.4. Polymer Liquids with the Interaction Site Model

The interaction site approach can be applied to polymers. For simple linear polymers such as polyethylene, each monomer is represented by a single site, thus giving a representation at the same level of coarse-graining as the UA simulations. For long polymers, the effects of distinguishibility of monomers due to their relative proximity to the end of the chain is small and confined to a small fraction of monomers near the ends, and so treating all sites to follow a chain-averaged tcf is a good approximation for most applications. Thus the RISM Matrix equations for the tcfs reduce to the scalar equation for the average monomer-monomer tcf

$$\hat{h}^{mm}(k) = \hat{\omega}^{mm}(k) \left[\hat{c}^{mm}(k)\hat{\omega}^{mm}(k) + \rho_m \hat{c}^{mm}\hat{h}^{mm}(k) \right] , \tag{II.10}$$

known as the polymer-RISM (PRISM) generalized Ornstein-Zernike equation, and where $\hat{\omega}^{mm}(k)$ is the average pair distribution of monomers around monomers on an individual chain in the system.

There is an idealized limiting case of PRISM that can be solved analytically that is of some theoretical interest known as the Percus-Yevick thread limit. In this idealization, the direct correlation function in real space is taken to be a delta function, or equivalently a constant value in Fourier space, $\hat{c}^{mm}(k) = c_0$. The limit of the PY closure approximation for hard sphere monomers is then applied, giving a condition for $r = 0$ that can be solved analytically using the rational function approximation form of the Debye intramolecular distribution

$$\frac{2}{k^4}(k^2 - 1 + e^{-k^2}) \approx \frac{1}{1 + k^2/2} . \tag{II.11}$$

The result gives for the direct correlation

$$c_0 = \frac{1}{\rho_m N} \left(\frac{R_g^2}{\xi_\rho^2} - 1 \right) \tag{II.12}$$

and for the total correlation

$$h^{mm}(r) = \left(\frac{3}{\pi\rho_m l_{eff}^2 r}\right)\left(e^{-\sqrt{2}r/R_g} - e^{r/\xi_\rho}\right) \ , \tag{II.13}$$

where the PY-thread density screening length is defined as $\xi_\rho = \left(\frac{\sqrt{2}}{R_g} + \frac{1}{3}\pi\rho_m l_{eff}^2\right)$.

Physically, the thread model describes a limit where the detailed nature of monomer pair interactions, and therefore of geometric packing among monomers, is totally irrelevant. For systems in this regime, properties of the system are universal to any architecture. For most real polymer melts at high densities, the packing among monomers is sufficiently dense relative to the range of inter-monomer interactions that this universality is lost and the PY thread model does not capture the full behavior of the system.[44]

Throughout this work, the term "PY thread model" will refer to this solution where the monomer-level problem is solved using the assumption that $\hat{c}^{mm}(k) \approx c_0$ for all k. In the following chapters the less drastic approximation that the direct correlation can be approximated over some finite range of small wave vectors that are relevant to a coarse-grained model will also be used. In this case, the direct correlation function is short relative to the length scales of interest, but not infinitesimal in range, and the direct correlation parameter, c_0, is found from

$$c_0 = 4\pi \int_0^\infty r^2 c^{mm}(r) dr \tag{II.14}$$

using the full form of $c^{mm}(r)$.

In the general case where the thread model does not apply because detailed packing of monomers is relevant, numerical solutions of the PRISM generalized Ornstein-Zernike equation can be used to obtain $c^{mm}(r)$. Specifically, a model which treats the repulsive interactions using a hard sphere potential and attractive part of monomer interactions via the attractive part of a Lennard-Jones potential can be used. The PY closure approximation is employed for the repulsive part and the molecular mean-spherical closure approximation is employed for the attractive component.[45]

II.2.5. Fictitious Sites in the Interaction Site Model

RISM in principle allows a choice of what sites to include and what part of the molecule these sites represent. In fact, RISM allows sites which do not represent any real part of the

molecule at all (termed "fictitious sites") to be included without any effect on real sites so long as the dcfs between fictitious sites and all other sites are everywhere zero. As was first proposed by Krakoviack and coworkers[34] and examined numerically using distribution functions obtained in computer simulations of polymer solutions,[36,37] this can be used to obtain coarse-grained potentials for cm coordinates if the intramolecular distribution(s) of real monomer sites with fictitious sites are taken to be the probability distribution(s) of monomers about their center of mass.

Using the PRISM PY-thread model, Guenza and collaborators were able to solve analytically for the form of the pair correlation functions for a representation including one cm site per polymer for polymer melts and mixtures and perform MD simulations using numerically-derived effective pair potentials in this representation[38,39] and for a soft dumbbell representation of diblock copolymers.[46] These were also extended to multiscale approaches that combined atomistic and mesoscale level simulation data to get descriptions accurate both on short and long length scales,[47] and to examine the approach to the spinodal phase transition in binary mixtures.[48] In the following chapter, this approach will be extended to characterize pair correlation functions in highly coarse-grained representations of melts whose polymers are represented by cm coordinates of arbitrary numbers of sub-chains long enough to exhibit Gaussian statistics. In chapters V and VI, the effective pair potentials based upon these structural pair correlation functions are considered.

II.3. Computer Simulations

Computer simulations will be used to test the ability of effective potentials in the coarse-grained representation to reproduce the properties of low-level representations, which in turn are known to reproduce experiments.

II.3.1. United Atom Simulations

United atom molecular dynamics (UAMD) simulations are computer simulations performed using the united atom representation described above where several atoms are represented by a single degree of freedom, and the time evolution of the system is calculated using molecular dynamics simulations. Effective pair potentials have been derived by fitting the

parameters of a Lennard-Jones interaction potential to experimental data. UAMD simulations using these force-fields have been tested against scattering data and reproduce experimentally determined structure factors very well.[20,21]

The available United Atom molecular dynamics (UAMD) simulations provide systems against which the detailed properties of more coarse-grained simulations can be tested. Specifically, in this document, results from our high-level representations are tested against United atom simulations provided by Grest[20] and Mavrantzas,[22] and new UAMD simulations performed by my colleague Jay McCarty using the same models. The new UAMD simulations performed in the group have allowed us to compare pressure and other thermodynamic quantities, as well as test our theories against a wider range of densities and chain lengths.

II.3.2. Mesoscale Molecular Dynamics

The dynamics of highly coarse-grained polymer models can be related to the underlying physical system by "projecting" the time evolution of the Hamiltonian onto the phase space of the coarse-grained degrees of freedom. This can be derived directly by the projection operator formalism starting from the Liouville equation of motion for the system. The time evolution of the coarse-grained cm points in the real system therefore follows time evolution equation with non-Hamiltonian memory and random force terms.[41] To understand and characterize dynamical correlations two main approaches may be taken. The first is to directly modify simulation algorithms to include random forces and memory and run computer simulations with these. This approach has been pursued recently by Padding and Briels in a series of papers.[30–33] The second approach, is to simulate Hamiltonian dynamics for the coarse-grained representation with mesoscale molecular dynamics (MSMD) simulations using effective pair potentials and separately derive the effects of non-Hamiltonian terms in the equations of motion on the dynamical correlations of interest.

The coarse-grained representations project in this research group, of which the research here is a part, has taken the latter approach. Work done by Ivan Lyubimov to derive the correction effects of non-Hamiltonian terms that allow for the reconstruction of the long-time dynamics, has been successful in predicting diffusive regime mean square displacements and other autocorrelations measured from UA simulations and experimental data using MSMD

simulations and analytically derived dynamical rescaling factors accounting for the change in friction and entropy between the UA representation and the soft sphere model, where each polymer is represented by a single center of mass point. This work has been published in a series of papers.[49,50] Preliminary work has suggested that the theory for the rescaling factors can be naturally extended to multiblock models where each chain is represented by large numbers of long chain subsections.[51]

Since the focus in this work will be entirely on addressing long-standing questions about equilibrium static time-invariant thermodynamic averages, these issues are not directly relevant here. They do however, motivate the choice of dynamical simulations to test these simulations, as these are necessary for input to the full theory for the structure and dynamics. The properties in question here could be tested via Monte Carlo simulations or non-Hamiltonian dynamical models, as all particle-based simulation approaches take effective pair potentials as input. The development and use of MSMD simulations to test static properties in this work is done to fit in the context of the large coarse-graining project, so they can be used in future work extending the dynamical reconstruction theories to lower level representations.

CHAPTER III

STRUCTURAL CORRELATIONS FOR A FAMILY OF HIGHLY COARSE GRAINED REPRESENTATIONS

The material in sections one through four of this chapter are adapted from "Mapping of Polymer Melts onto Liquids of Soft-Colloidal Chains," coauthored with my advisor Marina Guenza, who initially suggested the idea for this model and offered assistance through the derivation and in shaping the presentation of the theory in the article. This article was previously published in the Journal of Chemical Physics in 2010.[52]

III.1. Introduction

In previous work Guenza and collaborators have presented an analytical course-grained model that effectively maps a homopolymer melt onto a liquid of soft colloids. This model accurately reproduces the static structure of the melt on the molecular length scale and allows extensions of the range of systems that can be investigated through mesoscale simulations. In it, the polymers are described as point particles that interact via an effective pair potential with a range of the order of the polymer dimension, i.e. its radius-of-gyration, R_g.[38,39] This large-scale model, combined with local scale united atom simulations, provides a complete description of the structure of the polymer melt at length scales between the bond length and R_g, and it is sufficient to give the needed information for liquids of unentangled macromolecules.[47]

However, some important phenomena that occur in polymer liquids take place on intermediate length scales, smaller than the size of the molecule, but still much larger than the size of the monomers. These phenomena include, for example, dynamical entanglements, blob chains for polymers dissolved in "good" solvents, and polymer pearl-neckless structures.[7,16] For systems where intermediate length scales are important, representing the polymer as one soft-colloid is too drastic. Therefore it is necessary to develop a course-grained model that still averages out a large number of irrelevant degrees of freedom, to provide a reduction in required computation and make large-scale simulations of long-chain melts practical, while retaining enough effective internal degrees of freedom to describe internal structure on intermediate length scales.[30,31] In addition, while most highly coarse-grained theories of polymer melts, including this

approach, make the reasonable approximation of treating bulk polymers as spherically symmetric objects in light of their random orientations and the interest in long time and large length scale behavior, individual melt polymer configurations have, on average, some asphericity.[53] The inclusion of multiple submolecular degrees of freedom allows the chain configurations that are aspherical on the molecular level to arise naturally in simulations while still using spherically symmetric interaction potentials[15]

Presented here is a model of this kind, where each chain is represented by a collection of identical shorter chains, so-called "blocks", connected together. Each short chain is mapped onto a point particle located at its center of mass, effectively replacing the long polymer by a chain of soft blocks. Each block is treated approximated to be spherically symmetric. Because we treat homopolymer liquids, intra- and inter-molecular interactions are identical. However, if the blocks in a chain were chemically different, the theory could be implemented to include repulsive or attractive interactions between blocks of different chemical nature, and the model would describe a liquid of coarse-grained block copolymers.[46]

Inputs to mesoscale simulations of coarse-grained systems are the effective potentials acting between effective units or blocks, which are calculated from the intermolecular block-block pair distribution functions by enforcing a closure equation. Intermolecular pair distributions are derived from first-principles liquid state theory using a generalized Ornstein-Zernike equation (OZ) where the monomeric units of the polymers are modeled as interacting rigid spheres. The course-grained description arises from adding imaginary, non-interacting sites fixed to lie at the center of mass of each block within each chain. The resulting equations can be solved to give analytical predictions in Fourier space for the pair correlations between block-center sites on different chains within the melt, allowing it to be immediately applied to a wide range of thermodynamic conditions and polymer types. Approximate analytical forms are then derived for the total pair correlations between blocks in real space. This contrasts with other course-graining schemes that have been applied to describe polymers as chains of soft-colloids, which are numerical, and require simulations to be performed for each set of system parameters in order to determine effective potentials.[54]

The equilibrium intramolecular structure of polymers formed by distinct sub-blocks enter the generalized OZ equation. This includes all pair correlations involving monomers or

block-centers, which are formulated using the ideality of intra-chain statistics for polymers in a melt. The Gaussian approximation for the block-monomer correlation, which was successful in representing the correlation between a site and block center previously for the soft-colloid[38,39] and diblock[46] models, still applies for sub-chains including a number of monomers higher than $N = 30$ for relatively small numbers of blocks, but can lead to significant errors for blocks representing shorter sub-chains. We propose a more general approximation for the intermolecular correlation functions in real space, using the freely jointed chain model, which gives analytic dependence on system parameters, and can be extended naturally to different models of the intramolecular structure. Derived expressions for intra and intermolecular monomer and block correlations throughout are compared with United Atom Molecular Dynamics simulations of a melt of 96 site polyethylene chains[20,21] and one of 224 site polyethylene chains[22,23] with good agreement, supporting the validity of the proposed equations.

The chapter is structured as follows. In the first section we present the generalized Ornstein Zernike equation for the coarse-graining of the homopolymer liquid into chains of soft blocks. Three sections follow in which we report the intramolecular monomer-monomer (mm), block-monomer (bm), and block-block (bb) distribution functions. While the intramolecular Gaussian distribution works well for blocks of long chains, a more refined distribution is necessary for short blocks and for chains with a high number of blocks. We propose a freely-jointed description which agrees well with data from united atom simulations. In the following three sections we present solutions for the total correlation functions between any combination of block and monomer pair interactions. An analytical solution for the freely-jointed chain model shows improved agreement with simulation data when compared to the more traditional Gaussian distribution model. The improvement is more pronounced when the homopolymer is represented as a chain of short blocks, with a higher number of blocks. Finally, a block-averaged description is formulated for long multiblock chains that will be used in the derivation of effective potentials in the following chapter.

III.2. Generalized Ornstein-Zernike Equation for Block-level Coarse-graining

The liquid-state approach introduced here represents a homopolymer as a chain of non-interacting soft colloids or blocks. The block-level intermolecular correlations are

derived following the solution of a generalized Ornstein-Zernike equation where the monomer representation is described by real sites, while the coarse-grained sites are fictitious. No direct correlation is present between fictitious sites, and between real and fictitious sites.[34] This approach is an extension of our method to represent diblock copolymers as dumbbells of soft colloids of possible different chemical nature and/or degree of polymerization.[46] Our previous work also included a theory to coarse-grain homopolymers and their mixtures at the polymer center-of-mass level, where the whole chain is represented as a single soft colloidal particle.[38]

The new model introduced here describes homopolymer chains as a collection of an arbitrary number, n_b, of chemically identical blocks. Each block contains a number of sites N_b, such that $n_b \times N_b = N$, with N the total number of sites in a chain. Intra- and inter-molecular total correlation correlation functions are derived for each possible pairing of sites among the block center-of-mass (cm) and monomeric sites.

These intermolecular total correlation functions (tcfs) are of great relevance, since they are the starting point for the calculation of all the properties of interest, thermodynamic and dynamic, to describe the coarse-grained system. These include the effective potential between a pair of coarse-grained sites, which is the necessary input to mesoscale simulations of the coarse-grained system. Because the effective potential is a free-energy, and therefore a function of the system parameters, such as temperature, density, and degree of polymerization, different systems have different effective potentials. In this respect it is convenient to have analytical forms of the effective potentials, as are those in our treatment, because their parameter dependence is explicit, and they are directly applicable to different systems of interest, i.e. they are transferable.

The generalized OZ equation is formulated using the polymer reference interaction site model (PRISM). Extending the block-PRISM equations[55] by including fictitious sites, which have no site-site direct correlation with other sites, at the center of mass of each block, the resulting matrix equations are

$$\hat{\mathbf{h}}^{mm(n_b)}(k) = \hat{\omega}^{mm(n_b)}(k)\hat{\mathbf{c}}(k)\left(\hat{\omega}^{mm(n_b)}(k) + N_b\rho_c\hat{\mathbf{h}}^{mm(n_b)}(k)\right) \ , \tag{III.1}$$

$$\hat{\mathbf{h}}^{bm(n_b)}(k) = \hat{\omega}^{bm(n_b)}(k)\hat{\mathbf{c}}(k)\left(\omega^{mm(n_b)}(k) + N_b\rho_c\hat{\mathbf{h}}^{mm(n_b)}(k)\right) \ , \tag{III.2}$$

$$\hat{\mathbf{h}}^{mb(n_b)}(k) = \hat{\omega}^{mm(n_b)}(k)\hat{\mathbf{c}}(k)\left(\omega^{mb(n_b)}(k) + N_b\rho_c\hat{\mathbf{h}}^{mb(n_b)}(k)\right) \ , \tag{III.3}$$

and

$$\hat{\mathbf{h}}^{bb(n_b)}(k) = \hat{\omega}^{bm(n_b)}(k)\hat{\mathbf{c}}(k)\left(\omega^{mb(n_b)}(k) + N_b\rho_c\hat{\mathbf{h}}^{mb(n_b)}(k)\right) \ . \tag{III.4}$$

Here ρ_c is the number density of chains. We denote correlations involving block-center sites by superscript b, and those involving real monomer sites by superscript m, and Greek indices are used to label the number of a block along a chain. The element $\hat{c}_{\alpha\beta}(k)$ denotes the direct correlation between the average monomer site on block α on one polymer and the average monomer site on block β on another. $\hat{\omega}_{\alpha\beta}^{mm(n_b)}(k)$ is the intramolecular distribution between a monomer site on block α and a monomer site on block β of a given polymer, which has a number of blocks equal to n_b. The correlation between the block-center site on block α and a monomeric site on block β in the same chain is $\hat{\omega}_{\alpha\beta}^{bm(n_b)}(k)$. Analogous formalism is adopted for the intermolecular tcfs**;** for example, $\hat{h}_{\alpha,\beta}^{bm(n_b)}(k)$ is the correlation between the block-center site on block α and a monomeric site on block β on different chains. The intermolecular and intramolecular correlations that comprise these matrices are illustrated in Figures III.1 and III.2 respectively.

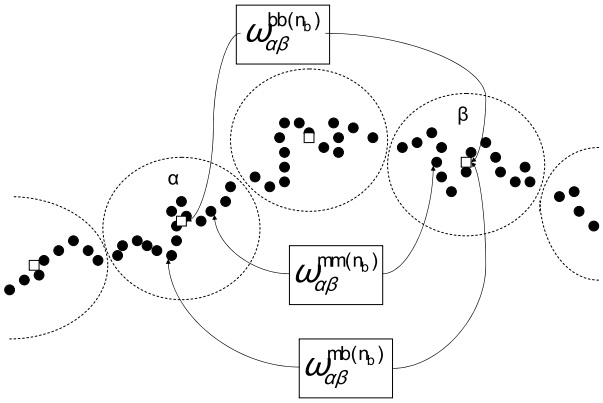

FIGURE III.1. Schematic illustration of the various block-averaged intramolecular distributions between sites on the same molecule. Filled circles represent monomers and the open circles with dashed borders represent the effective soft sphere each block on the chain is mapped onto, and the center-of-mass of each block is represented by an open box.

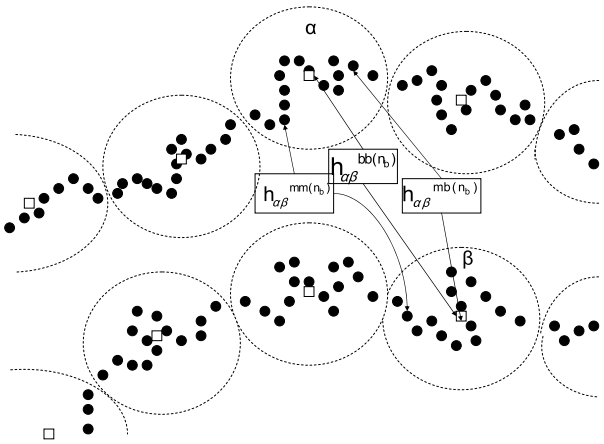

FIGURE III.2. Schematic illustration of the various block-averaged tcfs between sites on different molecules. Same notation as in Figure III.1.

All the sites inside one block are assumed to be equivalent. However, different blocks in the polymer remain distinguishable by their different distances from the end of the chain. To further clarify our treatment, we adopt for the block block matrix the following notation: $h^{bb(n_b)}$, where n_b is the number of blocks included in the polymer. In this way, the generic matrix element $h_{ij}^{bb(n_b)}$ expresses, for example, the position of block i inside a chain of n_b blocks, indicating if each block is central or terminal in the chain. This set of equations allows for the solution of the matrices $\hat{h}^{bb(n_b)}(k)$, $\hat{h}^{bm(n_b)}(k)$, and $\hat{h}^{mb(n_b)}(k)$, which provides the block course-grained description of the polymer melt, once the monomer level direct and intramolecular correlations are specified.

Assuming that all direct correlations are identical, since all monomers are identical, models of the system with different numbers of blocks can be related using only the intramolecular distributions. In particular, the soft colloid description can be recovered if the intramolecular distributions and any of the block-block tcfs are known. For example, using the block-level tcf between an end block on each polymer, the soft colloid (1-block) tcf is

$$\hat{h}^{bb(1)}(k) = \left[\frac{\hat{\omega}^{bm(1)}(k)}{\sum_{\gamma=1}^{n_b}\hat{\omega}_{\gamma}^{bm(n_b)}(k)}\right]^2 \hat{h}_{11}^{bb(n_b)}(k) \ . \tag{III.5}$$

The one-block description recovers the equations for the com derived in our previous papers,[38,39] given that $\hat{\omega}^{cm}(k) \equiv \hat{\omega}^{bm(1)}(k)$ and $\hat{h}^{cc}(k) \equiv \hat{h}^{bb(1)}(k)$ with the index c indicating the com of the polymer. Here $\hat{\omega}^{cm}(k)$ is the distribution of monomers about the polymer center-of-mass and $\hat{h}^{cc}(k)$ is the tcf between the coms of two different chains.

III.3. Intramolecular Structure. Monomer-monomer Distributions

It is a long-established result that on large length scales, positions of monomeric units within a long polymer molecule in a melt follow, to very good approximation, the same statistical distribution as the steps in an unbiased, memoryless random walk, which is Gaussian. This behavior is due to the presence of forces from enough surrounding molecules to nearly cancel the excluded volume forces that would tend to swell the distribution, producing an "unperturbed" chain distribution.[7] Furthermore, local semiflexibility and barrier crossing become irrelevant when correlation functions describing the overall static structure of long polymers in a melt are under study, e.g. distributions of all sites about another site or point.[56] Finally, course-grained models of polymer systems, which are under study here, describe properties measured on length scales much larger than the monomeric units. For these models, the detailed properties of the interactions between monomers and their local conformational transitions are irrelevant because local degrees of freedom are averaged out, and the continuum Gaussian distribution becomes well justified.[16]

At the monomer level, the intramolecular structure factors in the Gaussian approximation for whole chains[16] and diblocks[57] are well-known. Here we extend the model to a multi-block description of a homopolymer chain. In our notation, Greek indices are used to label the number of a block along a chain as before, and Latin indices are introduced to label the number of a site within that block, so that, for example, the i-th site on the α-th block is labeled by α_i. Consider two sites on different blocks, namely α_i and β_j, where the blocks α and β satisfy the condition $\beta \geq \alpha$, and denote the effective bond length as l_{eff}. The correlation between the two sites in a completely flexible polymer or in a semiflexible polymer on scale larger than the polymer persistence length, is given by

$$\hat{\omega}^{mm(n_b)}_{\alpha_i,\beta_j}(k) = e^{-y\frac{l^2_{eff}k^2}{6}} \ . \tag{III.6}$$

In the block-site notation used here, y is given as $y = |j - i|$ for sites on the same block, while for different blocks, where $\alpha < \beta$, as $y = N_b + (\beta - \alpha - 1)N_b + j - i$. This counts the chain steps from one block to an adjacent block with the first, i.e. $N_b + 1 - i$ is the distance from site i to the first segment on the next block.

The average pair correlation between a site on block α and one on block β, which is input to Equations (III.1)-(III.3), is then

$$\hat{\omega}_{\alpha\beta}^{mm(n_b)}(k) = \frac{1}{N_b} \sum_{i=1}^{N_b} \sum_{l=1}^{N_b} \hat{\omega}_{\alpha_i\beta_l}^{mm(n_b)}(k) \tag{III.7}$$

In the continuum limit, Equation (III.7) recovers for sites on the same block the equation for the undivided chain, but with the number of sites on the block in place of the number of sites on the chain. For sites on different blocks, however, a new form is obtained. Defining the radius of gyration of a block as $R_{gb}^2 = N_b l_{eff}^2/6$ and adopting a new index $\gamma = |\alpha - \beta|$ to identify the number of blocks separating two sites, Equation (III.7) reduces to

$$\hat{\omega}_{\alpha\beta}^{mm(n_b)}(k) = \hat{\omega}_{\gamma}^{mm(n_b)}(k) = \begin{cases} \frac{N_b}{(kR_{gb})^4}(k^2 R_{gb}^2 - 1 + e^{-k^2 R_{gb}^2}) & \text{if } \gamma = 0 \\ \frac{N_b}{(R_{gb}k)^4} e^{-(\gamma-1)R_{gb}^2 k^2} \left(1 - e^{-R_{gb}^2 k^2}\right)^2 & \text{if } \gamma \neq 0 \end{cases} \tag{III.8}$$

For the case $n_b = 2$ these reduce down to familiar results used in the context of diblock copolymers,[57] and for $n_b = 1$ it reduces down to the overall chain result.[16]

To test the validity of our treatment, Figure III.3 shows the comparison between Equations (III.8) and data from a United Atom Molecular Dynamics (UA-MD) simulation of polyethylene chains with a number of monomer per chain $N = 96$, at $T = 453\ K$ with density $\rho_c = 3.28 \times 10^{-2}\ \mathring{A}^{-3}$.[20] The value of the average block radius of gyration, used in the formulas above, is calculated from the radius of gyration of the chains measured in the UA-MD simulations, $R_g = 281.70\ \mathring{A}$, by applying the relation $R_{gb}^2 = R_g^2/n_b$.

Good agreement is observed for large lengthscales, i.e. small k, except for the same-block correlation in the $n_b = 4$ case, where the block size ($N_b = 24$) becomes so small that short-range and finite-chain effects start to dominate.

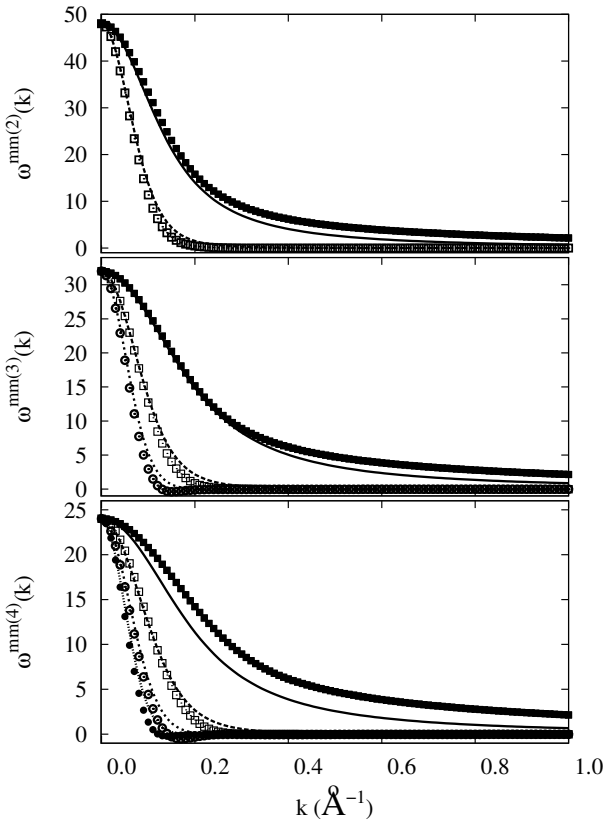

FIGURE III.3. Intramolecular site-site distributions for two, three, and four block models compared to polyethylene 96 simulation data. Predicted curves are shown for the possible block separations of the sites involved, with solid lines and filled boxes for sites on the same block, dashed lines and open boxes for sites on adjacent blocks, dotted lines and open circles for sites two blocks apart, and dotted-dashed lines and filled circles for sites three blocks apart. For the n_b=4 case, the block size ($N_b = 24$) becomes so small that short-range and finite-chain effects start to dominate.

III.3.1. Distributions of Monomers about Block Centers

Given the intramolecular pair correlation between site i on block β and the center of block α, $\hat{\omega}^{bm}_{\alpha\beta_i}(k)$, the site-averaged distribution function is defined as

$$\hat{\omega}^{bm}_{\alpha\beta}(k) = \sum_{i=1}^{N_b} \hat{\omega}^{bm}_{\alpha\beta_i}(k) \ . \tag{III.9}$$

In the case that the site and block center considered are on the same block, Equation (III.9) recovers the single-chain distribution of sites around their center-of-mass. The derivation of

an analytical form for this quantity is well-established,[56] and it is extended here to the case of different blocks, $\alpha \neq \beta$.

Let us denote the vectors from the center site of block α to sites i on block α and j on block β as $\vec{S}_{\alpha\alpha_i}$ and $\vec{S}_{\alpha\beta_j}$, respectively. The bond vector from the i-th site on the α-th block to the next site, $i+1$, on the chain is $\vec{r}_{\alpha_i}$. Assuming for convenience that $\beta > \alpha$, as the polymer chain is symmetric with respect to the center of the chain, we have that

$$\vec{S}_{\alpha\beta_j} = \frac{1}{N_b}\sum_{i=1}^{N_b}\sum_{k=i}^{N_b}\vec{r}_{\alpha_k} + \sum_{\gamma=\alpha+1}^{\beta-1}\sum_{k=1}^{N_b}\vec{r}_{\gamma_k} + \sum_{k=1}^{j-1}\vec{r}_{\beta_k} \ , \tag{III.10}$$

where the first term represents the contribution related to the com of the block α, the second term is the vector connecting block α to block β, and the third contribution gives the vector connecting to the site k on block β.

In the freely-jointed chain model, where the probability distribution of finding a certain displacement between a pair of monomers is an isotropic Gaussian, the probability distribution of a sum of monomer-monomer displacement vectors, such as the block com distribution, will also be Gaussian. As a consequence, the probability of finding a site at a given distance from the block center is fully determined by the second moment of the Gaussian distribution. Because in this model different bond vectors are totally uncorrelated, $\langle \vec{r}_{\alpha_i} \cdot \vec{r}_{\beta_j} \rangle = l_{eff}^2 \delta_{\alpha,\beta}\delta_{i,j}$, from Equation (III.10) the second moment is found to be

$$\langle S_{\alpha\beta_j}^2 \rangle = Q_{\alpha,\beta}^{(n_b)} + \frac{6}{N_b}(j-1)R_{gb}^2 \ , \tag{III.11}$$

where $Q_{\alpha,\beta}^{(n_b)} \equiv 2\left(R_{gb} + \frac{1}{2N_b}R_{gb}\right)^2 + \frac{3}{N_b}R_{gb}^2 + 6(\beta-\alpha-1)R_{gb}^2 - \frac{6}{N_b}R_{gb}^2 \approx 2R_{gb}^2 + 6(\beta-\alpha-1)R_{gb}^2$.

The probability distribution of finding a site j on block β a distance from the center of block α corresponding to wave vector k, $\hat{\omega}_{\alpha\beta_j}^{bm(n_b)}(k)$, is then given by

$$\hat{\omega}_{\alpha\beta_j}^{bm(n_b)}(k) = e^{-\frac{1}{6}\langle S_{\alpha\beta_j}^2 \rangle} \ , \tag{III.12}$$

which yields for the averaged quantity, with $\gamma = |\alpha - \beta|$ as before,

$$\hat{\omega}_{\alpha\beta}^{bm(n_b)}(k) = \hat{\omega}_{\gamma}^{bm(n_b)}(k) = \begin{cases} \left(\frac{N_b\sqrt{\pi}}{R_{gb}k}\right)\left(\mathrm{erf}\left[\frac{1}{2}kR_{gb}\right]\right)e^{-\frac{R_{gb}^2k^2}{12}} & \text{if } \gamma = 0 \\ \frac{N_b}{k^2R_g^2}e^{-\frac{1}{6}Q_\gamma^{(n_b)}k^2}\left(1 - e^{-R_{gb}^2k^2}\right) & \text{if } \gamma \neq 0\ . \end{cases} \tag{III.13}$$

In Figure III.4, Equations (III.13) are compared to data from the simulation of polyethylene melts with $N = 96$. Again good agreement is observed for small k except for the same-block correlation in the $n_b = 4$ with $N_b = 24$ case. In this case, blocks are too short for their internal structure to be well-approximated by this model, when correlations on the same block are calculated. However, monomer-block correlations follow the Gaussian statistics when the segment and the block-center are far apart on the same chain.

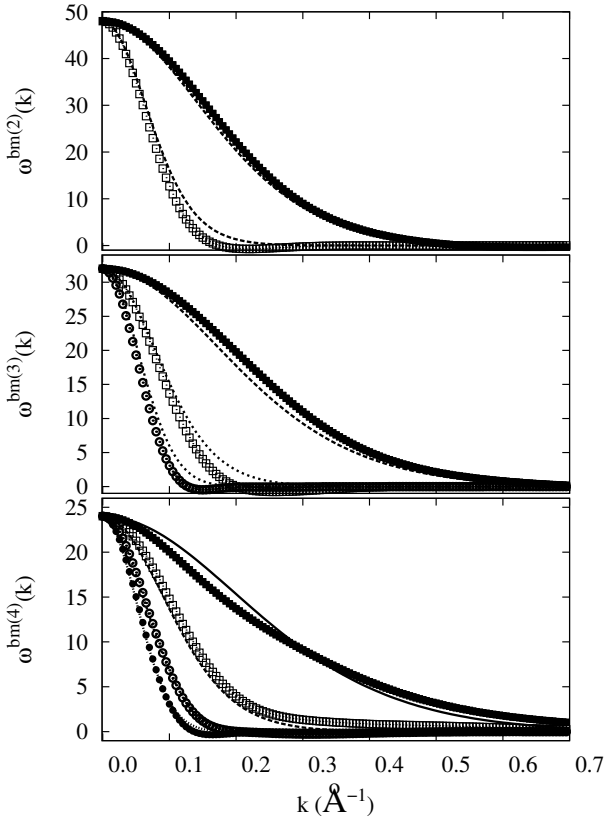

FIGURE III.4. Intramolecular block-center to site correlations for two, three, and four block models compared to simulation data of polyethylene with N=96. Same notation as in Figure III.3.

III.3.2. Pair Distributions between Block Centers

It is important to calculate the intramolecular distributions between block centers in a chain, even if these quantities do not directly appear in the definition of the intermolecular tcfs, because they provide the needed formal background to calculate intramolecular effective potentials between blocks to be used as an input to molecular dynamics simulations of the block-coarse-grained polymer liquid.

Distributions for the separation of the centers of mass of a pair of blocks can be found by following an analogous procedure. We denote the vector from the center of block α to the center of block β as $\vec{X}_{\alpha\beta}$. Because the distribution is Gaussian, only the second moment, $\langle \vec{X}^2_{\alpha\beta} \rangle$, is needed to calculate the block-center properties of the system. The relative positions of the two block centers can be written as linear combinations of Gaussian-distributed variables as $\vec{X}_{\alpha\beta} = \vec{S}_{\alpha\beta_j} - \vec{S}_{\beta\beta_j}$. Using this definition and the result from the previous section for $S_{\alpha\beta_j}$ together with the known expression for $\vec{S}_{\beta\beta_j}$[56]

$$\vec{S}_{\beta\beta_j} = \frac{1}{N_b} \sum_{i=1}^{N_b} \left(\Theta(j-i) \sum_{l=i}^{j-1} \vec{r}_{\beta l} - \Theta(i-j) \sum_{l=j}^{i-1} \vec{r}_{\beta l} \right) \ , \tag{III.14}$$

the second moment can be evaluated as

$$\langle \vec{X}^2_{\alpha\beta} \rangle = Q^{(n_b)}_{\alpha,\beta} + L + (j-1) l^2_{eff} \ , \tag{III.15}$$

with $L = R^2_{gb} \left(2(1 - \frac{5}{N_b})(1 - \frac{1}{N_b}) + 3(\frac{1}{N_b} + \frac{1}{N_b^2}) - \frac{12}{N_b^2} \right) \approx 2R^2_{gb}$, and $Q^{(n_b)}_{\alpha,\beta}$ as defined previously. The distribution between a pair of block-center sites with block separation $\gamma = |\beta - \alpha|$ is

$$\omega^{bb(n_b)}_{\alpha\beta}(k) = e^{-[\frac{1}{6}(Q^{(n_b)}_{\gamma} + L) + (\gamma - 1)R^2_{gb}]k^2} \ . \tag{III.16}$$

The comparison of Equation III.16 against simulations of polyethylene $N = 96$, displayed in Figure III.5, shows good agreement in the large-scale regime. In general, the predicted forms for the intramolecular distributions show good agreement with the simulation data for small k, with larger deviations at larger wave vectors. The deviations at large wave vector are likely due to anomalous local scale behavior, such as excluded volume effects due to finite monomer size, and short range stiffness effects, that are neglected in this model.

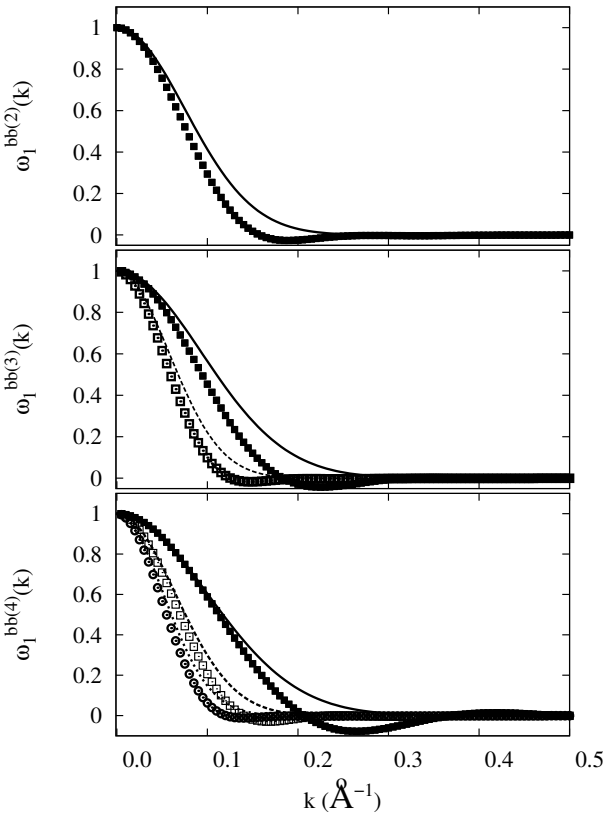

FIGURE III.5. Intramolecular correlations between block-centers for two, three, and four block models compared to simulation data of polyethylene N=96. Same notation than in Figure III.3.

Once the numerical inverse transform of the intramolecular forms is performed, and data are compared with simulations, our formalism is found to accurately predict the intramolecular structure at large length scales, while a small deviation is observed at short length scales, as shown for the site to block-center correlations in a diblock model in Figure III.6. Because in a course-grained description detailed features on short length scales are averaged out, small local-scale deviations are irrelevant and it is only necessary to accurately describe features on long length scales to obtain an accurate block-level description to be input to the OZ calculation of the intermolecular tcfs.

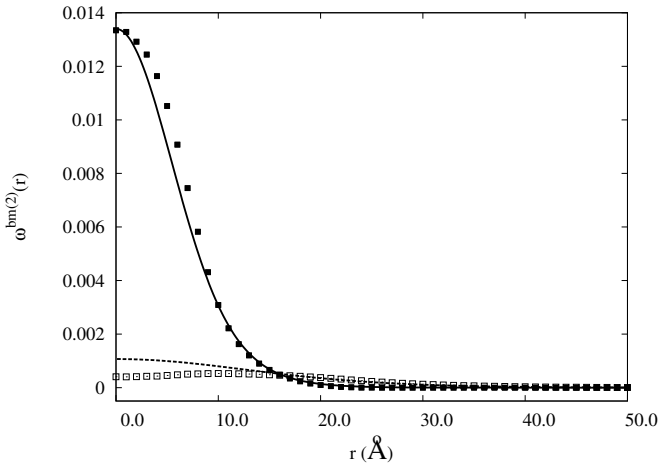

FIGURE III.6. Intramolecular correlations between sites and block-centers in real space for two block model: theoretical predictions (filled line) and simulations (filled squares) for sites and center on the same block; theoretical predictions (dashed line) and simulations (open squares) for sites and center on different blocks.

III.4. Solution of the Intermolecular Total Correlation Functions

The solution of the intermolecular tcfs must start from a series of approximations for the liquid structure at the monomer level. The block-block correlation functions can be expressed in terms of the overall monomer-monomer distribution, the block-monomer intramolecular distributions, and the direct correlation function. The latter is assumed to be identical for all monomers on all blocks, since all sites are chemically identical and interact by the same pair potentials.

For two blocks, correlations between any pair of blocks are indistinguishable:

$$\hat{h}^{bb2}_{\alpha\beta}(k) = \frac{\hat{c}(k)(\hat{\omega}^{bm(2)}_0(k) + \hat{\omega}^{bm(2)}_1(k))^2}{1 - N\rho_c\hat{\omega}^{mm(1)}(k)} \ , \tag{III.17}$$

where we used the fact that the overall chain intramolecular distribution $\hat{\omega}^{mm(1)}(k)$, can be written in terms of the block-level intramolecular distributions as:

$$\hat{\omega}^{mm(1)}(k) = \frac{1}{n_b}\sum_{\alpha=1}^{n_b}\sum_{\beta=1}^{n_b}\hat{\omega}^{mm(n_b)}_{\alpha\beta}(k) \ . \tag{III.18}$$

The notation in Equation (III.17) is the one defined for Equation (III.8).

For three blocks and higher, distinct block-block correlations occur due to the distinguishability of blocks depending on their distance from a chain end. Specifically for the three block case, there are three distinct total correlations, as there are two end-blocks and one interior block:

$$\hat{h}^{bb(3)}_{11}(k)=\hat{h}^{bb(3)}_{13}(k) = \hat{h}^{bb(3)}_{31}(k) = \hat{h}^{bb(3)}_{33}(k) \ , \tag{III.19}$$

$$=\frac{\hat{c}(k)(\hat{\omega}^{bm(3)}_0(k)+\hat{\omega}^{bm(3)}_1(k)+\hat{\omega}^{bm(3)}_1(k))^2}{1-\hat{c}(k)N\rho_c(\hat{\omega}^{bm(1)}(k))} \ ,$$

$$\hat{h}^{bb(3)}_{12}(k)=\hat{h}^{bb(3)}_{23}(k) = \hat{h}^{bb(3)}_{21}(k) = \hat{h}^{bb(3)}_{32}(k) \ , \tag{III.20}$$

$$=\frac{\hat{c}(k)(\hat{\omega}^{bm(3)}_0+2\omega^{bm(3)}_1)(\hat{\omega}^{bm(3)}_0(k)+\hat{\omega}^{bm(3)}_1(k)+\hat{\omega}^{bm(3)}_2(k))}{1-\hat{c}(k)N\rho_c(\hat{\omega}^{mm(1)}(k))} \ ,$$

and

$$\hat{h}^{bb(3)}_{22}(k)=\frac{\hat{c}(k)(\hat{\omega}^{bm(3)}_0(k)+2\omega^{bm(3)}_1(k))^2}{1-\hat{c}(k)N\rho_c(\hat{\omega}^{mm(1)}(k))} \ . \tag{III.21}$$

In general, for n_b blocks, the intermolecular tcf between blocks α and β, for $\alpha, \beta \leq (n_b + 1)/2$ can be written

$$\hat{h}_{\alpha\gamma}^{bb(n_b)}(k) = \left(\frac{N^2 \hat{c}(k) \hat{W}_{\alpha\gamma}^{bm(n_b)}(k)}{1 - \hat{c}(k) N \rho_c (\hat{\omega}^{mm(1)}(k))} \right) , \tag{III.22}$$

with

$$\hat{W}_{\alpha\gamma}^{bm(n_b)}(k) = \frac{1}{N^2} \prod_{\eta=\alpha,\gamma} \left[\hat{\omega}_0^{bm(n_b)}(k) + 2 \sum_{\epsilon=1}^{\Delta\eta_{e<}} \hat{\omega}_\epsilon^{bm(n_b)}(k) + \sum_{\epsilon=\Delta\eta_{e<}+1}^{\Delta\eta_{e>}} \hat{\omega}_\epsilon^{bm(n_b)}(k) \right] , \tag{III.23}$$

where the shorter and longer chain separations of site η from the end of the chain are given by

$$\Delta\eta_{e<} = \begin{cases} \eta - 1 & \text{if } \eta \leq \frac{n_b}{2} \\ n_b - \eta & \text{if } \eta \leq \frac{n_b}{2} \end{cases} \tag{III.24}$$

and

$$\Delta\eta_{e>} = \begin{cases} n_b - \eta & \text{if } \eta \leq \frac{n_b}{2} \\ \eta - 1 & \text{if } \eta \leq \frac{n_b}{2} \end{cases} \tag{III.25}$$

respectively.

In the systems of interest here, where Gaussian statistics hold, the size of the soft blocks that represent the polymer are much larger than the size of the monomers. Therefore, in order to make analytical progress, the assumption is made that the monomer direct correlation is of much much shorter range in space than the tcfs between soft blocks, and therefore that the monomer direct correlation in reciprocal space can be assumed to be constant ($\hat{c}^{mm}(k) \approx c_0$) over the range where the tcf between any pair of blocks, $\hat{h}_{\alpha\gamma}^{bb(n_b)}(k)$, differs significantly from 0. Note that this does not assume that the direct correlation parameter c_0 is given by the thread-PY model, just that the monomer direct correlation can be approximated as a constant in the coarse-grained function.

Defining the parameter $\Gamma_b = -N_b \rho_m c_0$, the general form of the block-block tcf in Fourier space can be rewritten

$$\hat{h}_{\alpha\gamma}^{bb(n_b)}(k) \quad = \quad -\frac{N_b n_b^2 \Gamma}{\rho_m}\left(\frac{\hat{W}_{\alpha\gamma}^{bb(n_b)}(k)}{1-n_b\Gamma(\hat{\Omega}^{mm(1)}(k))}\right) \ , \tag{III.26}$$

with $\hat{\Omega}^{mm}(k)) = \hat{\Omega}^{mm(1)}(k))/N$

III.4.1. Approximate Analytical Forms for the Block Total Correlation Functions of a Freely-jointed Chain

The tcf can be asymptotically expanded for large Γ_b as

$$\hat{h}_{\alpha\gamma}^{bb(n_b)}(k) = -\frac{N_b}{\rho_m}\left[\hat{X}_{0\alpha\gamma}^{bm(n_b)}(k) - \frac{1}{\Gamma_b}\hat{X}_{1\alpha\gamma}^{bm(n_b)}(k) + \frac{1}{\Gamma_b^2}\hat{X}_{2\alpha\gamma}^{bm(n_b)}(k) - ...\right] \tag{III.27}$$

where

$$\hat{X}_{i\alpha\gamma}^{bm(n_b)}(k) = \frac{2\pi^2 W_{\alpha\gamma}^{bm(n_b)}(k)}{n_b^{i-1}(\hat{\Omega}^{mm}(k))^{i+1}} \ , \tag{III.28}$$

and r is expressed in units of R_{gb}, and k in units of R_{gb}^{-1}.

The inverse transform can then be expressed in terms of the inverse transforms of the $\hat{X}_i^{bm(n_b)}$ functions as

$$h_{\alpha\gamma}^{bb(n_b)}(r) \approx -\frac{N_b}{2\pi^2\rho_m R_{gb}^3}\left[X_{0\alpha\gamma}^{bm(n_b)}(r) - \frac{1}{\Gamma_b}X_{1\alpha\gamma}^{bm(n_b)}(r) + \frac{1}{\Gamma_b^2}X_{2\alpha\gamma}^{bm(n_b)}(r) - ...\right] \ . \tag{III.29}$$

The form of the tcfs in real space can be further decomposed into terms arising from different intramolecular contributions. If the polymer chain is represented as one block, the centers-of mass tcf, which has no block-level intramolecular contributions, to leading order, is

$$h^{bb(1)}(r) = -\frac{N_b}{2\pi^2 R_{gb}^3\rho_m}\left[\left(\Phi_0^{(s,1)}(r)\right) + \frac{1}{\Gamma}\left(\Phi_0^{(s,2)}(r)\right)\right] \ , \tag{III.30}$$

with $\Gamma = N\rho_m|c_0|$ the expansion parameter for the soft sphere representation.

The tcf for two blocks can be written

$$h^{bb(2)}(r)=-\frac{N_b}{2\pi^2 R_{gb}^3\rho_m}\left[\left(\Phi_0^{(s,2)}(r)+2\Phi_0^{(c,2)}(r;1)+2\Phi_0^{(m,2)}(r;1,1)\right)\right. \tag{III.31}$$

$$\left.+\frac{1}{\Gamma_b}\left(\Phi_1^{(s,2)}(r)+2\Phi_1^{(c,2)}(r;1)+2\Phi_1^{(m,2)}(r;1,1)\right)\right] .$$

with η_γ defined as $\eta_\gamma = Q_\gamma/R_{gb}^2 \approx 6(\beta-\alpha)-4$

This can be continued for an arbitrary number of blocks by decomposing the X distributions defined above as

$$X_{i\alpha\gamma}^{bm(n_b)}(k)=\Phi_i^{(s,nb)}(r)+\sum_{\eta=\alpha,\gamma}\left[2\sum_{\epsilon=1}^{\Delta\eta_{e<}}\Phi_i^{(s,nb)}(r;\epsilon)+\sum_{\epsilon=\Delta\eta_{e<}+1}^{\Delta\eta_{e>}}\Phi_i^{(s,nb)}(r;\epsilon)\right]$$

$$+4\sum_{\epsilon=1}^{\Delta\alpha_{e<}}\sum_{\epsilon'=1}^{\Delta\gamma_{e<}}\Phi_i^{(s,nb)}(r;\epsilon,\epsilon')+2\sum_{\epsilon=\Delta\alpha_{e<}+1}^{\Delta\gamma_{e>}}\sum_{\epsilon'=1}^{\Delta\gamma_{e<}}\Phi_i^{(s,nb)}(r;\epsilon,\epsilon') \tag{III.32}$$

$$+2\sum_{\epsilon=1}^{\Delta\alpha_{e<}}\sum_{\epsilon'=\Delta\gamma_{e<}+1}^{\Delta\gamma_{e>}}\Phi_i^{(s,nb)}(r;\epsilon,\epsilon')+\sum_{\epsilon=\Delta\alpha_{e<}+1}^{\Delta\alpha_{e<}}\sum_{\epsilon'=\Delta\gamma_{e<}}^{\Delta\gamma_{e>}}\Phi_i^{(s,nb)}(r;\epsilon,\epsilon')$$

The Φ_j functions for the freely-jointed chain model are defined as

$$\Phi_j^{(s,n_b)}(r)\equiv\frac{\pi n_b^{j+1}}{r}\int_0^\infty k\sin(kr)\left(\frac{k^{4j+2}\mathrm{erf}^2[\frac{1}{2}k]e^{-\frac{1}{6}k^2}}{[2(n_bk^2-1+e^{-n_bk^2})]^{j+1}}\right)dk\ , \tag{III.33}$$

$$\Phi_j^{(c,n_b)}(r;\epsilon)\equiv\frac{n_b^{j+1}\pi^{\frac{1}{2}}}{2r}\int_0^\infty k\sin(kr)\left(\frac{k^{4j+1}\mathrm{erf}[\frac{1}{2}k]e^{-(\frac{1}{12}+\frac{1}{6}\mu_\epsilon)k^2}(1-e^{-k^2})}{[2(n_bk^2-1+e^{-n_bk^2})]^{j+1}}\right)dk\ , \tag{III.34}$$

and

$$\Phi_j^{(m,n_b)}(r;\epsilon;\epsilon')\equiv\frac{n_b^{j+1}}{r}\int_0^\infty q\sin(kr)\left(\frac{k^{4j}e^{-\frac{1}{6}(\mu_\epsilon+\mu_{\epsilon'})k^2}(1-e^{-k^2})^2}{[2(n_bk^2-1+e^{-n_bk^2})]^{j+1}}\right)dk\ . \tag{III.35}$$

These functions represent respectively the contributions to the correlation between a given pair of blocks on two chains propagating through only directly through the two blocks involved, propagating directly through one involved block on one chain and indirectly through another block on the other chain, and indirectly through other blocks on both of the chains.

Note that shape of the the Φ functions defined here depend only on the number of blocks, n_b. Because the dependence on all the system parameters (ρ, N_b, and R_{gb}) is expressed in the analytical prefactors, once the number of blocks n_b is defined, our formalism can be directly applied to any polymer melt of interest, including more accurate descriptions of semiflexibility, polymer architecture, and possibly even good solvent conditions, without the need to re-derive approximations.

The most important physical consequence of this series expansion form is that the dependence on Γ_b, and therefore on the direct correlation between monomers, vanishes from the leading order term. This means that to leading order the tcfs between large blocks in high density melts do not depend at all on monomer interactions. In the large-block, high density limit the tcf for a given n_b approaches a universal form with a prefactor and width scaling that depending only on N_b, ρ_m, and R_{gb},

$$h_{\alpha\gamma}^{bb(n_b)}(r) \rightarrow -\frac{N_b}{2\pi^2\rho_m R_{gb}^3} X_{0\alpha\gamma}^{bm(n_b)}(r) \ . \tag{III.36}$$

For a system of finite but large blocks and high density, all dependence on the monomer direct correlation, and therefore the details of the monomer interactions, is contained in the very small correction. This result has major implications for the reliability of schemes to construct effective pair potentials from structural correlations, as will be discussed in chapters V and VI.

A useful first approximation for the value of the direct correlation parameter is given by the thread model, where, as was discussed in chapter III, the form of the direct correlation is taken to be $c^{mm}(r) = c_0\delta(r)$, and an analytical solution for hard-sphere sites given by $c_0 = \frac{1}{N\rho_m}\left(\frac{\xi_c}{\xi_\rho} - 1\right)$ where the density screening length is $\xi_\rho = \left(\frac{\sqrt{2}}{R_g} + \frac{1}{3}\pi\rho l_{eff}^3\right)^{-1}$, the correlation hole length scale is $\xi_c = R_g/\sqrt{2}$, with the statistical segment length $l_{eff} = R_g/\sqrt{N}$.[44] Therefore, it gives in the limit of long chains $\lim_{N\rightarrow\infty} c_0 = -2\pi^2\rho l_{eff}^6$.

Figures III.7 and III.8 show that this "large block" approximation works well for any case under study. Reasonable agreement is seen even for three blocks, where $N_b = 32$, and chains start

to be too short for random walk statistics to be replaced by the Gaussian limiting forms assumed to derive these results. The result of keeping the second order term in $1/N_b$ is also shown for the three-block case to demonstrate that the deviations from the exact result, observed at small separation for the first order form, are overcome when the second order correction is included. This shows that deviations of our freely-jointed chain solution from the exact numerical result are due solely to the relatively small number of sites on each block ($N_b = 32$). Additionally, a comparison of the second order form for the two and four block models with a simulation of longer chains ($N = 224$) by Mavrantzas[22,23] is shown in figures III.9 and III.10 respectively.

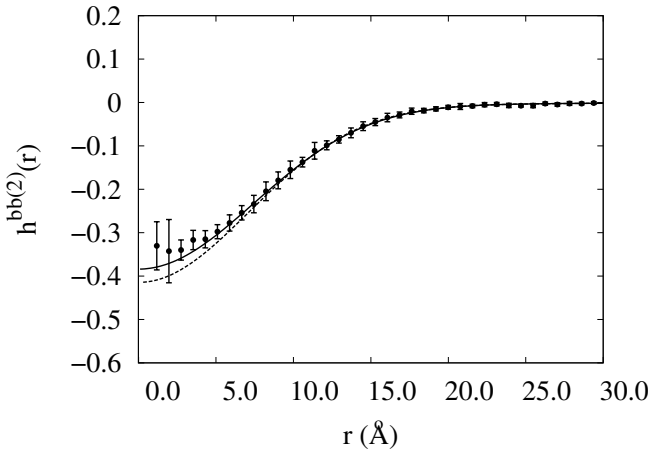

FIGURE III.7. Large block approximation form (full line) for the intermolecular block-center to block-center distribution for the 2-block model compared to polyethylene 96 simulations (symbols) and numerical inverse transform (dashed line).

III.4.2. Analytical Total Correlation Functions in the Gaussian Approximation

While the approximate solution for the coarse-grained liquid of freely-jointed chains gives predictions in quantitative agreement with exact solutions of the integral, and simulations, in this section we want to compare the quality of agreement observed in this model against our traditional Gaussian model, which we have adopted in our previous papers.[38,39,46] The Gaussian model provides an analytical formalism for the tcfs and effective potentials, in quantitative agreement with simulations, when polymer chains are represented as soft colloidal particles or soft-colloidal dumb-bells.

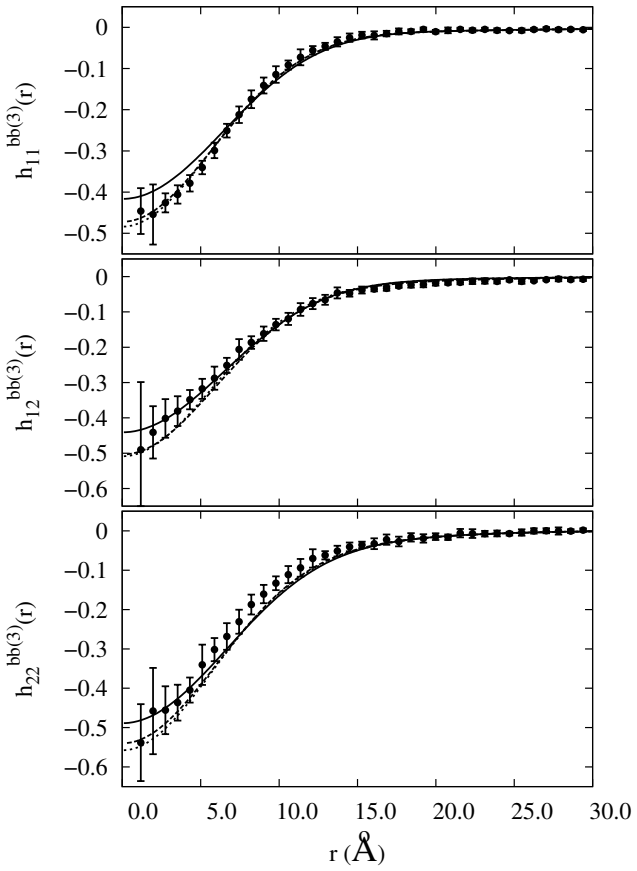

FIGURE III.8. Large-block approximation forms to leading order (full line), and second order (dotted line) form for the intermolecular block-center to block-center distribution for the 3-block model compared to polyethylene 96 simulations (symbols) and numerical inverse transform (dashed line).

Extending the traditional Gaussian approach for diblock copolymer course-graining,[46] we assume that all intramolecular block-monomer distributions are Gaussian. The total correlations can then be written in terms of a simple, analytical functional form, derived in the original coarse-graining analysis of polymer melts.

The Gaussian approximation, for a chain divided into n_b blocks, takes the form

$$\hat{\omega}_{\gamma}^{bm}(k) \quad \approx \quad N_b e^{-Y_{n_b,\gamma} k^2} \ , \tag{III.37}$$

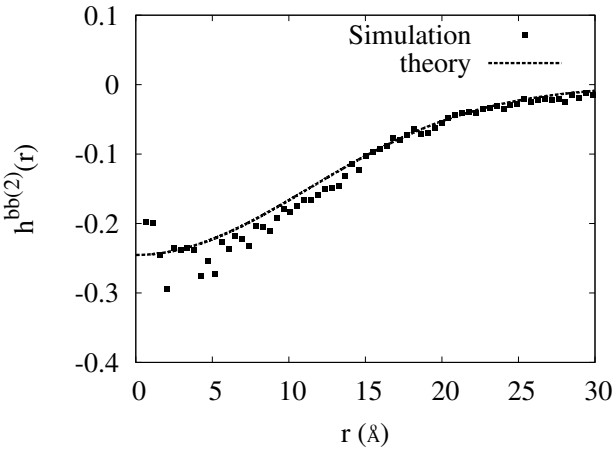

FIGURE III.9. Large-block approximation forms to second order (dotted line) form for the intermolecular block-center to block-center distribution for the 2-block model compared to polyethylene 224 simulations (symbols).

with $Y_{n_b,\gamma} = \frac{R_{n_b,\gamma}}{6}$. Here $R_{n_b,\gamma}$ is the calculated average separation of sites between a block center and sites on a block, which is γ blocks away. Using this together with the standard Padé approximation to the Debye form for the overall monomer-monomer intramolecular distribution, $\hat{\omega}^{mm(1)}(k) \approx N/(1+\xi_c^2 k^2)$, and the definition of the density screening length (in the thread limit) $\xi_\rho = \xi_c/\sqrt{(1-\rho_c c_0)}$, the total correlations can be written in terms of the form:[38,39,46]

$$\hat{T}_0(k;Y) = \left(\frac{N_b^2 c_0 \xi_\rho^2}{\xi_c^2}\right) \frac{(1+\xi_c^2 k^2) e^{-2Yk^2}}{1+\xi_\rho^2 k^2} \ . \tag{III.38}$$

The inverse transform of Equation (III.38) is given by

$$T_0(r;Y) = \frac{1}{8\pi^{\frac{3}{2}}} \left(\frac{\xi_c^2}{\xi_\rho^2}\right) e^{-\frac{r^2}{4Y}} + \frac{1}{8\pi\xi_\rho^2}\left(\frac{\xi_c^2}{\xi_\rho^2} - 1\right) \tag{III.39}$$

$$\times \ \frac{e^{\frac{Y}{\xi_\rho^2}}}{r}\left(e^{\frac{r}{\xi_\rho}} \operatorname{erfc}\left[\frac{\sqrt{Y}}{\xi_\rho} + \frac{r}{2\sqrt{Y}}\right] - e^{\frac{-r}{\xi_\rho}} \operatorname{erfc}\left[\frac{\sqrt{Y}}{\xi_\rho} - \frac{r}{2\sqrt{Y}}\right]\right) \ . \tag{III.40}$$

For two blocks the total correlation functions are simply given by

$$h^{bb(2)}(r) = \frac{N_2^2 c_0 \xi_\rho^2}{\xi_c^2}(T_0(r;2Y_{2,0}) + T_0(r;2Y_{2,1}) + 2T_0(r;Y_{2,0}+Y_{2,1})) \ , \tag{III.41}$$

where $h_{11}^{bb(2)} = h_{12}^{bb(2)} = h_{21}^{bb(2)} = h_{22}^{bb(2)}$. For three blocks the three distinct correlations become

$$h_{11}^{bb(3)} = \frac{N_3^2 c_0 \xi_\rho^2}{\xi_c^2}(T_0(r;2Y_{3,0}) + T_0(r;2Y_{3,1}) + T_0(r;2Y_{3,2}) + 2T_0(r;Y_{3,0}+Y_{3,1}) \tag{III.42}$$

$$+2T_0(r;Y_{3,0}+Y_{3,2}) + 2T_0(r;Y_{3,1}+Y_{3,2}))\ ,$$

$$h_{12}^{bb(3)} = \frac{N_3^2 c_0 \xi_\rho^2}{\xi_c^2}(T_0(r;2Y_{3,0}) + 2T_0(r;2Y_{3,1}) + 3T_0(r;Y_{3,0}+Y_{3,1}) \tag{III.43}$$

$$+T_0(r;Y_{3,0}+Y_{3,2}) + 2T_0(r;Y_{3,1}+Y_{3,2}))\ ,$$

$$h_{22}^{bb(3)} = \frac{N_3^2 c_0 \xi_\rho^2}{\xi_c^2}(T_0(r;2Y_{3,0}) + 4T_0(r;2Y_{3,1}) + 4T_0(r;Y_{3,0}+Y_{3,1}))\ . \tag{III.44}$$

Similar forms can be written for higher numbers of blocks, and they are not reported here. Using the definition of $c_0 = \left(1 - \xi_c^2/\xi_\rho^2\right)/N\rho_m$ and $\xi_\rho' \equiv 3/(\pi\rho_c l_{eff}^2) = N/(2\pi\rho_c R_g^2)$ to eliminate the density, we recover for the two blocks the form derived previously in the context of diblock copolymers.[46] When compared with simulation data, the Gaussian formalism shows good, but less quantitative, agreement than the freely jointed chain approximation, which is more precise.

Figures III.11 and III.12 show the Gaussian approximation compared to exact results and polyethylene simulation data for the two and three block models. The Gaussian approximation shows increasing deviation from the numerically-derived form and from simulation data for three blocks. This suggests the need for a more accurate approximation, such as the proposed freely jointed chain formalism, when chains containing more than two blocks are under study.

In our previous papers on homopolymer and diblock copolymer course-graining, the intramolecular distributions of monomers about fictitious center sites was successfully approximated using the Gaussian function. The Gaussian approximation works well for these

models because it is a very good description of the distribution at small wave vectors (large length scales), which dominate the total correlations for large chains with a small number of blocks. However, its accuracy decreases on larger wave vectors as more blocks are added to each chain: our study suggests that in this case the total correlations between block centers come to depend more and more on the intermediate wave vector values of the intramolecular distribution, causing the total correlation to suffer increasing contribution on short length scales from the region of the Gaussian distribution considered unreliable, i.e. large k regime.

To demonstrate this effect, consider the functional form in momentum space of the contribution to the lowest order asymptotic expansion form of the tcf $\hat{h}^{bb(n_b)}(k)$ given in Equation (III.27) that arises from correlations between real monomers that are on the same block as the block center site involved for both chains, $\hat{F}_{bb}(k) \propto \frac{(\omega_0^{bm(n_b)})^2(k)}{\omega^{mm}(k)}$. Using the continuum freely-jointed chain correlations and explicitly writing the chain radius of gyration in terms of the block radius of gyration, the result for various numbers of blocks is given by

$$\hat{F}^{bb}(k) \equiv \frac{n_b \pi (R_{gb}k)^2 \mathrm{erf}^2[\frac{1}{2}R_{gb}k]}{2(n_b(R_{gb}k)^2 - 1 + \exp[-n_b(R_{gb}k)^2])} \ . \tag{III.45}$$

Figure III.13 shows this function vs wave vector for chains with increasing numbers of blocks with the length of each block fixed. As the number of blocks is increased, the maximum of the function moves from $k = 0$ to a value just below $k = 2/R_{gb}$. The contribution of this term to the total correlation in real space therefore is increasingly composed of values at wave vectors away from $k = 0$. Other terms arising from contributions to the tcfs due to sites on different blocks show a similar onset of intermediate wave vector dominance that starts at higher numbers of blocks, leading to the overall result for the total block-block tcf to become increasingly sensitive to the intermediate-wave vector values of the distribution of sites about the block center. For this reason approximations formulated for accuracy at very small wave vectors such as the Gaussian approximation (for length scales long compared to the block radius) should be expected to yield increasing error for larger numbers of blocks.

III.5. Block-averaged Description and $n_b \to \infty$ Infinite Chain Limit

III.5.1. Block-Averaged Total Correlation In Fourier Space

For larger numbers of blocks, n_b, the chains become dominated by blocks far from the end of the chain. In this regime, it is useful to formulate a simpler block-averaged description that captures the structural correlations of blocks far from the end well.

The average tcf between blocks on the chain, is given by

$$\hat{h}^{bb(n_b)}(k) = \frac{1}{n_b^2}\sum_{\alpha=1}^{n_b}\sum_{\gamma=1}^{n_b} h_{\alpha\gamma}^{bb(n_b)}(k) = \frac{N_b n_b^2 \Gamma_b}{\rho_m}\frac{(\hat{\Omega^{bm}}(k))^2}{1+n_b\Gamma_b\Omega^{mm}(k)} \tag{III.46}$$

where the unit normalized block-averaged intramolecular distribution of monomers about block centers in reciprocal space is given by

$$\hat{\Omega}^{bm}(k) = \sum_{\alpha=1}^{n_b}\sum_{\gamma=1}^{n_b}\hat{B}_{\alpha,\beta}(k) \tag{III.47}$$

The notation $\hat{h}^{bb(n_b)}(k)$ and $h^{bb(n_b)}(r)$ without subscripts is used throughout the remainder of the work to denote the block-averaged tcfs. Using the general result for $W_{\alpha,\beta}(k)$ given by Equation III.23, the sum can be evaluated to give

$$\hat{\Omega}^{bm}(k) = \frac{1}{n_b}\left[\frac{\sqrt{\pi}}{k}\mathrm{erf}(\frac{k}{2})e^{-\frac{k^2}{12}} - 2\left(\frac{e^{-n_b k^2} - n_b e^{-k^2} + n_b - 1}{n_b(e^{-k^2}-1)^2}\right)e^{-k^2/3}\right] . \tag{III.48}$$

III.5.2. Block-Averaged Total Correlation in Real Space

$$h^{bb}(r) = -\frac{N_b}{2\pi^2\rho_m R_{gb}^3}\left[X_0(r;n_b) + \frac{1}{\Gamma_b}X_1(r;n_b)\right] , \tag{III.49}$$

where

$$X_0(r;n_b) = \frac{1}{r}\int_0^\infty sin(kr)\frac{(\hat{\Omega}^{bm}(k))^2}{\hat{\Omega}^{mm}(k)} \tag{III.50}$$

and

$$X_1(r;n_b) = \frac{1}{n_b r}\int_0^\infty sin(kr)\frac{(\hat{\Omega}^{bm}(k))^2}{(\hat{\Omega}^{mm}(k))^2}\ . \tag{III.51}$$

The block-block tcfs are characterized by a primary block correlation hole (region of depletion) of the range of the block radius of gyration, and a secondary, shallower molecular correlation hole scaling with the size of the molecular radius of gyration, R_g, which reflects the average depletion in the space surrounding a block due to the presence of the other blocks on the chain. The function $X_0(r;n_b)$ is the dominant contribution to both regions, while the $X_1(r;n_b)$ correction essentially contributes only a small correction to the block correlation hole.

As $n_b \to \infty$, the primary peak of $\hat{X}_0(k)$ at small k narrows in width proportional to $\sqrt{n_b}$, and for approximately $n_b \geq 5$ it is well approximated at small k by its limiting form, which is the familiar DeBye function, which can be well approximated by a rational interpolating function for most purposes as

$$\hat{X}_0(k) \to \frac{2}{n_b^2 k^4}\left(n_b k^2 - 1 + e^{-n_b k^2}\right) \approx \frac{1}{1 + n_b k^2/2}\ . \tag{III.52}$$

This form then gives the function $X_0(r;n_b)$ at large r to be

$$X_0(r;n_b) \approx (\frac{\pi}{n_b r})Exp\left(-\sqrt{\frac{2}{n_b}}r\right)\ , \tag{III.53}$$

and therefore for the tcf for $r >> 1$

$$h^{bb}(r) \approx -(\frac{N_b}{2\pi n_b \rho_m R_{gb}^3 r})Exp\left(-\sqrt{\frac{2}{n_b}}r\right)\ . \tag{III.54}$$

Calculated example block-averaged tcf curves for are shown in Figure III.14.

III.6. Conclusion

We have presented a model based in first-principles, microscopic liquid state theory that provides a complete description of structure on the length scales of long sub-blocks on long homopolymer chains in a melt. The model gives analytic forms, which allow it to be applied directly to a wide variety of different polymer types and thermodynamic conditions. It is capable of describing effects within a polymer that occur on length scales which are smaller than the

size of the polymer but much larger than the size of the monomers it is comprised of, while still providing a dramatic degree of simplification over full monomer-level models.

This fills a gap between the drastic molecular course-graining model previously outlined, where a polymer chain was represented as a soft colloidal particle, and monomer level descriptions. The single soft colloid representation has the disadvantage that it cannot be used to describe processes that occur on shorter length scales than the molecular size, while many interesting phenomena in polymer physics occur on the sub-molecular length scale, i.e. entanglement constraints. Our coarse-graining model overcomes the limitations of the monomer-level models, for which the needed computational power makes simulating large systems impossible, while still allowing for relevant degrees of freedom within the each molecule to be retained.

The advantage of our multiblock model with respect to other models present in the literature is that our formalism contains an explicit dependence on the molecular and thermodynamic parameters of the system. For this reason our effective potential is readily applicable to different polymeric systems. The derived effective potentials will be used in future work to map a homopolymer melt onto a fluid of short coarse-grained interacting chains. This should allow for the extension of the range in time and length scales where polymer liquids and composites can be simulated, further into the regime of long chains, where multi-chain entanglement significantly effects the dynamics of the system.

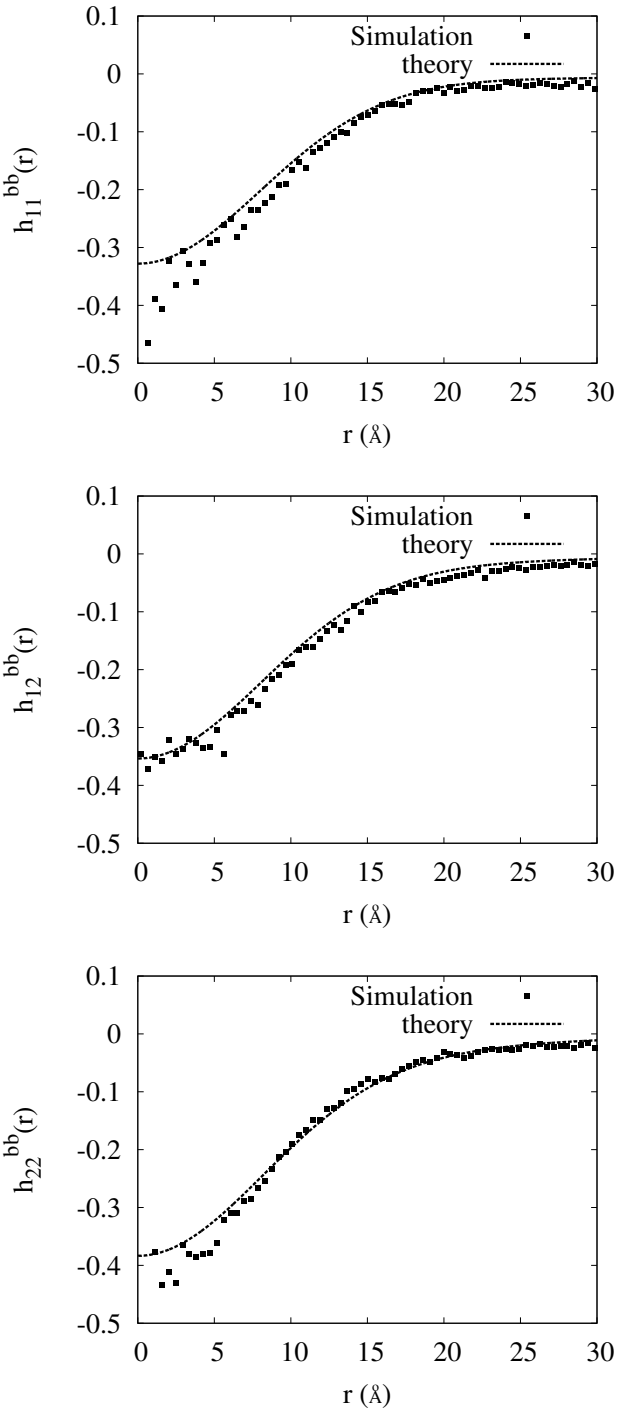

FIGURE III.10. Large-block approximation forms to second order (dotted line) form for the intermolecular block-center to block-center distribution for the 4-block model compared to polyethylene 224 simulations (symbols). From top to bottom: end block with end block, end block with interior block, and interior block with interior block

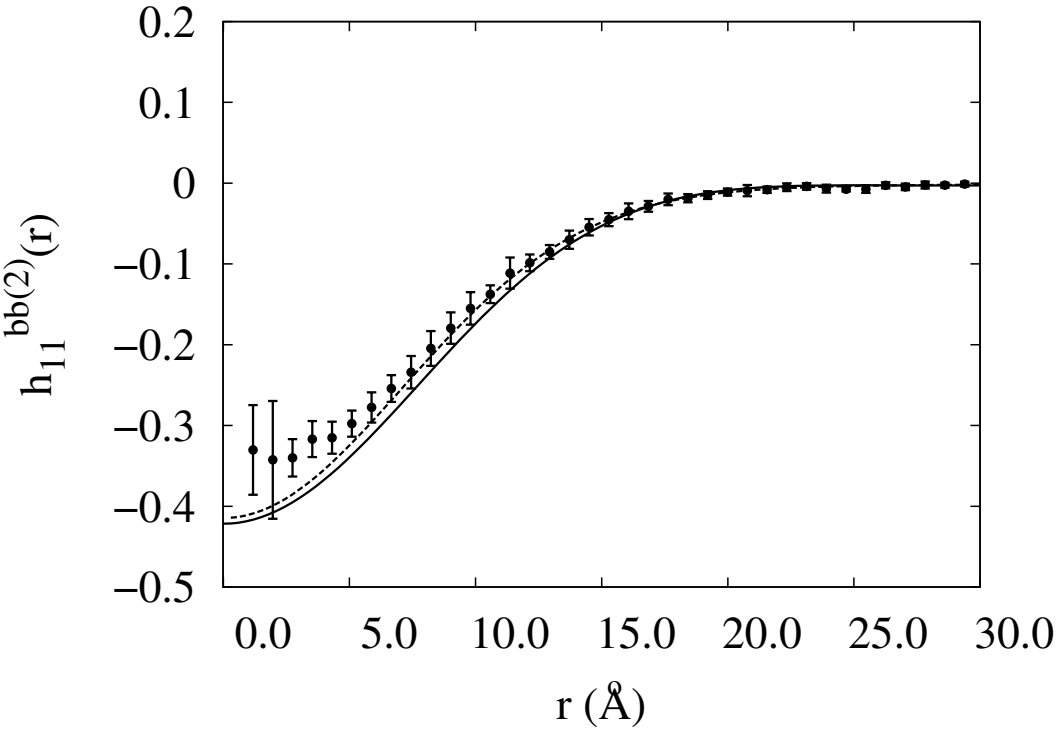

FIGURE III.11. Gaussian approximation for intermolecular block-center to block-center distribution for the 2-block model (full line) compared to the polyethylene 96 simulations (symbols) and numerical transform of exact derived form (dashed line).

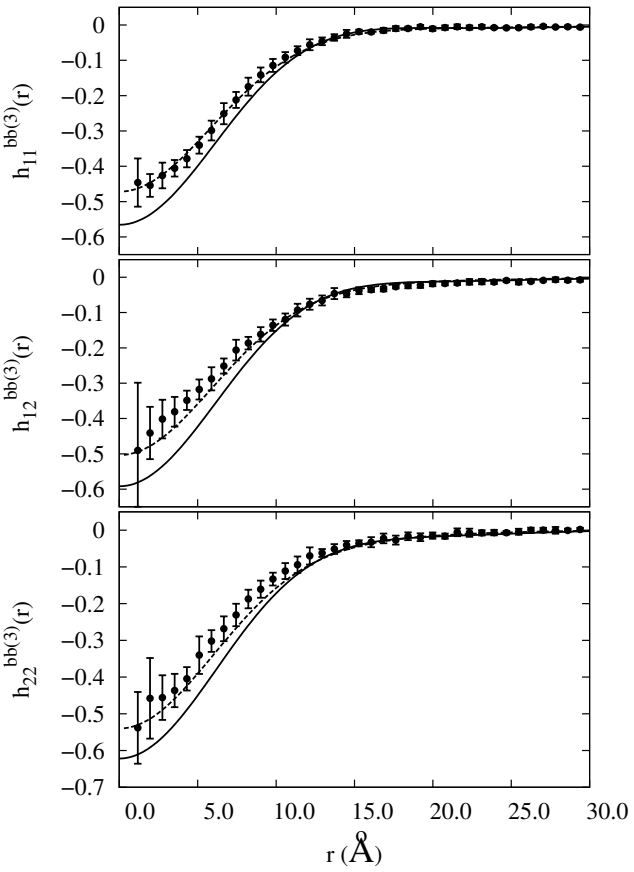

FIGURE III.12. Gaussian approximation for intermolecular block-center to block-center distribution for the 3-block model compared to the polyethylene 96 similuations and numerical transform of exact derived form.

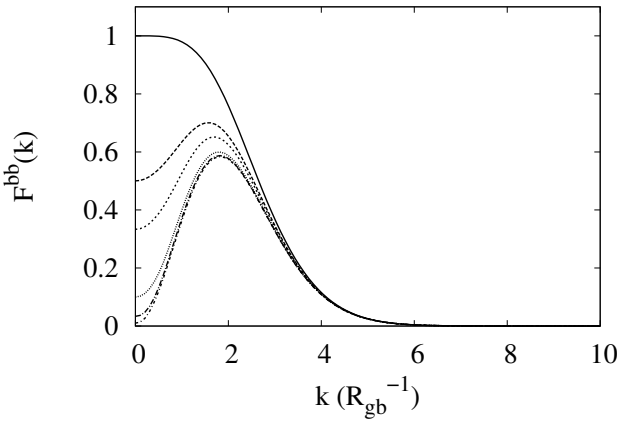

FIGURE III.13. Functional form of the $F^{bb}(k)$ contribution to the tcf for fixed block length for chains comprised of several numbers of blocks shows that the function is increasingly dominated by a peak at nonzero wave vector. Similar behavior is observed for other terms that contribute to the tcfs for large numbers of blocks. Shown are 1 (solid line) 2 (long-dashed line), 3 (short-dashed line), 10 (dotted line), 30 (long-dash-dotted line), and 100 (short-dashed-dotted line) blocks

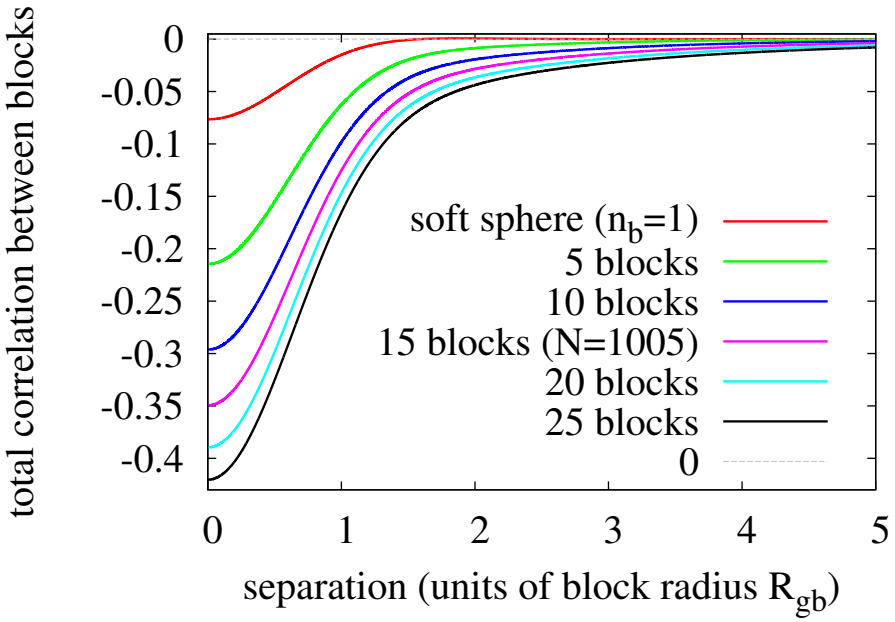

FIGURE III.14. Example curves for the block-level tcfs for various representations of the same system representing a Polyethylene melt with N=1000 with (from top to bottom) n_b=1, n_b=5, n_b=10, n_b=15 (N=1005), n_b=20, andn_b=25, plotted against the block radius of gyration (R_gb) for their respective models. All models feature a primary correlation (block) hole of range a small number of block radii, R_{gb}. Higher multiblock models exhibit a secondary (molecular) correlation hole persisting to increasing ranges beyond this ($r>>2R_{gb}$)

CHAPTER IV

EFFECTIVE POTENTIALS AND FORCES

This chapter is adapted from the short letter "Thermodynamic Consistency in Variable-Level Coarse Graining of Polymeric Liquids" which appeared in 2012 in the journal Physical Review Letters[58] and the longer and more detailed article "Theoretical Characterization of Effective Pair Potentials that Map the Structure and Thermodynamics of Polymer Melts onto Soft Colloidal Liquids" which is undergoing final revisions and will be submitted for publication soon. Both papers are co-authored with Jay McCarty, Ivan Lyubimov and Marina Guenza. To the material used in this chapter, all three co-authors have contributed useful discussions and help in formulating and editing the manuscript, and in particular Marina Guenza has provided insights used in the interpretation of the scaling of the effective potentials at long range.

In this chapter, the structural correlations derived in chapter IV for the multiblock model are used to derive and characterize effective interaction potentials. The mapping is based on the block-averaged tcf forms derived at the end of the previous chapter. To do this an effective direct correlation acting between the coarse-grained cm sites is first defined by a PRISM generalized Ornstein-Zernike equation, and its form is characterized. The effective potential and force curves are then obtained using standard liquid state closure approximations. The forms obtained indicate that an effective long-ranged "tail" develops at high levels of coarse-graining, which represents the average effects of interactions involving three or more mutually geometrically interpenetrating polymers. The infinite chain limit, $N \to \infty$ is considered in detail theoretically for two representations of interest: the limit where whole chains of increasing length are represented by a single cm degree of freedom, and the limit where each chain is represented by increasing numbers of fixed-length subchains ($n_b \to \infty$).

IV.1. Mapping onto Interacting Soft-colloid Chains

Starting from the block-averaged tcfs given in Fourier space in Equation III.46, the block-chain averaged direct correlation between soft blobs on each soft colloid chain is defined by the PRISM generalized Ornstein-Zernike equation for a chain of length n_b with block-averaged tcf $\hat{h}^{bb}(k)$,

$$h^{bb}(k) = n_b \hat{\Omega}^{bb}(k) c^{bb}(k) \left[n_b \hat{\Omega}^{bb}(k) + \rho_b h^{bb} \right] \ , \tag{IV.1}$$

where the block-averaged intramolecular distribution between block centers, obtained by taking the average of Equation III.16 over all block combinations, is given by

$$\hat{\Omega}^{bb}(k) = \frac{1}{n_b} + 2 \left[\frac{e^{-k^2} - n_b e^{-k^2} + (n_b - 1)}{n_b^2 (e^{-k^2} - 1)^2} \right] e^{-2k^2/3} \ , \tag{IV.2}$$

and ρ_b is the number density of blocks, ρ_m / n_b.

The direct correlation in Fourier space with wave vectors expressed in units of R_{gb}^{-1} is therefore

$$c^{bb}(k) = \frac{c_0 N_b^2 (\hat{Y}^{bm(n_b)})^2}{1 + \Gamma_b \hat{Z}^{bm(n_b)}(k)} \ . \tag{IV.3}$$

where the notation

$$\hat{Y}^{bm(n_b)}(k) = \hat{\Omega}^{bm}(k) / \hat{\Omega}^{bb}(k) \ , \tag{IV.4}$$

and

$$\hat{Z}^{bm(n_b)}(k) = n_b \left[\hat{\Omega}^{mm}(k) - (\hat{\Omega}^{bm}(k))^2 / \hat{\Omega}^{bb}(k) \right] \ . \tag{IV.5}$$

with $\hat{\Omega}^{bm}(k)$ as given in Equation III.47 and $\Omega^{mm}(k) = 2(n_b k^2 - 1 + e^{-n_b k^2})/(n_b^2 k^4)$ (with k in units of R_{gb}^{-1}) has been introduced for the two relevant combinations of intramolecular distributions. The first characterizes respectively the ratio of the distribution of monomers about block centers to the distribution of blocks about other blocks and the second the difference between the distribution of monomers about other monomers with a combination block-monomer and block-block distributions.

IV.1.1. Limits of Interest

The systems of interest in our study are in the limit of long chains at high densities, for which direct atomistic-level simulations are the most difficult to equilibrate and very time consuming, and coarse-graining is most relevant and useful. With this in mind we consider

two limiting regimes of this theory. The first case is a high-density melt where each polymer is represented by a single soft sphere in the limit that the chain length is large ($n_b = 1$, $N_b = N =\rightarrow \infty$). In this description no information about intramolecular processes is preserved in the coarse-grained representation. In practice polymer chains with $N > 30$ are well represented by this analytical soft-sphere model. For chain with $N < 30$ the numerical solution of the OZ coarse-graining equation becomes necessary.[38,39]

The second limit considered is that where the length of the constituent polymer chains is taken to infinity by adding more blocks of fixed size to each chain ($N_b > 30$ constant, $n_b \rightarrow \infty$). In this description, information about the intramolecular structure of the chain is retained on length scales larger than the block size. In practice the $n_b \rightarrow \infty$ limit is reached quickly for the effective direct correlations, requiring only about $n_b \geq 5$ for the infinite block chain result to be a very good approximation for a multiblock model with the same physical parameters and number of monomers per block, N_b. The functional form of the structure also approaches this limit relatively fast, although the "shielding" effects of surrounding blocks on the same chain require slightly larger n_b to reach a limiting form. Given that coarse-grained representations are likely to be of most interest to systems where the use of United Atom (UA) molecular dynamics simulations becomes impractical ($N >> 100$), and in order to include relevant sub-molecular modes would likely need $30 < N_b < 100$, this limit should be applicable to most systems of interest.

The tcfs and numerically integrated potentials in the *soft sphere limit* have been treated extensively in our previous papers.[38,39,47] This limit is recovered from the general multiblock model when $n_b = 1$. Here the effective potentials are characterized analytically in detail for the first time. The total and direct correlations, using the notation adopted in our most recent papers, are given by

$$\hat{h}^{cc}(k) = -\frac{N\Gamma}{\rho_c}\frac{(\hat{\Omega}^{cm}(k))^2}{1+\Gamma\Omega^{mm}(k)} \ , \tag{IV.6}$$

where $\rho_c = \rho_m/N$ is the polymer density with ρ_m the monomer density, $\Gamma = -N\rho_m c_0$, and c_0 the $k = 0$ value of the monomer-level PRISM direct correlation function in reduced units of R_g^{-1}. To connect to previous work, note that $\Gamma = \xi_c^2/\xi_\rho^2 - 1$ with the definitions $\sigma\xi_\rho^{-1} =$

$\sqrt{12(N^{-1}-\rho_m c_0)}$ for the density fluctuation correlation length, and $\xi_c = R_g/\sqrt{2}$ for the radius-of-gyration correlation length. The effective segment size σ satisfies the relation $R_g = \sigma\sqrt{N}/\sqrt{6}$.

The intramolecular monomer-monomer distribution function is given by

$$\hat{\Omega}^{mm}(k) = \frac{2}{k^4}\left(k^2 - 1 + e^{-k^2}\right) , \tag{IV.7}$$

and the center-of-mass monomer distribution function is

$$\hat{\Omega}^{cm}(k) = \frac{\sqrt{\pi}}{k}\mathrm{erf}(\frac{k}{2})e^{-\frac{k^2}{12}} . \tag{IV.8}$$

The direct correlation function, using the center of mass notation for Equations IV.4 and IV.5, reduces to

$$c^{cc}(k) = \frac{c_0 N^2 (\hat{Y}^{cm})^2}{1 + \Gamma \hat{Z}^{cm}(k)} , \tag{IV.9}$$

with $\hat{Y}^{cm}(k) = \Omega^{cm}(k)$ and $\hat{Z}^{cm}(k) = \hat{\Omega}^{mm}(k) - \left(\hat{\Omega}^{cm}(k)\right)^2$.

The *infinite soft-colloid chain limit* is described in our formalism in the limit of $n_b \to \infty$. In this limit the direct correlation reduces to

$$\hat{c}^{bb}(k) = \frac{N_b^2 c_0 (\hat{Y}^{bm}(k))^2}{1 + \Gamma_b \hat{Z}^{bm}(k)} , \tag{IV.10}$$

with

$$\hat{Y}^{bm(\infty)}(k) = \frac{(\sqrt{\pi}k\mathrm{erf}(k/2)e^{-k^2/12} + 2e^{-k^2/3})(e^{-k^2}-1)}{\left[e^{-k^2} - 1 - 2e^{-2k^2/3}\right]k^2} \tag{IV.11}$$

and

$$\hat{Z}^{bm(\infty)}(k) = \frac{2}{k^2} - \frac{(\sqrt{\pi}k(e^{-k^2}-1)\mathrm{erf}(k/2)e^{-k^2/12} + 2(e^{-k^2}-1)e^{-k^2/3})}{\left[(e^{-k^2}-1)^2 - 2(e^{-k^2}-1)e^{-2k^2/3}\right]k^4} . \tag{IV.12}$$

IV.1.2. The Effective Direct Correlation in Fourier Space

The combination that appears in the denominator of the Fourier transform of Equation (IV.3) can be approximated near $k = 0$ by its leading order series expansion about $k - 0$ as $\hat{Z}^{bm}(k) = \Omega^{mm}(k) - (\Omega^{bm}(k))^2/\hat{\Omega}^{bb}(k) \approx \frac{k^4}{45} + O(k^6)$. This results in a peak in $c^{bb}(k)$ whose width decreases as $\Gamma_b^{-1/4}$, so for fixed c_0 and monomer density the peak decreases in width as $N^{-1/4}$ (with k in units of R_g). At large k the function decays approximately as a Gaussian.

A limiting form for the peak at small k can be obtained by factoring out the overall factor of Γ_b, re-scaling wave vector units to fix the width of the peak, $k \rightarrow k\Gamma_b^{1/4}$, and expanding in powers of $1/\Gamma_b^{1/4}$ around $1/\Gamma_b^{1/4} \rightarrow 0$. The first two non-zero terms of this expansion give

$$\hat{c}^{bb}(k) \approx \frac{-N\Gamma}{\rho_m}\left[\frac{45}{45+\Gamma_b k^4} - \frac{5k^2}{28}\frac{13\Gamma_b k^4 - 3780}{(\Gamma_b k^4 + 45)^2}\right] , \tag{IV.13}$$

where k is expressed in units of R_{gb}^{-1}. For sufficiently large Γ ($\Gamma_b >> 10$), this form is a good approximation for $k << 1$. The second term is of order $\Gamma_b^{-1/2}$ smaller than the first in this region.

At large wave vectors for systems where Γ is large, ($k >> R_{gb}^{-1}$), $\hat{c}^{bb}(k)$ can be expanded in an asymptotic series about $1/\Gamma_b \rightarrow 0$. Summarizing these results

$$\hat{c}^{bb}(k) \approx \begin{cases} \frac{-N_b\Gamma_b}{\rho_m}\left[\frac{45}{45+\Gamma k^4} - \frac{5k^2}{28}\frac{13\Gamma_b k^4 - 3780}{(\Gamma_b k^4+45)^2}\right] & \text{if } k << 1 \\ \frac{-N_b\Gamma_b}{\rho_m}\sum_j \Gamma_b^{-j}\frac{(\hat{\Omega}^{cm}(k))^2}{(\hat{\Omega}^{mm}(k) - (\hat{\Omega}^{cm}(k))^2)^j} & \text{if } k >> 1 \end{cases} . \tag{IV.14}$$

IV.2. Effective Potentials and Forces

The effective potentials between coarse-grained units that give rise to the predicted tcfs must be "soft" since the tcfs give a nonzero chance of finding any separation distance. In this work, we use the term "soft" to describe systems where the effective potentials are never much larger than k_bT, and large variations of the potential relative to the characteristic energy scale (k_BT) of the system do not occur. For such "soft" systems, the Hypernetted-Chain (HNC) closure is known to give a good approximation to the relationship between the direct correlation and the pair potential.[41] Applying the HNC closure gives

$$V^{bb}(r) = -k_bT\left[c^{bb}(r) - h^{bb}(r) + ln(1 + h^{bb}(r))\right] . \tag{IV.15}$$

When $|h^{bb}(r)| << 1$, which always holds at large separations ($r >> 1$ in units of R_{gb}) and at any separation for representations with large N_b and high densities, this further simplifies to

$$V^{bb}(r) \approx -k_b T c^{bb}(r) \ . \tag{IV.16}$$

This formula is referred to as the mean spherical approximation (MSA) or random phase approximation in the literature. We choose here to refer to it as the MSA in this article to emphasize that it does not make the assumption of incompressibility in the melt, which has sometimes been associated with theories using the random phase approximation. It is, rather, arrived at here as a well-justified approximation of the HNC closure when the tcf is small in absolute value.

Figure IV.1 shows some example curves for the effective force $(-\partial V^{bb}(r)/\partial r)$ found using the numerical inverse transform of the effective direct correlation. The multiblock potentials for the same block size and system conditions approach a fixed form rapidly with increasing n_b. Thus for any soft-colloid chain model with $n_b >> 1$ it is a good approximation to replace the interaction potential with the potential found in the limit $n_b \to \infty$, which justifies the choice to examine only the $n_b \to \infty$ multiblock limit in detail.

IV.2.1. The Effective Direct Correlation and MSA Potential at Large Separations in Real Space

For large separations, $r >> 1$ (in R_{gb} units), the inverse transform integral is sufficiently dominated by $\hat{c}^{cc}(k)$ at small wave vectors that the large wave vector contribution can be entirely neglected. Furthermore, since the expansion for small wave vectors is bounded at large k, the error incurred in using the small k form with the integral bounds extended to infinity is small, so for $r >> 1$

$$c^{bb}(r)\approx\frac{-N_b\Gamma}{2\pi^2\rho_m R_{gb}^3 r}\int_0^\infty\left(k\sin(kr)\left[\frac{45}{45+\Gamma k^4}-\frac{5k^2}{28}\frac{13\Gamma_b k^4-3780}{(\Gamma_b k^4+45)^2}\right]\right)dk$$

$$=\Big[\left(\frac{45\sqrt{2}N_b\Gamma_b^{1/4}}{8\pi\sqrt{3}\sqrt[4]{5}\rho_m R_{gb}^3}\right)\frac{\sin(Q'r)}{Q'r}e^{-Q'r}-\left(\frac{\sqrt{5}N_b}{672\pi\rho_m\Gamma_b^{1/4}R_{gb}^3}\right)\big[(13Q^3(Q'r-4))cos(Q'r) \tag{IV.17}$$

$$+\left(\frac{945+13Q^4}{\Gamma_b^{1/4}}\right)r\sin(Q'r)+\frac{945r}{\Gamma_b^{1/4}}cos(Q'r)\big]\frac{e^{-Q'r}}{Q'r}\Big]\ ,$$

where $Q'=5^{1/4}\sqrt{3/2}\Gamma^{-1/4}$ and $Q\equiv Q'\Gamma^{1/4}$.

IV.2.2. The Form of the Effective Direct Correlation and MSA Potential at Small Separations

Since the region of interest is a finite domain of separations around $r\ =\ 0$, the most straightforward approach to approximating the form of the direct correlation/MSA potential is using a truncated power series. A series expansion in powers of the separation r can be obtained by expanding the sine function in the inverse Fourier transform. The generic result for the direct correlation is

$$c^{bb(n_b)}(r)=-\frac{N}{2\pi^2R_{gb}^3}\sum_{j=0}^{j_{max}}A_j^{(n_b)}(\Gamma)r^{2j}\ , \tag{IV.18}$$

where the $A_j(\Gamma_b)$, defined by

$$A_j^{(n_b)}(\Gamma_b)=\frac{\Gamma_b}{(2j+1)!}\int_0^\infty k^{2j+2}\frac{(\hat{\Omega}_{av}^{bm}(k)/\hat{\Omega}_{av}^{bb}(k))^2}{1+n_b\Gamma_b[\hat{\Omega}^{mm}(k)-(\hat{\Omega}_{av}^{bm}(k))^2/\hat{\Omega}_{av}^{bb}(k)]}dk\ , \tag{IV.19}$$

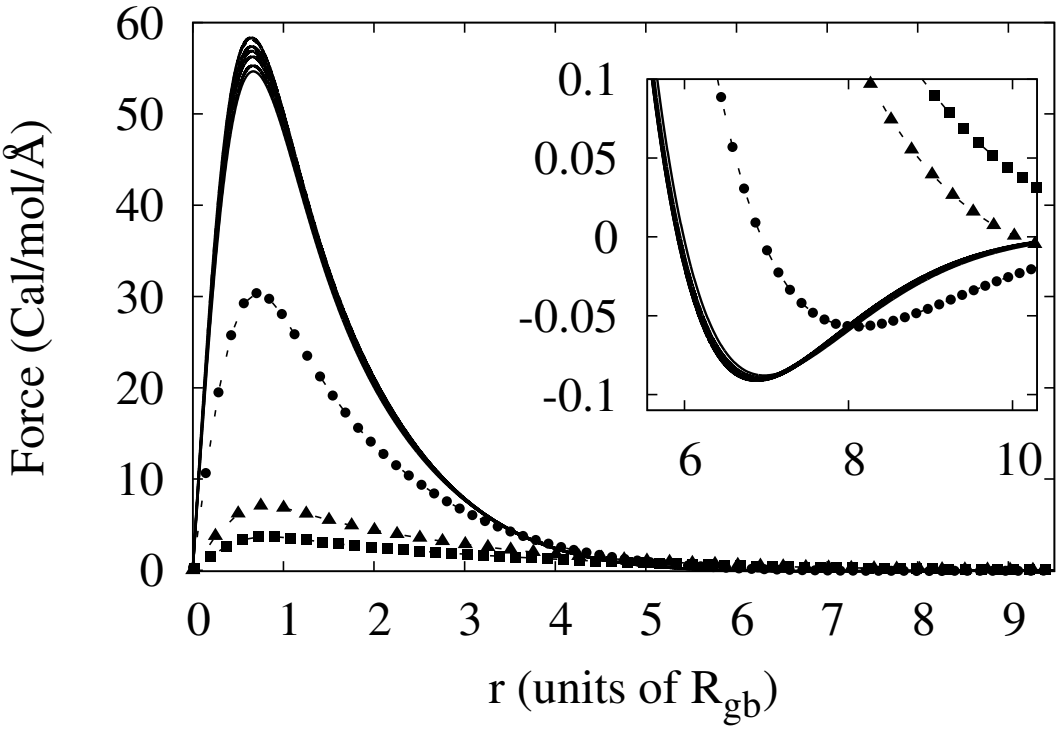

FIGURE IV.1. The multiblock force curves for a family of systems with $\rho_m|c_0|$=1 represented by the center of mass of sub-chains of length N_b=50 (solid lines) for increasing degrees of polymerization–from bottom to top, N=50, N=100, N=250, N=500, N=1000, N=10000, and N=100000. The soft sphere force curves for the N=100 (circles with dashed connecting lines), N=500 (triangles with dashed connecting lines), and N=1000 (squares with dashed connecting lines) systems with each chain represented by a single com site are also shown for comparison. The soft sphere potentials, which are plotted with separation distance in terms of the chain radius of gyration so that they can be shown on the same plot, show dramatic change with increasing degree of polymerization, while the potentials with a fixed block size show only small differences near their peaks over a wide range of chain lengths. The inset shows a close-up of the minima of the N_b=50 multiblock potentials, which are so close as to be nearly indistinguishable in this region, in contrast to the soft sphere (1 block) potentials for the same systems, which increase in range much faster than their physical size.

are functions of the system parameters through the combination Γ_b, and j_{max} is the order at which the series is truncated. Numerical integration suggests $j_{max} \approx 10$ is necessary to achieve a good approximation to the function on the range of interest (to about $r = 1$). The problem of characterizing the parameter dependence of the effective direct correlation at short range is thus reduced to that of characterizing the expansion coefficients. In the following sections we outline the results for the two limits of interest described above. Since the limiting form of the effective potentials as $n_b \to \infty$ is approached rapidly, the $n_b \to \infty$ limit can be applied for multiblock systems with $n_b > 5$ with negligible error.

In the soft sphere limit for $N \to \infty$ and therefore $\Gamma \to \infty$, the two approximations for large and small wave vectors converge to approximately the same value at $k = 1$, and so the integrals for the $A_j(\Gamma_b)$ coefficients can be taken to good approximation using the two region piece-wise form using these forms, with the division point at $k = 1$.

The generic form of the coefficients in this limit is that for $\Gamma >> 100$ $A_0 = a_0'\Gamma^{1/4} - a_0$, $A_1 = a_2 - a_2'/\Gamma^{1/4}$, with $a_0' \approx 19.30$ and $a_2' \approx 37.09$, and all higher coefficients approximately independent of Γ, $A_j^{(1)}(\Gamma) = a_j$ for $j > 2$. All a_j and b_j coefficients are numerical coefficients independent of system parameters Details of the derivation of these forms and tables of estimated values of the numerical coefficients are presented in the appendix.

The effective potential and force curves in the infinite soft sphere limit have the form (in units of R_g)

$$V_{MSA}^{cc}(r) \approx \begin{cases} \left(\frac{k_bT}{2\pi^2\rho_c R_g^3}\right)\left[\left(a_0^{(3/4)}\Gamma^{1/4} - a_0^{(1)}\right) - \left(a_2^{(1)} - \frac{a_2^{(\prime)}}{\Gamma^{1/4}}\right)r^2 + \sum_{j=2}^{j_{max}} a_{2j}r^{2j}\right] & \\ & \text{if } r < 1 \\ k_BT\Big[\left(\frac{45\sqrt{2}N\Gamma^{1/4}}{8\pi\sqrt{3}\sqrt[4]{5}\rho_m R_g^3}\right)\frac{\sin(Q'r)}{Q'r}e^{-Q'r} & \\ -\left(\frac{\sqrt{5}N}{672\pi\rho_m\Gamma^{1/4}R_g^3}\right)\left[(13Q^3(Q'r-4))cos(Q'r)\right. & \\ \left.+\left(\frac{945+13Q^4}{\Gamma^{1/4}}\right)r\sin(Q'r) + \frac{945r}{\Gamma^{1/4}}cos(Q'r)\right]\frac{e^{-Q'r}}{Q'r}\Big] & \text{if } r > 1 \end{cases} \tag{IV.20}$$

and

$$F^{cc}_{MSA}(r) \approx \begin{cases} \frac{\Gamma k_B T}{2\pi^2 \rho_c R_g^4} \left[2\left(\frac{a_2^{(1)}}{\Gamma} - \frac{a_2^{(5/4)}}{\Gamma^{5/4}} \right) r - \frac{2}{\Gamma} \sum_{j=2} j a_{2j} r^{2j-1} \right] & \text{if } r < 1 \\ \left(\frac{15N}{12\pi\sqrt{5} R_g^4 r^2} \right) \left[\left(Q'r - \Gamma^{-1/2} \eta_c(r) \right) cos(Q'r) \right. & \\ - \left. \left(1 + Q'r - \Gamma^{-1/2} \eta_s(r) \right) \sin(Q'r) \right] e^{-Q'r} & \text{if } r > 1 \end{cases} , \qquad \text{(IV.21)}$$

where the polynomial coefficient functions $\eta_c(r) = 13\sqrt{5}(4 - Q'r + Q'r[4 + Q'r])/336$ and $\eta_s(r) = 5^{3/4}\sqrt{3/2}Q'r(1890r + 13Q^4 r + 13Q^3[Q'r - 4])/3780$ are defined to simplify the expression. The convergence of this form to the numerically integrated exact form is shown in Figure IV.2.

In the infinite multiblock limit, the total degree of polymerization, N, goes to infinity, but the number of monomers per block, N_b, remains finite, and therefore all systems with $\Gamma_b >> 1$ values are potentially of interest. When Γ_b is not large enough for the system to be in the asymptotic regime, the large and small wave vector limiting series approximations presented previously do not converge to the same value near $k = 1$, and therefore the piece wise approximation must be extended to include a third form in the region around $k = 1$. The form in this "crossover" region, $1-\epsilon < k < 1+\epsilon$, is obtained by a series expansion of the direct correlation around $k = 1$.

The large k asymptotic form fails to converge even for the low order terms for approximately $\Gamma_b < 40$ (terms of higher order in j become non-convergent first as Γ_b is decreased), and so this regime is not approachable by this method, and numerical integration must be used. The general form for $\Gamma_b > 40$, the form of the approximation for the jth coefficient is

$$A_j^{(\infty)}(\Gamma_b) = B_0(\Gamma_b) + B_1(\Gamma_b) + \sum_{m=0}^{m_{max}} I_m^{(\infty)}(\Gamma_b)\eta_{j,m}(\epsilon) + \sum_{l=1}^{l_{max}} (a_j^{(\infty)}/\Gamma_b)^{l-1} , \qquad \text{(IV.22)}$$

where $B_0(\Gamma_b)$, $B_1(\Gamma_b)$, and $I_m^{(\infty)}(\Gamma_b)$ are functions of the parameter Γ_b whose derivations and forms are given in the appendix and the a_j and η_j are parameter independent numerical constants, for which a table and generating formula respectively are given in the appendix.

For systems with $\Gamma < 40$, where these formulae are not applicable, numerically integrated values are used.

The effective potential and force curves, in units of R_{gb}, are given by

$$V_{MSA}^{bb}(r) \approx \begin{cases} \left(\frac{N_b k_b T}{2\pi^2 \rho_m R_{gb}^3}\right) \left[\sum_{j=0}^{j_{max}} A_j(\Gamma_b) r^{2j}\right] & \text{if } r < R_g \\ k_B T \Big[\left(\frac{45\sqrt{2} N \Gamma_b^{1/4}}{8\pi\sqrt{3}\sqrt[4]{5}\rho_m R_g^3}\right) \frac{\sin(Q'r)}{Q'r} e^{-Q'r} & \\ - \left(\frac{\sqrt{5}N}{672\pi\rho_m \Gamma_b^{1/4} R_g^3}\right) \left[(13Q^3(Q'r-4))cos(Q'r)\right. & \\ \left. + \left(\frac{945+13Q^4}{\Gamma_b^{1/4}}\right) r\sin(Q'r) + \frac{945r}{\Gamma_b^{1/4}} cos(Q'r)\right] \frac{e^{-Q'r}}{Q'r} \Big] & \text{if } r > 1 \end{cases} \quad \text{(IV.23)}$$

and

$$F_{MSA}^{bb}(r) \approx \begin{cases} \left(\frac{N_b k_b T}{\pi^2 \rho_m R_{gb}^3}\right) \left[\sum_{j=0}^{j_{max}} j A_j(\Gamma_b) r^{2j-1}\right] & \text{if } r < R_g \\ \left(\frac{15N}{12\pi\sqrt{5} R_g^4 r^2}\right) \Big[\left(Q'r - \Gamma_b^{-1/2}\eta_c(r)\right) cos(Q'r) & \\ - \left(1 + Q'r - \Gamma_b^{-1/2}\eta_s(r)\right) \sin(Q'r)\Big] e^{-Q'r} & \text{if } r > R_g \end{cases}, \quad \text{(IV.24)}$$

with the $A_j(\Gamma_b)$ coefficients given by Equation IV.22 if $\Gamma_b > 40$, or by numerical integration for values of Γ_b to small for this approximation. Figure IV.3 shows this approximation against numerically integrated forms.

IV.2.3. Effective Potential and Force Curves

IV.3. Analysis

In this section, interpretation of the effective pair potentials as is presented. The features of the effective potentials, particularly the long-range tail, can be seen as representing the average effect of many polymer correlations amongst strongly interpenetrating polymers in the surrounding liquid. The scaling of this effective tail with the parameter Γ_b, and therefore

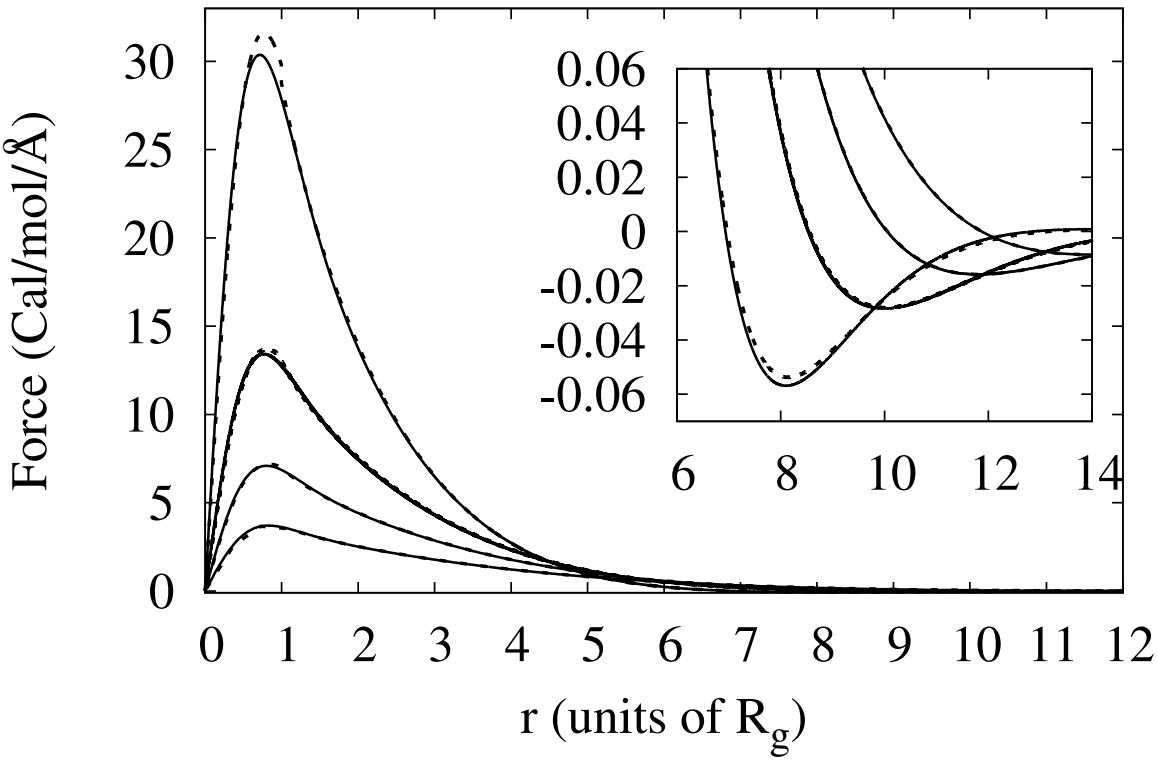

FIGURE IV.2. Convergence of the two region piece-wise approximation (dashed line) to the numerically integrated form of the force curve (solid lines) in the soft sphere model with (from top to bottom in main figure, bottom to top in inset) N=100, 250, 500, and 1000. Inset shows the small attractive part of the potential. All systems have density $0.03355\mathring{A}^{-3}$, effective bond length $4.372\mathring{A}$, and c_0 taken from UA simulations or the fit of the UA simulation values to the form $a + b/N$

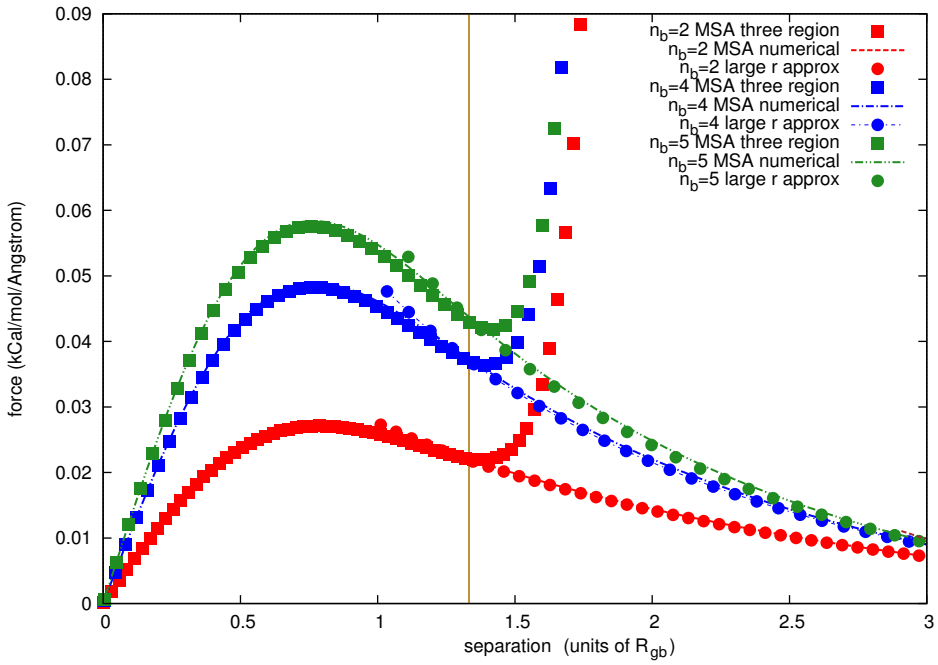

FIGURE IV.3. Comparison of small and large r approximate forms for the force with numerically calculated force for the infinite multiblock model for various subdivisions of the same example PE200 system for density ρ_m=0.03656$\mathring{A}^{-3}$ at 400K. The vertical orange line shows the proposed cutoff point between large and small r approximations.

density and the number of monomers represented by each coarse-grained degree of freedom is then discussed.

IV.3.1. Physical Interpretation of the Effective Direct Correlation and Pair Potential

The Ornstein-Zernike equation which defines the effective direct correlation in real space can be expanded for the direct correlation

$$c^{bb}(r)=-\frac{N_b\Gamma_b}{\rho_m}\big[(Y^{bm}*Y^{bm})(r)-\Gamma_b(Z^{bm}*Y^{bm}*Y^{bm})(r) \tag{IV.25}$$

$$+\Gamma_b^2(Z^{bm}*Z^{bm}*Y^{bm}*Y^{bm})(r)\ -...\big],$$

where the "*" operator indicates a convolution, and the distributions $Z^{bm}(r)$ and $Y^{bm}(r)$ are the inverse Fourier transforms of the Fourier space intramolecular distributions $\hat{Z}^{bm}(k)$ and $\hat{Y}^{bm}(k)$ defined above.

Consider first the simple case of the soft sphere representation where the polymer can be approximated as infinitely short ranged. In this case the application of the Percus-Yevick closure allows an analytical solution for the monomer direct correlation parameter, $c_0 \approx= -2\pi^2\rho l_{eff}^6$.[44] Since c_0 in this regime is proportional to density, the parameter Γ is proportional to $\rho_m^2 N$, and is therefore proportional to the average number of other polymers found in the characteristic volume of one (roughly a sphere of volume R_g). For the soft sphere model $Y^{bm}(r) = \Omega^{cm}(r)$, and $Z^{cm}(r) = \Omega^{mm}(r) - (\Omega^{cm} * \Omega(cm))(r)$. The parameter $\Gamma_b = \Gamma = -N\rho_m c_0$ is large in systems with a high level of geometric interpenetration of coarse grained units is (large $N\rho_m$) and strong monomer interactions (large $|c_0|$), and small when the coarse-grained units have little geometric overlap and typical monomer interactions are small. In the limit that Γ is very small, the correction term in the OZ integral equation becomes negligible. Therefore the effective direct correlation is simply proportional to the self-convolution of the density pair correlation of monomers about the center of mass, which is just the average overlap of molecules with a given center of mass separation. For the soft sphere model,

$$lim_{\Gamma\to 0} c^{cc}(r) = [-\frac{N\Gamma}{\rho_m}](\Omega^{cm} * \Omega cm)(r) \approx [-\frac{N\Gamma}{\rho_m}](\frac{3\sqrt{3}}{8\pi^{3/2}})e^{3r^2/4} \ . \qquad \text{(IV.26)}$$

When Γ is nonzero, however, some interpenetrating configurations will contribute, and the effective direct correlation is no longer simply proportional to this average density overlap. For small Γ, the deviation from the intuitive low interpenetration/interaction form is determined by the difference in the pair density distribution of monomers about other monomers from the self-convolution of the pair density distribution of monomers about the center of mass. The difference correlation, $Z^{cm}(r)$ characterizes how much of the correlation between two monomers cannot be mapped through the center of mass as pair interactions. The first correction term of the expansion describes contributions from correlations that propagate between two polymers through the "hidden" processes in a third that overlaps in space with both; correlations from the cm of the first to a monomer on the first, to a monomer on the third, through cm "hidden" intramolecular processes to another monomer in the third, to a monomer on the second, and

finally to the center of mass of the second. Higher correction terms involve additional steps through the cm "hidden" processes on additional intermediate overlapping polymers.

When $\Gamma >> 1$, essentially all polymers in any probable configuration overlap significantly with at least several others in all probable equilibrium configurations, and so the effects of paths through "hidden" correlations on any sequence of polymers in the system are included. The result found above for the effective pair potential between chain cms therefore reflects the average effect of how these interactions "propagate through the network of interpenetrating polymers. At finite Γ this resulting effect remains of finite range, but as $\Gamma \rightarrow \infty$ the range of the contribution to the direct correlation from these processes grows without bound. In this simple scaling limit, the result can be envisioned as a random walk on the network of jointly-interpenetrating polymers. Since the number of interpenetrating polymers in the volume of any other scales as $N^{1/2}$ and the intramolecular "hidden correlations" propagate through chain segments that follow random walk statistics, their effects propagate out with a scaling $(N^{1/2})^{1/2} = N^{1/4}$

In systems where the non-zero range of the interactions between monomers becomes of importance and the details of monomer interactions become important because of local packing properties of the monomers, the monomer direct correlation parameter c_0 is no longer proportional to ρ_m, and the universal scaling with geometric interpenetration is lost, as the effect of the specific monomer interactions as well as the geometric interpenetration are wrapped into Γ.

This interpretation can be extended straightforwardly to the multiblock-level distributions, but the relevant distributions describing correlations involving monomers and block centers are all modified to be divided in Fourier space by a factor of the average correlation of block-centers with other block centers. Because the latter distribution is smaller, this actually makes its value larger for $k > 0$, and has the effect of keeping the distribution much closer to the same form as $\hat{\Omega}^{cm}(k)$ (but in units of block radius). To leading order the $\Gamma \rightarrow 0$ limiting form can be approximated by the same Gaussian form. The mathematical result reflects the fact that the surrounding monomers on the same chain are explicitly represented in the model and removes the long range component in $\Omega^{bm}(r)$ that scales in range with the size of the molecule. A schematic illustration of the various correlations described here is shown in Figure IV.4

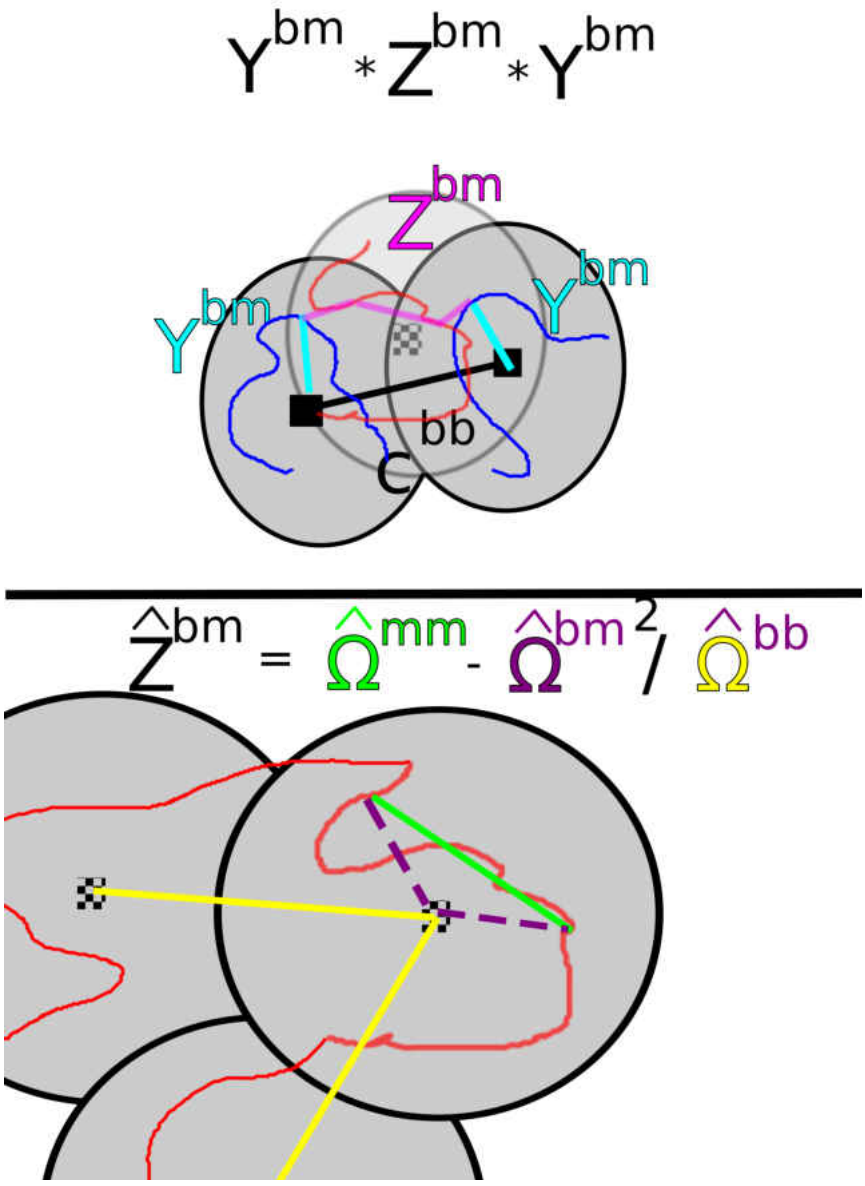

FIGURE IV.4. Schematic Illustration of the processes mapped into effective pair potentials when coarse-grained units have a high level of geometric overlap

IV.3.2. Properties of the Effective Pair Force

The effective pair force is characterized by a short range soft repulsive part that grows away from 0 at $r = 0$ and reaches a peak value before $r = 1$, and a long repulsive tail and small attractive part that scales in range faster than the radius of gyration of the molecule, as $\Gamma^{1/4}$. The relevant features of the effective potential that characterize its physical properties are the position and magnitude of the force peak (the inflection point in the effective potential) at short range and the position and magnitude of the attractive part of the effective potential. The first two non-zero separations where the force is zero characterize the attractive region of the potential and also serve as points where the potential may be truncated for computer simulations so as to not introduce a discontinuity in the force.

The position and magnitude of the peak force can be approximated from the series expansion explicitly by defining $\delta = 1 - r$, and expanding the series form from the previous section around $\delta = 0$ to quadratic order. Generically, in terms of the $A_j(\Gamma)$ coefficients, the separation of peak force is given by

$$r_{pk} \approx 1 - \frac{M_1(\Gamma_b)}{2M_2(\Gamma_b)} + \frac{1}{2}\sqrt{\frac{M_1^2(\Gamma_b)}{M_2^2(\Gamma_b)} - \frac{4M_0(\Gamma_b)}{M_2(\Gamma_b)}} \ , \tag{IV.27}$$

where $M_0(\Gamma_b) = \sum_{j=0}^{j_{max}} jA_j(\Gamma_b)$, $M_1(\Gamma_b) = 2\sum_{j=0}^{j_{max}} j(2j-1)A_j(\Gamma_b)$, and $M_2(\Gamma_b) = \sum_{j=0}^{j_{max}} j(2j-1)(2j-2)A_j(\Gamma_b)$.

In the soft sphere limit, the estimates for the $A_j(\Gamma)$ give the particularly simple form

$$r_{pk} \approx 1 - \left[-0.203664 + 0.195141\sqrt{1 + 14.0663\Gamma^{-1/4}}\right] \ . \tag{IV.28}$$

Inserting this back into the series expansion for the force $(-k_BT\partial c^{cc}(r)/\partial r)$ at small separations, expanding in powers of $1/\Gamma^{1/4}$ and discarding terms that fall off faster than $1/\Gamma^{5/4}$, the magnitude of the peak force for the soft sphere model is approximately

$$F^{cc}(r_{pk}) \approx \left(\frac{k_BT\Gamma}{2\pi^2\rho_c R_g^3}\right)\left(-\frac{38.3438}{\Gamma} + \frac{43.5344}{\Gamma^{5/4}}\right) \ . \tag{IV.29}$$

Plots of the properties described here for the soft sphere model in Figure IV.5. Highly similar forms can be found with slightly different coefficients for the same assumptions in the

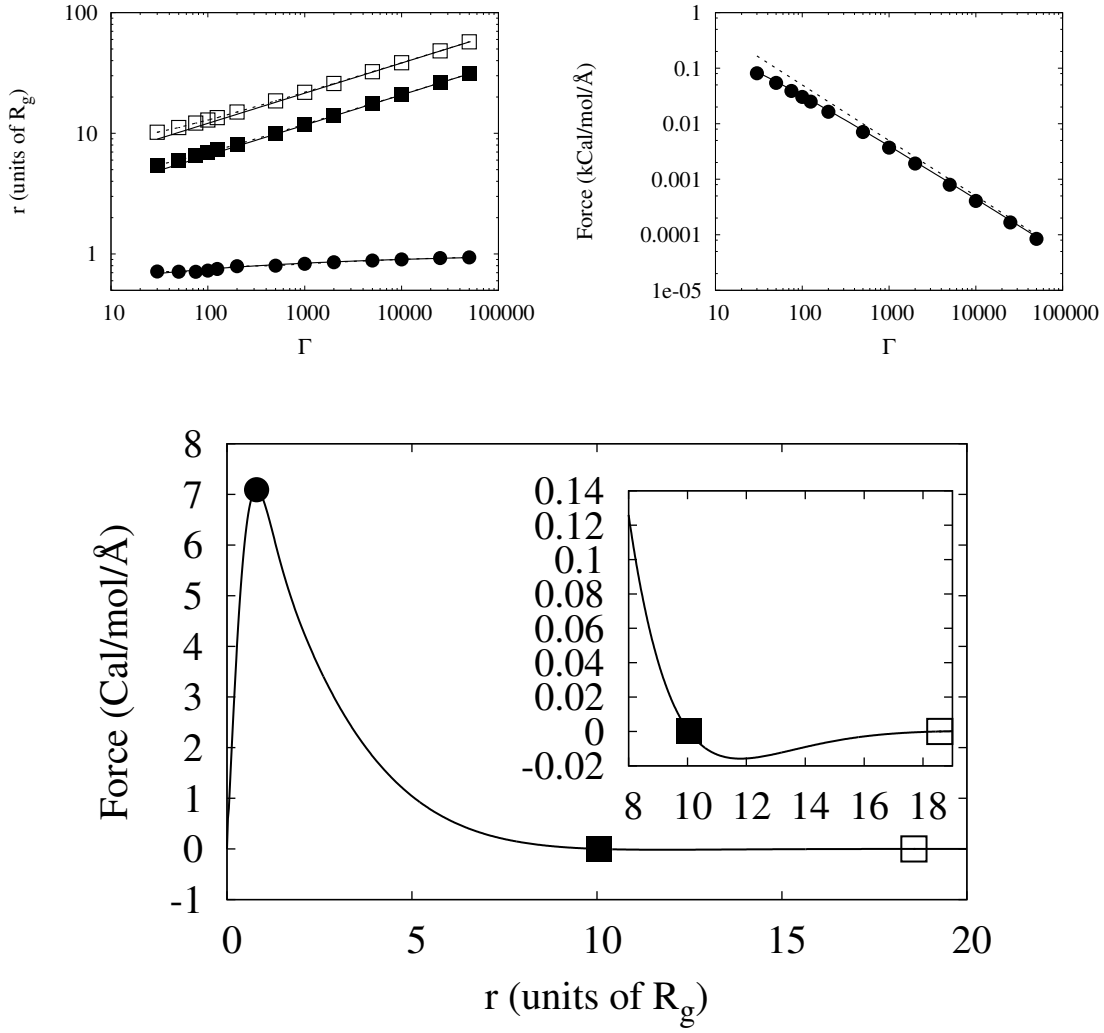

FIGURE IV.5. Approach of the separation of peak force (circles connected by dashed lines), and the first to nonzero separations of zero force (filled and open squares respectively connected by dashed lines) of the numerically integrated potential to the limiting forms for these quantities described in the text (solid lines).

$\Gamma_b \to \infty$ limit of the multiblock model, however in the limit of interest where $n_b \to \infty$ with fixed block sizes, no further simplification for the force peak is possible. The forms at small Γ (but $\Gamma > 40$) can be written in terms of the $A_j(\Gamma_b)$ forms derived in appendix b.

The nonzero separations where the pair force vanishes characterize the range of the interaction, and serve as points where the interaction can be truncated in simulations without a resulting discontinuity in the force. Since all these zeros occur at $r >> R_{gb}$, for any system with Γ_b large enough that the correction terms of order $1/\sqrt{\Gamma_b}$ can be neglected, the large r limiting form can be used to estimate the separation distances for these. This form predicts zeros at all the roots of the transcendental equation

$$tan(Q'r) = \frac{Q'r}{1 + Q'r} \ . \tag{IV.30}$$

The first two nonzero solutions to this can be estimated numerically and give $r_{01} \approx 2.08\Gamma_b^{1/4}$ and $r_{02} \approx 3.82\Gamma_b^{1/4}$. Truncating the effective potential at the second force zero is usually sufficient to reproduce thermodynamics to within negligible error, while truncating at either the first or second force zero is quite sufficient to reproduce structure as well.

This scaling of the range of the effective potential (and force) has important practical implications for simulations using the effective pair potentials. Since the box dimensions required for a simulation scale with the box size (the side length must be twice the cutoff range for a cubic simulation box with periodic boundaries)[59] higher levels of coarse-graining require larger box sizes. Thus, while the reduced number of degrees of freedom and friction in a soft sphere simulation always allows for the fastest MSMD simulation of a system of a given box size, if a smaller box size can adequately capture the desired properties of the system the efficiency of the simulation of a given system can be optimized by choosing a multiblock model and simulating the system with a smaller box size. Physically, this non-trivial scaling of the range suggests that lower levels of coarse-graining than would naively be assumed may be required to resolve processes that take place on a give thength scale, as effective pair potentials represent only only the average effects of many polymer interactions on this range.

IV.3.3. Sensitivity to Monomer Interaction Properties

The theory presented here predicts the effective potentials in terms of parameters from the monomer-level theory, specifically the density, radius of gyration and the direct correlation parameter c_0. The former two are straightforward properties of melts, while the latter is specific to integral equation theory and reflects the average direct influence exerted on one monomer by each monomer on each other chain in the system. Most generally it therefore is determined by the local pair potential between monomers and inter-chain packing effects. Extensive previous work on PRISM has developed approaches to numerically calculate monomer-level direct correlation functions, from which c_0 can be estimated.[45]

Physically, c_0 can potentially depend on density, temperature, chain architecture, and nature of the monomer interaction potential. Since both the overall magnitude and shape of the monomer effective pair potentials depend on c_0, the effective coarse grained potentials remain dependent on all of these properties even in the high density and infinite chain limits. This contrasts with the static structure reflected in the tcfs, which become asymptotically insensitive to c_0 in the high density/long chain limit. For large Γ the tcf for a melt depends only on the chain length, density and radius of gyration, as Equation III.49 reduces to

$$h^{cc}(r) \approx -\frac{N}{\rho_m R_g^3} X_0(r) \ . \tag{IV.31}$$

In the highly coarse-grained limit, therefore, the structure may show no difference between systems with very different effective potentials and very different thermodynamic properties. The implications of this for virial route thermodynamics represented by coarse-grained models based on structural optimization will be discussed in the next chapter.

CHAPTER V

THERMODYNAMIC CONSISTENCY IN COARSE-GRAINED MODELS: PRESSURE, COMPRESSIBLITY AND EQUATION OF STATE

This chapter is adapted from the short letter "Thermodynamic Consistency in Variable-Level Coarse Graining of Polymeric Liquids" which appeared in 2012 in the journal Physical Review Letters[58] and the longer and more detailed article "Theoretical Characterization of Effective Pair Potentials that Map the Structure and Thermodynamics of Polymer Melts onto Soft Colloidal Liquids" which is undergoing final revisions and will be submitted for publication soon. Both papers are co-authored with Jay McCarty, Ivan Lyubimov and Marina Guenza. To the material used in this chapter, Jay McCarty has contributed new United atom simulations that allow for the comparison of pressure with the coarse-grained representation and did the initial calculations for the virial equation of state for the soft sphere model using the potential I derived. Ivan Lyubimov contributed some MSMD trajectories using the soft sphere model. All three co-authors have contributed useful discussions and help in formulating and editing the manuscript.

V.1. Simulations of Multiblock Models

V.1.1. Intramolecular Interactions

To extend the simulations to the multiblock model, intramolecular interactions are added that on average enforce the predicted intramolecular distributions predicted from random walk statistics. To obtain interactions that enforce these distributions, we first impose an interaction potential whose force on average cancel out the net force due to the other surrounding molecules. Because the system is a dense melt, a repulsive potential between bonded block cms is required to cancel the forces due to the surrounding molecules. The effective potential between to block cms interacting via the pair potential in the field of the surrounding molecules is the definition of the potential of mean force, which in terms of the known tcf is $-k_BTln(1+h^{bb}(r))$. Thus in order to provide a stabilizing potential against the forces from the surrounding fluid, a repulsive interaction equal to the difference between the intermolecular pair potential and the potential of mean force is imposed between all adjacent block centers on each chain. With the effect of the

potential due to the surrounding molecules canceled out to good approximation, the Gaussian distribution of block centers can be enforced by imposing the harmonic potentials found from the direct Boltzmann inversion of $\omega^{bb}(r)$, and solving for the effective potential (direct Boltzmann Inversion) The net result between bonded atoms is

$$V_{bond}^{bb} = 3k_BTr^2/(8R_{gb}^2) + V^{bb}(r) + k_BTln(1 + h^{bb}(r)) \ . \tag{V.1}$$

An angle potential is similarly derived by direct inversion of the angle distribution predicted from Gaussian melt statistics, which has been previously derived by others.[61] Additional correlations between monomers farther apart on the chain (dihedrals, etc.) are taken to be small enough to be negligible in this soft regime. All simulation tests with the soft multiblock model are implemented as classical MD simulations in the NVE ensemble using the LAMMPS simulation package[60] and the effective potentials described above.

Since the effective block cm chain is very flexible, all other block cms separated by more than one other block cm are assumed to be indistinguishable from block cms on different molecules, and therefore to interact with the intermolecular pair potential.

V.2. Equilibrium Thermodynamics

V.2.1. Compressibility

The total correlation function in this blob description gives isothermal compressibility, $\kappa_T = [k_BT\rho_m(1 + \Gamma_b)/N]^{-1}$, with k_B the Boltzmann constant and T the temperature, which is consistent with the compressibility in the atomistic description.[44] Intra- and inter-molecular pair distribution functions and the structure factor, are consistent with their atomistic counterpart for distances $r > R_{gb}$ and wave vectors $k < 2\pi/R_{gb}$.

V.2.2. Pressure and Virial Equation of State

Using established formalism for chain molecules by Honnell et al,[62] the virial equation of state can be decomposed into a kinetic term plus contributions from intramolecular and intermolecular forces as

$$P = P_{kin} + P_{inter} + P_{intra} \ , \tag{V.2}$$

where, in the notation used here and under with all intermolecular interactions and tcfs assumed equal, and all intramolecular potentials and pair correlations assumed to depend only on the number of intervening monomers on the chain,

$$P_{kin} = \frac{\rho_m k_B T}{N_b} \ , \tag{V.3}$$

$$P_{inter} = -\frac{2\pi\rho_m^2}{3N_b^2}\int_0^\infty r^3(1+h^{bb}(r))\frac{\partial V^{bb}(r)}{\partial r} \ , \tag{V.4}$$

and

$$P_{intra} = -\frac{4\pi\rho_m(n_b-1)}{3N}\int_0^\infty r^3\omega_1^{bb}(r)\frac{\partial V_{bnd}(r)}{\partial r}dr - \frac{4\pi\rho_m}{3N}\sum_{\epsilon=3}^{n_b-1}(n_b-\epsilon)\int_0^\infty r^3\omega_\epsilon^{bb}(r)\frac{\partial V^{bb}(r)}{\partial r} \ . \tag{V.5}$$

The predicted pressure is the same to good approximation for all numbers of blocks. In the large N limit, $h^{cc}(r) \approx 0$ everywhere, and so the intermolecular contribution may be approximated using the result for a particles of a perfectly uniform liquid interacting with the MSA potential, giving total pressure in the soft sphere limit of

$$P_{tot} \approx P_{kin}^{(ss)} + P_{inter}^{(0)} = \frac{\rho_m k_B T}{N} - \frac{2\pi\rho_m^2}{3N^2}\int_0^\infty r^3\frac{\partial V^{bb}(r)}{\partial r} \ . \tag{V.6}$$

This intermolecular contribution is referred to hereafter as the uniform MSA contribution. The generalization of the uniform MSA contribution to multiblock models in the regime here considered ($N_b > 30$) yields the same result regardless of the number of blocks, n_b. Additional contributions to the pressure arising from the intramolecular interactions between blocks on the same chain, the increasing non-uniformity of the liquids structure on the block level, and the kinetic contribution due to the additional degrees of freedom represented on each chain cancel each other to leave the pressure the same across different levels of representation. Specifically, the additional kinetic contributions and the contributions from the harmonic bonds cancel each other exactly, and the intramolecular repulsive interactions compensate for the reduction in

the intermolecular pressure due to the depletion in other chains in the surrounding space due to the presence of blocks on the same chain. In the relatively high density, long chain systems examined here, the latter effects (the canceling effects of intramolecular repulsion and shielding) are generally a small fraction of the total pressure.

Intermolecular contributions

The intermolecular contribution for a system interacting with the force obtained using the HNC closure approximation can be decomposed into a term that is dominant for high density long chain systems, which is the only surviving term in the large block, high density regime where $|h^{bb}(r)| \rightarrow 0$ for all r, plus a set of correction terms arising from the non-uniformity of the structure of the liquid or $P_{inter} = P^{(0)}_{inter} + P^{(1)}_{inter}$, where, with r in units of R_{gb}

$$P^{(0)}_{inter} = \frac{-2\pi\rho_b^2}{3} R_{gb}^4 \int_0^\infty r^3 F^{bb}_{MSA}(r) dr \ , \tag{V.7}$$

with the number density of blocks $\rho_b = \rho_m / n_b$, and

$$P^{(1)}_{inter} = \frac{-2\pi\rho_b^2}{3} R_{gb}^4 \int_0^\infty \left[r^3 F^{bb}_{MSA}(r) h^{bb}(r) + k_B T h^{bb}(r) \frac{dh^{bb}}{dr} \right] dr \ . \tag{V.8}$$

The dominant term can be decomposed into integrals over the piece-wise form of the MSA force given above and evaluated as

$$P^{(0)}_{inter} = -\frac{2\pi\rho_b^2 k_B T}{3} \left[I_{Psr} + I_{Plr} \right] \ , \tag{V.9}$$

with

$$I_{Psr} = \int_0^{r_{cut}} r^3 F^{bb}_{eff}(r) dr = \frac{2N}{\pi\rho_m} \sum_{j=1}^{j_{max}} \frac{j A_j(\Gamma_b)}{2j+3} r_{cut}^{2j+3} \ , \tag{V.10}$$

and

$$I_{Plr}=\int_{r_{cut}}^{\infty} r^3 F_{eff}^{bb}(r)dr \tag{V.11}$$

$$\approx -\left(\frac{N_b\Gamma_b}{4\pi\rho_m}\right)\left[3(w_1\Gamma_b^{-1/4}+1)cos[w_1\Gamma_b^{-1/4}]+(3w_1\Gamma_b^{-1/4}+1)Sin[w_1\Gamma_b^{-1/4}]\right]e^{-w_1/\Gamma_b^{1/4}}\ ,$$

where $w_1 = (5^{1/4}\sqrt{3}r_{cut})/(\sqrt{2})$, and where the contribution from the correction term to the force at long range have been neglected as it is less than 1% of the value of the contribution from the leading order term in Γ_b for all $\Gamma_b >> 1$.

The finite tcf correction term contains contributions from two integrals

$$P_{inter}^{(1)} = -\frac{-2\pi\rho_b k_B T}{3}\left[I_{Pi11}+I_{Pi12}\right]\ , \tag{V.12}$$

with

$$I_{Pi11} = \int_0^{\infty} r^3 \frac{c^{bb}(r)}{dr} h^{bb}(r)dr \tag{V.13}$$

and

$$I_{Pi12} = \int_0^{\infty} r^3 h^{bb}(r)\frac{dh^{bb}(r)}{dr}dr = \frac{3}{2}\int_0^{\infty} r^2 (h^{bb}(r))^2 dr = \frac{3}{16\pi^3}\int_0^{\infty} k^2(\hat{h}^{bb}(k))^2 dk\ . \tag{V.14}$$

where integration by parts and Plancherel's theorem (for the asymmetric normalizations used here for the Fourier transforms) are employed to obtain the second and third forms. These correction terms are integrated numerically and shown in Figure V.1 for an example polyethylene melt with $N = 1000$ represented by various multiblock models.

In the case of the infinite soft sphere, $h^{bb}(r) \to 0$ both of these corrections are negligible.[63] For the infinite multiblock chain, however, they remain significant both due to the finite value of $h^{bb}(r)$, and the presence of the secondary correlation hole feature in $h^{bb}(r)$, which grows in range with the size of the molecule.

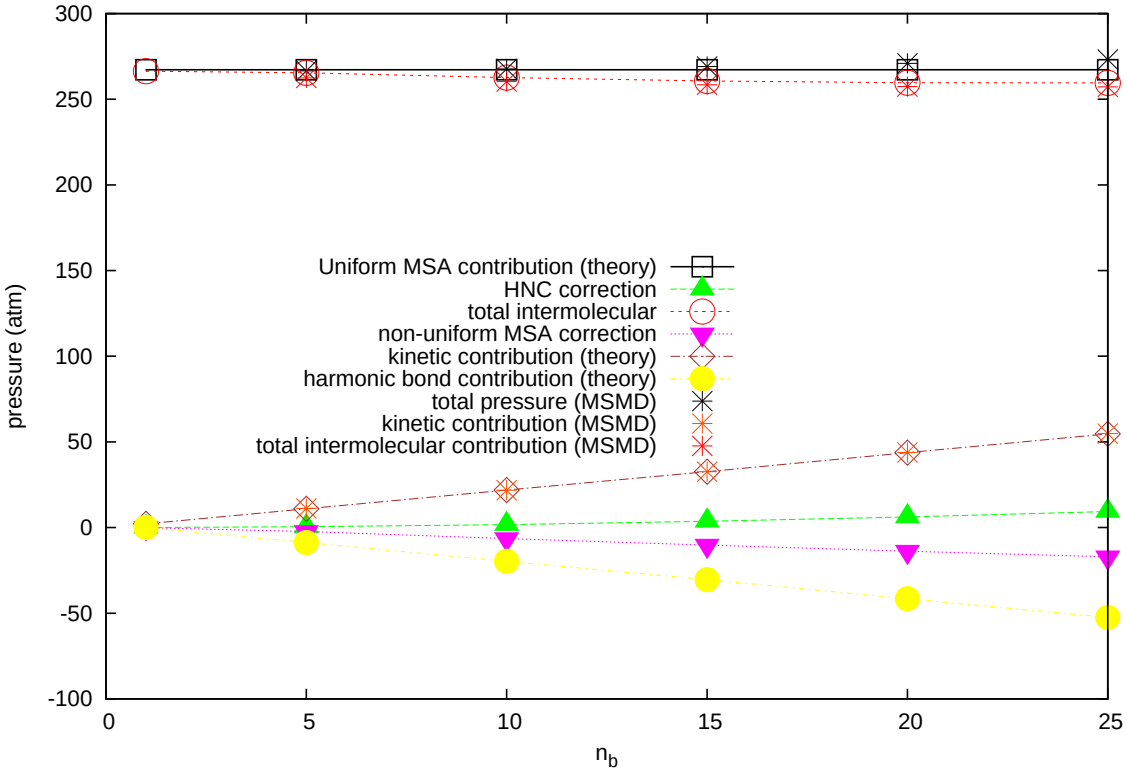

FIGURE V.1. The decomposition of contributions to pressure for various multiblock models representing the same system (PE1000 at 509K)

Intramolecular contributions

The intramolecular contribution to the virial-route pressure can be decomposed into contributions from the harmonic part of the bond interactions (P_{bharm}), the repulsive part of the bond interactions (P_{brep}), and the non-bonded repulsive interactions (P_{nb}):

$$P_{bharm} = -\frac{4\pi\rho_m(n_b-1)}{3N}\int_0^\infty r^3\omega_1^{bb}(r)\frac{\partial V_{bharm}(r)}{\partial r}dr \ , \tag{V.15}$$

$$P_{brep} = -\frac{4\pi\rho_m(n_b-1)}{3N}\int_0^\infty r^3\omega_1^{bb}(r)\frac{\partial V_{brep}(r)}{\partial r}dr \ , \tag{V.16}$$

and

$$P_{nb} = -\frac{4\pi\rho_m}{3N}\int_0^\infty r^3\omega_{>3}^{bb}(r)\frac{\partial V^{bb}(r)}{\partial r} \ , \tag{V.17}$$

with

$$V_{bharm} = \frac{3k_bT}{8}r^2 \ , \tag{V.18}$$

$$V_{brep} = V^{bb}(r) + k_BTln(1+h^{bb}(r)) \ , \tag{V.19}$$

and

$$\begin{aligned}\omega_{>3}^{bb}(r) &= \sum_{\epsilon=3}^{n_b-1}(n_b-\epsilon)\omega_\epsilon^{bb}(r) \\ &= \frac{1}{2\pi^2 r R_{gb}}\int_0^\infty ksin(kr)\frac{e^{-6k^2}(n_b-3)+e^{-2k^2(n_b+1)}-e^{-8k^2}(n_b-2)}{(1-e^{-2r^2})^2}dk \ ,\end{aligned} \tag{V.20}$$

where in r is as usual expressed in units of R_{gb}.

The contribution from the harmonic bonds can be integrated analytically and gives the equipartition result,

$$P_{bharm} = -\frac{\rho_m k_B T (n_b - 1)}{N} \ , \tag{V.21}$$

and so combined with the kinetic contribution gives

$$P_{kin} + P_{bharm} = \frac{\rho_m k_B T}{N} \ , \tag{V.22}$$

independent of n_b. The other contributions from the intramolecular repulsive contributions can be integrated numerically to show their approximate cancellation with the intermolecular HNC and shielding corrections for the systems considered here. Figure V.1 shows this decomposition for an example system.

V.2.3. Sensitivity of Pressure to the Total Correlation Function at Large Separations

The effective pair potential can be obtained theoretically from the structure in the above way, but at higher levels of coarse graining and higher densities, the predicted effective pair potentials become sensitive to smaller variations in tcf at longer ranges relative to the size of the coarse-grained unit. The effect occurs at all levels of representation, but we focus here on the soft sphere limit, as the simplest example.

If a small variation at large r, $\delta h^{cc}(r)$, is introduced, giving a small variation at low wave vector $\hat{\delta h}^{cc}(k)$, the modified effective direct correlation and therefore MSA potential, neglecting the term proportional to the small correction, is given by

$$c_\delta^{cc}(r) = \left(-\frac{\Gamma N}{2\pi^2 r R_g^3} \int_0^\infty \frac{h^{cc}(k) k \sin(kr)}{1 + \rho_c h^{cc}(k) + \rho_c \hat{\delta h}^{cc}(k)} \right) \ . \tag{V.23}$$

The larger Γ is, the smaller $\hat{\delta h}^{cc}(k)$ at small k, and therefore the smaller $\delta h^{cc}(r)$ at large r must be in order for the error in $c_\delta^{cc}(r)$ to be small. In the infinite chain limit of the soft sphere representation, the error that can be tolerated without a significant effect on the direct correlation and therefore the pair potential and thermodynamic properties of the system goes to zero.

In a simulation-based coarse-graining procedure, the structure used to obtain the potential is calculated from a small atomistic-level simulation. Since it is desirable to use as small an atomistic simulation as possible because of the high computational expense, it is natural to

choose a simulation box size just large enough to capture the apparent nontrivial structure of the pair correlations. For a soft level of description, the observed structure is dominated by the well-known correlation hole, which occurs for separations less than $2R_g$. The structure beyond this appears by examination to be a uniform liquid with $h^{cc}(r) \approx 0$. However, the tail of the effective potential in the theory presented above depends on the structure well beyond this correlation hole. To demonstrate this effect, simulation tests using the methods described previously are also performed using a modified soft potential produced by taking the tcf to go to exactly zero at a range of a fixed number of R_g, based upon where it visually appears to have no further nontrivial structure. Inspection of the tcfs shows that $h^{cc}(r) \approx 0$ appears to be a good approximation for about $r > 3.5R_g$ (anywhere between 3 and 4 R_g). In terms of the formalism above

$$\delta h^{cc}(r) = \begin{cases} 0 \text{ if} & r \leq 3.5R_g \\ -h^{cc}(r) \text{ if} & r > 3.5R_g \end{cases} . \tag{V.24}$$

The result of this procedure is a force curve very close to the unmodified force curve at short range, but with a tail range now fixed to the size of the coarse grained chain, R_g. Results for the pressure at varying chain length (Figure V.3) and densities (Figure V.4) are presented along with the results of UA simulations and mesoscale simulations with the full effective potentials. The results show that the apparently reasonable truncation of the tcf changes the pressure measured in the mesoscale simulation dramatically. The tcfs measured from simulations using the full and cut potentials (shown in Figure V.2), however, do not show any significant difference. From this, we conclude that the inability of numerical structure based coarse-graining alone to reproduce equilibrium thermodynamic averages consistent with atomistic representations is due to the extreme sensitivity to small features of the tcfs beyond the correlation hole. For highly coarse-grained representations, the necessity of measuring structure in these regions to high precision to determine the tail of the effective potential accurately will require such a large box size to make the determination of thermodynamically consistent effective potentials with IBI procedures that optimize structure alone impractical or impossible. Such techniques should be limited, therefore, to low levels of coarse graining or low densities, where the many-polymer contributions to effective pair potentials due to the interpenetration of coarse-grained units are small.

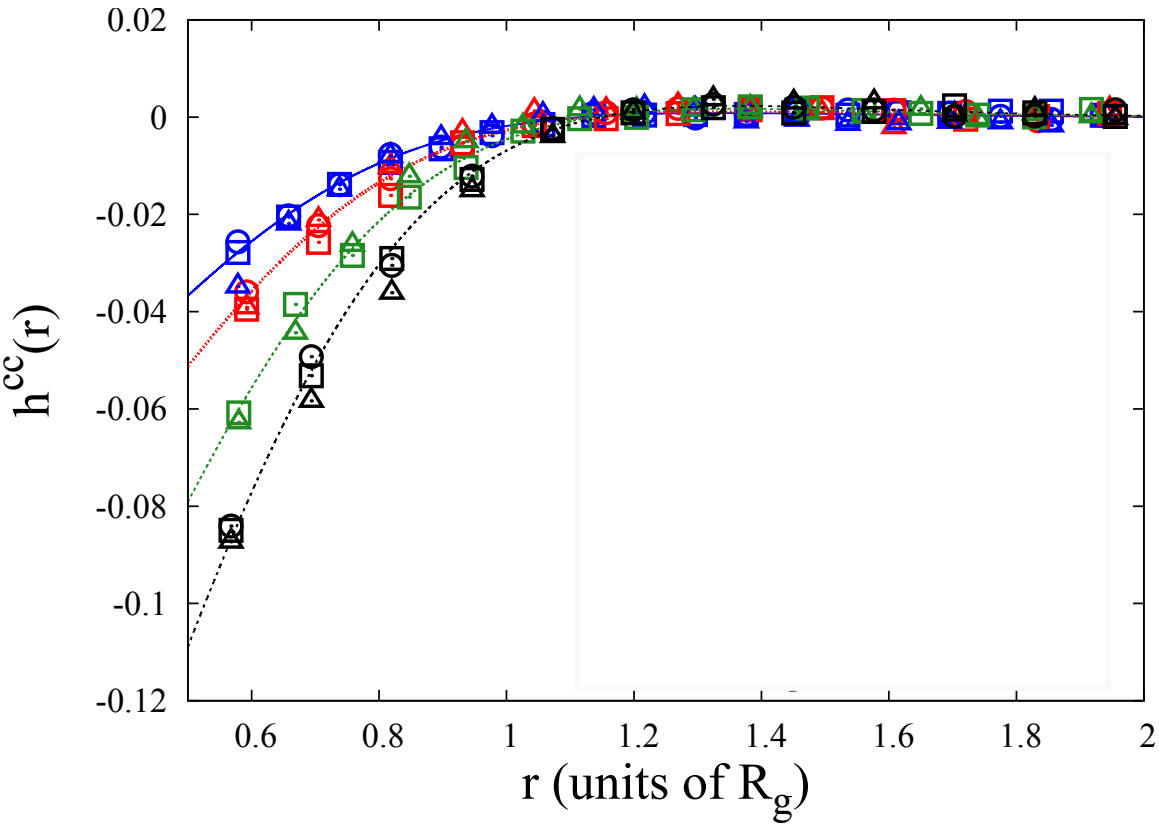

FIGURE V.2. The cm tcf, $h^{cc}(r)$ for N=100 (black/lowest at small r), N=200 (green/second lowest at small r), N=500 (red/second highest at small r), and N=1000 (blue/highest at small r) is compared for results from theory (lines), mesoscale soft sphere simulations (circles), mesoscale soft sphere simulations with the potential derived by cutting $h^{cc}(r)$ at r=3.5R_g (squares) and mesoscale simulations performed using blocks of length N_b=50 (triangles). All three produce the same approximate structural tcf, but while the mesoscale soft sphere and multiblock simulations reproduce pressure consistent with each other and with the United Atoms simulation data where it is available, the soft sphere simulations performed with the potentials derived using the cutoff tcf give much different pressures.

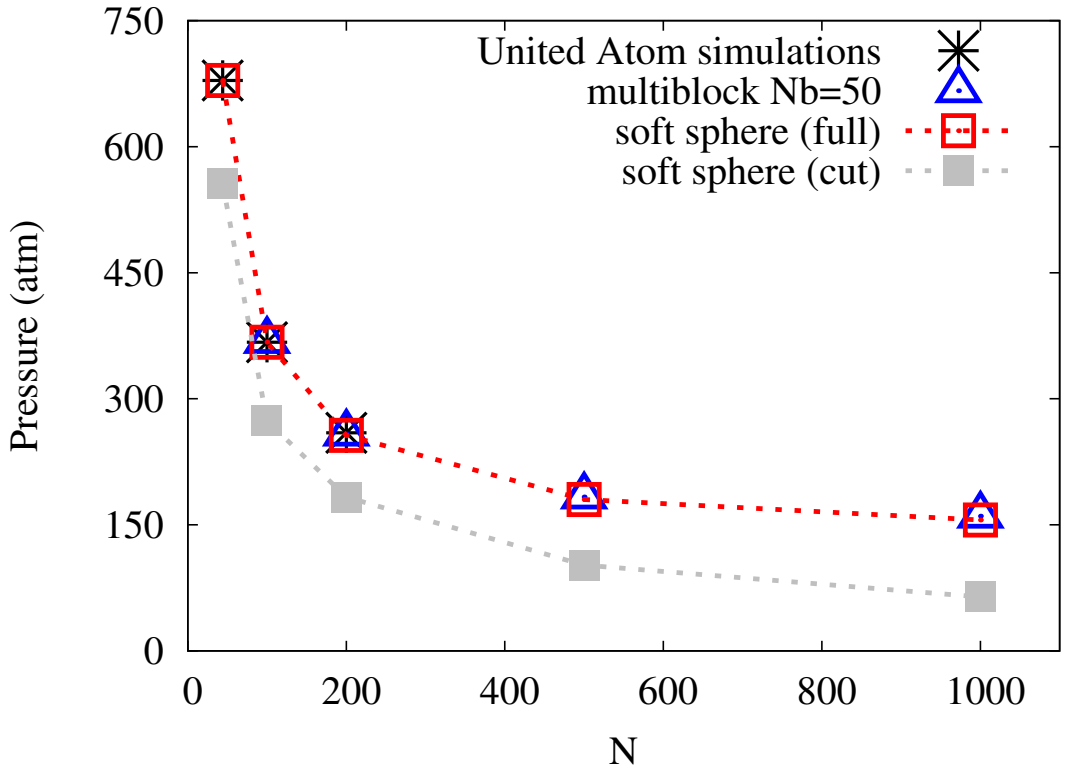

FIGURE V.3. Pressure measured from MSMD simulations performed either using the full tail in the effective potentials (open squares) and using an example modified tail potential formed by taking $h^{cc}(r)$=0 for r>3.5R_g (filled squares). Also shown are United Atom simulations (stars) for systems where they are available (N≤200) and soft multiblock simulations (open triangles). Data are collected for increasing degree of polymerization N. Despite both potentials reproducing the tcfs well, the potential with the modified tail produces dramatically different results for the measured pressure.

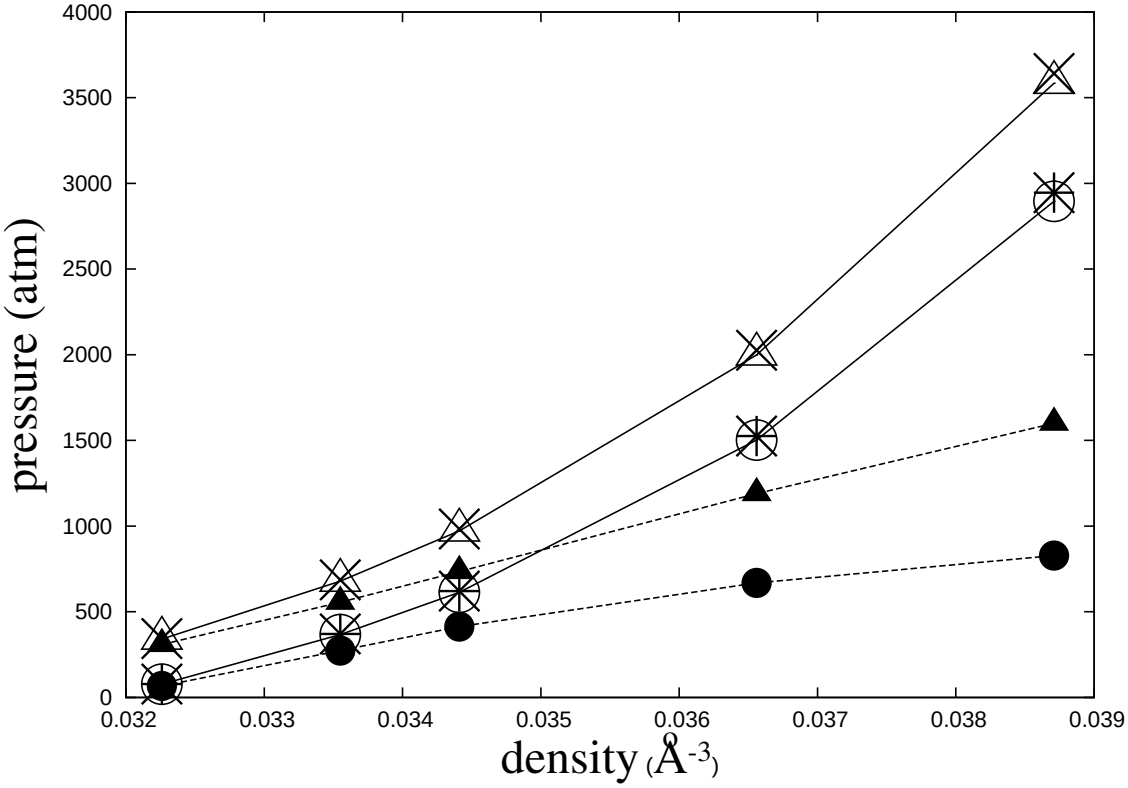

FIGURE V.4. Measured pressures from MSMD simulations, for N=44 (triangles) and N=100 (circles), performed with effective potentials where c_0 is determined from UAMD simulation, using the full tail of the potential (open symbols), using the potential modified with the $3.5R_g$ cutoff in $h^{cc}(r)$ (filled symbols). Also shown are the corresponding UAMD simulations (crosses for N=44 and stars for N=100). Connecting lines are added as a guide to the eye.

V.2.4. Effective Energy in the Coarse-grained Model

The average potential energy per molecule is not conserved across levels of coarse-graining, nor is the entropy. The effective potential energy of the coarse grained system is actually an "intermediate" free energy of the system which reflects the actual potential energy between monomers plus a contribution $-T\Delta S_{cg}$, where ΔS_{cg} is the reduction in entropy between the physical system and its coarse-grained representation. The contribution to the entropy of the system from configurations of block or chain cms is still present explicitly in the system. The consequenes of this, particularly for the dynamics produced in soft simulation will be of great intereset going forward, and current research is underway to develop the understanding of how entropy, energy, and free energy change at different levels of coarse grained representation.

Simulation tests and analytical results using the effective potentials show results consistent with the general predicted pattern, as the effective potential energy per polymer is observed to decrease as fewer degrees of freedom are included to represent each chain in the model. This decomposition is shown in Figure V.5 for multiblock models representing the same system used Figure V.1. The result seen is that as lower level representations with increasing average entropy are used, the effective potential energy per molecule of the system increases monotonically, reflecting the decreased entropic contribution. In the Gaussian multiblock regime, this increase in effective potential per polymer is observed to scale linearly with the number of blocks included in the representation, consistent with results for flexible chain models.

V.3. Conclusion

In conclusion, as the density or length of blocks used to represent a melt increases, the form and magnitude of the long tail of the potential have increasingly negligible effect on the structure measured by the cm tcf, but increasingly dominates the calculation of bulk thermodynamic quantities. For highly coarse-grained representations, this region dominates thermodynamic quantities calculated in the virial route. Because of the growth of the tail, energy route thermodynamic integrals for energy and pressure in the coarse-grained description remain finite in the infinite chain limit and thus intermolecular interactions are predicted to remain relevant even in the infinite chain limit. Because of the insensitivity of tcfs to the long tail of the potential, it is possible to construct effective pair potentials that reproduce indistinguishable

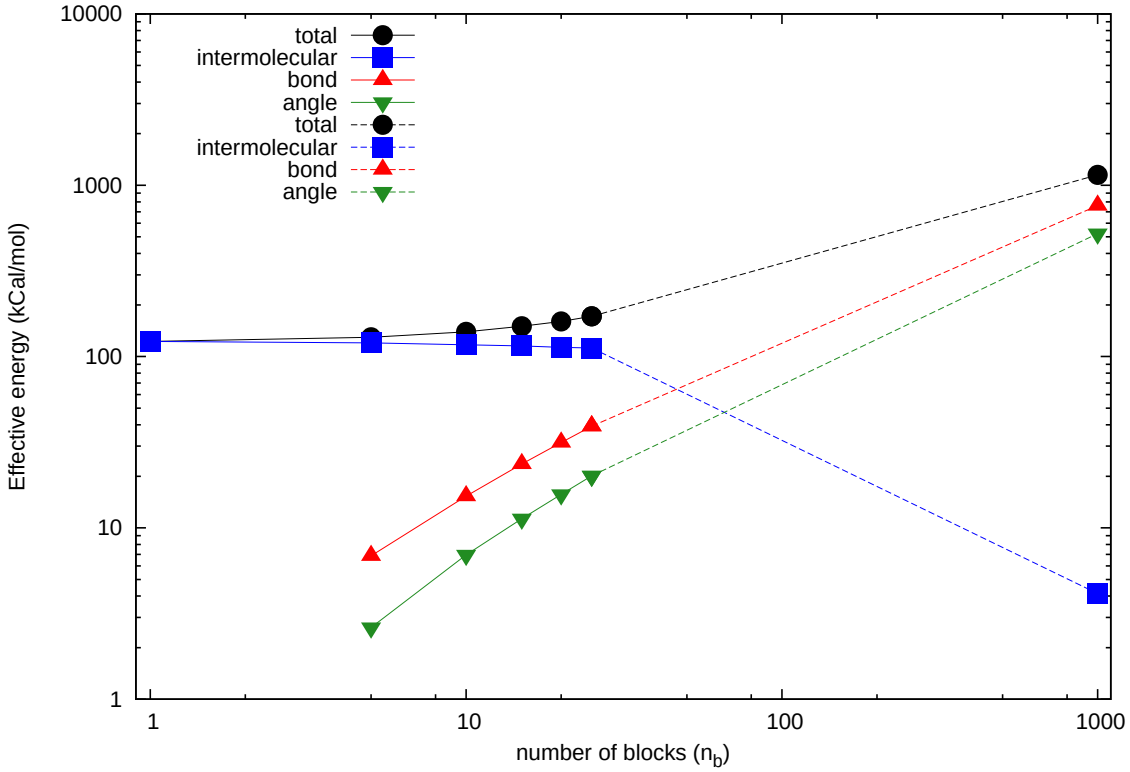

FIGURE V.5. The decomposition of contributions to energy for various multiblock models representing the same system (PE1000 at 509K) shown for the soft sphere (n_b=1) and multiblock models increasing in 5 block increments through n_b=25. United Atom data for the same system are shown with the same point types, connected by a dashed line as a guide to the eye through through the intermediate range of block numbers (n_b) where the block size is too small for Gaussian statistics to hold.

tcfs but yield dramatically different bulk thermodynamic quantities when used in molecular dynamics simulations. From this, we see why effective potentials numerically derived from the optimization of structural correlation functions alone are likely to produce thermodynamically inconsistent coarse-grained representations. There is therefore a large family of potentials that differ significantly in the shape and size of their tails, which yields tcfs different by vanishingly small amounts, and only at separations much larger than R_g, but substantially different thermodynamic properties. The implication for numerical coarse-graining potentials is that care must be taken to ensure that the coarse-grained model is actually representing the correct target system, which is not guaranteed by simply comparing tcfs.

The difference between the scaling predictions for the effective potential and the potential of mean force also has very important implications for theories of polymer melts. The strength of the potential of mean force, $w(r) = -k_B T ln(1 + h^{bb}(r))$, is found to scale for long chains, or large blobs, and high densities as $1/(\rho_m\sqrt{N})$ and its range as $N^{1/2}$ with c_0 becoming irrelevant and $w(r)$ vanishing in the infinite chain limit. Use of the $w(r)$ in thermodynamic relations therefore results in vanishing energies and pressures in the long chain/high density limit, which would imply the irrelevance of intermolecular interactions and allow reduction of the system to a single chain problem. While the effective pair potential at contact, $V^{bb}(0)$, still vanishes in the infinite chain limit, its tail increases in such a way that the Virial integral does not. Likewise the average effective energy in the system also does not vanish, and furthermore both depend on the monomer level direct correlation, and therefore on the monomer interaction potential. This implies that even in the infinite chain limit, intermolecular potentials do not become irrelevant, and therefore cannot generally be neglected, as it is conventionally done in the description of polymer melt dynamics.[16]

CHAPTER VI

CONCLUSION

This dissertation has presented a theory for the effective pairwise interaction potentials for a family of highly coarse-grained representations of polymer melts. Because the theory retains analytical dependence on system and thermodynamic parameters, the theory is transferable between different melts. This theory allows a detailed exploration of the properties of such highly coarse-grained effective potentials. This analysis is used to show that structure-based coarse-graining can produce potentials that accurately represent the thermodynamic state of the system along with structural correlations. Because the long range part of the effective potentials that dominates thermodynamics is sensitive to very small features in the structural correlations, however, numerical optimization schemes require unrealistically high precision measurements of structural correlations to generate thermodynamically consistent interactions.

VI.1. Summary of Results

In chapter III, the intramolecular distributions and tcfs of the multiblock model, wherein each chain is represented by the centers of mass of several identical chain subsections, were characterized. The theory predicted forms with analytical parameter dependence on system parameters and parameters from monomer-level theory. These forms were consistent with the results of low-level UAMD simulation results, which have in turn well-tested against experimentally determined structure and thermodynamic data. The specific nature of interaction potentials between monomers, carried through the PRISM dcf parameter, was found to become irrelevant at high levels of coarse-graining and high densities. Thus for high-level coarse-graining the tcfs approached a universal form depending only on the number of monomers per coarse-grained unit, number of coarse-grained units, the system density and the chain radius of gyration.

In chapter IV, the results for the tcf were mapped onto an effective soft-colloid chain model to obtain effective interaction potentials using the tcfs from chapter III and the HNC approximation. The effective potentials were observed to exhibit a small, exponentially decaying long-ranged tail that scaled beyond the physical size of the coarse-grained unit as $N^{1/4}$, and was dependent on the PRISM dcf parameter, and therefore on the specific monomer interactions in

the underlying physical system. The width of the long ranged tail was found to be a result of the many-polymer correlations among highly multiple highly interpenetrating polymer chains or coarse-grained sub-chains. In the limit of infinitesimally short-ranged monomer interactions, this scales universally with the average number of coarse-grained units found within the volume of one coarse-grained unit, while non-universal dependence on monomer interactions is found in situations where the local packing of monomers becomes important due to finite-ranged monomer interactions.

In chapter V, the effective potentials were used to calculate the viral route pressure both theoretically and through MSMD simulations. The results for all coarse-grained representations were verified to be consistent with each other and with well-tested UAMD simulations where available. Compressibility was also verified to be consistent across levels of representation. The consequences of the insensitivity of structural correlations to monomer interactions was discussed, and it was shown that the introduction of seemingly negligible errors to the long-range behavior of the tcf could result in a representation of effectively indistinguishable structure but very different pressure.

VI.2. Future Directions

The first direction of research in the immediate future will be to extend this coarse-graining method into the subgaussian regime (where each coarse-grained unit includes too few monomers for Gaussian statistics to apply), using the insight gained from this analytical theory. This will be of great interest to the field given the tremendous popularity of bead and spring simulations, as described in chapter 1. The next direction will be to extend the a posteriori dynamical reconstruction to long soft-colloid chain models. Along with this the general formalism and insight gained here can be applied to develop thermodynamically consistent analytical effective pair potentials for a variety of related systems, including mixtures, co-polymers, polymers in solution, and melts of other architectures, such as star polymers.

APPENDIX

SERIES EXPANSION COEFFICIENTS FOR EFFECTIVE POTENTIALS AT SHORT RANGE

A.1. Infinite Soft Sphere Limit

For the soft sphere model with $\Gamma >> 100$, the approximations for $\hat{c}^{bb}(k)$ at large and small wave vectors and the function itself converge to approximately the same value at $k = 1$. Therefore, the two region piece-wise approximation

$$\hat{c}^{cc}(k) \approx \begin{cases} \frac{-N}{\rho_m}\left[\frac{45}{45+\Gamma k^4}\right] & \text{if } k \leq 1 \\ \frac{-N\Gamma}{\rho_m}\frac{(\hat{\Omega}^{cm}(k))^2}{(\hat{\Omega}^{mm}(k)-(\hat{\Omega}^{cm}(k))^2)} & \text{if } k > 1 \end{cases} . \tag{A.1}$$

provides a good approximation in this limit. Note that because Γ is assumed to be very large here, only the leading order terms in Γ have been retained.

With this approximation, the $A_j^{(1)}(\Gamma)$ are given by

$$A_j^{(1)}(\Gamma) = \left(\frac{45\Gamma}{(2j+1)!}\right)\int_0^1 \frac{k^{2j+2}}{45+\Gamma k^4}dk + a_{2j} \ , \tag{A.2}$$

where a_{2j}, the large wave vector contribution given by

$$a_{2j} = \frac{1}{(2j+1)!}\int_1^\infty \frac{k^{(2j+2)}(\hat{\Omega}^{cm}(k)^2)}{\hat{\Omega}^{mm}(k)-(\hat{\Omega}^{bm}(k))^2}dk \tag{A.3}$$

is independent of Γ, and therefore may be estimated numerically without loss of physical generality. Estimated numerical values through order $j = 10$ are given in table A.1.

The first term (the integral over the small k form) becomes smaller with increasing order j, and in practice its value is negligibly small for $j \geq 2$. The first two terms can be evaluated in terms of elementary functions, and in this very large Γ limit these results can be expanded in powers of $1/\Gamma^{1/4}$, neglecting terms that fall off faster than $1/\Gamma^{1/4}$:

$2j$	a_{2j}
4	15.55
6	-6.644
8	2.339
10	-0.6812
12	0.1677
14	-0.03564
16	0.006648
18	-0.001104
20	0.0001653
22	-0.00002250

TABLE A.1. Numerically integrated values for the soft sphere large wavevector coeficients a_{2j}

$$\begin{aligned}(45\Gamma)\int_0^1 \tfrac{k^2}{45+\Gamma k^4}dk &= \left(\tfrac{\Gamma}{45}\right)^{\frac{2j+3}{4}}\left[\tfrac{1}{4\sqrt{2}}\Big(-2tan^{-1}[1-\sqrt{2}(\sqrt[4]{45/\Gamma})]+2tan^{-1}[1+\sqrt{2}(\sqrt[4]{45/\Gamma})]\right.\\ &\quad \left.+ln[\tfrac{1-(2\sqrt{2}(\sqrt[4]{45/\Gamma}))}{(1+(\sqrt[4]{45/\Gamma})(\sqrt{2}+(\sqrt[4]{45/\Gamma})))}]\Big)\right]\\ &\approx 19.30\Gamma^{1/4}-45.0+2.728\times 10^{-15}\Gamma^{-1/4}\\ &\approx 19.30\Gamma^{1/4}-45.0\end{aligned} \tag{A.4}$$

and

$$\begin{aligned}\left(\tfrac{45\Gamma}{6}\right)\int_0^1 \tfrac{k^4}{45+\Gamma k^4}dk &= \left(\tfrac{\Gamma}{45}\right)^{\frac{2j+3}{4}}\left[(\sqrt[4]{45/\Gamma})+\tfrac{1}{(2\sqrt{2})}\Big(tan^{-1}[1-\sqrt{2}(\sqrt[4]{45/\Gamma})]\right.\\ &\quad \left.-tan^{-1}[1+\sqrt{2}(\sqrt[4]{45/\Gamma})]-tanh^{-1}[(\sqrt{2}(\sqrt[4]{45/\Gamma}))/(1+(\sqrt[4]{45/\Gamma})^2)]\Big)\right]\\ &\approx 15.0-43.16\Gamma^{-1/4}\ .\end{aligned} \tag{A.5}$$

Combining these results, the overall form of the effective direct correlation at small separations is

$$c_s^{cc}(r)\approx -\frac{\Gamma}{2\pi^2\rho_c R_g^3}\left[\Big(19.30\Gamma^{1/4}-7.276\Big)-\left(37.09-\frac{21.58}{\Gamma^{1/4}}\right)r^2+\frac{1}{\Gamma}\sum_{j=2}a_{2j}r^{2j}\right]\ . \tag{A.6}$$

A.2. Infinite Multiblock Limit at High Densities

When Γ_b is large but non-infinite, neither the large k asymptotic expansion nor the small k limiting expansion represent good approximations to the form of the direct correlation near $k = 1$. For a tractable approximation in this range we use the direct Taylor series expansion of the functional form in k space about $k = \alpha$

$$\frac{\Gamma_b}{(2j+1)!}\frac{Y^{bm}(k)}{1+\Gamma_b Z^{bm}(k)} \approx \frac{1}{(2j+1)!}\sum_{m=0}^{m_{max}} I_m(\Gamma_b)(k-\alpha)^m \ , \tag{A.7}$$

where

$$I_m^{\infty}(\Gamma_b) = \Gamma_b \left(\frac{d^m}{dk^m}\hat{c}^{bb}_{norm}(k)\right)\Big|_{k=\alpha} \tag{A.8}$$

The direct correlation is then taken to be

$$\hat{c}^{bb}(k) \approx \begin{cases} \frac{-N\Gamma}{\rho_m}\left[\frac{45}{45+\Gamma_b k^4} - \frac{5k^2}{28}\frac{13\Gamma_b k^4 - 3780}{(\Gamma_b k^4+45)^2}\right] & \text{if } k \le 1-\epsilon \\ \frac{1}{(2j+1)!}\sum_{m=0}^{m_{max}} I_m(\Gamma_b)(k-\alpha)^m & \text{if } 1-\epsilon < k \le 1+\epsilon \\ \frac{-N\Gamma}{\rho_m}\sum_{j}^{j_{max}} \Gamma^{-j}\frac{(\hat{\Omega}^{cm}(k))^2}{(\hat{\Omega}^{mm}(k)-(\hat{\Omega}^{cm}(k))^2)^j} & \text{if } k > 1+\epsilon \end{cases} . \tag{A.9}$$

A.2.1. Contribution from Small Wave Vectors

As for the infinite soft sphere case treated in appendix (a), only the order $j = 0$ and $j = 1$ terms of the integral over the small wave vector region contribute significantly, as the increasing powers of k in the integrand of the higher terms makes it smaller for $k < 1$ with increasing j. Since Γ_b cannot be assumed to be arbitrarily large here, both the leading order limiting form and the first correction term (of relative order $\sqrt{\Gamma_b}$) are included in the integral. The results of these integrals are

$$B_0(\Gamma_b)=\frac{5(1-\epsilon_s)\left(\frac{251}{4\left(\frac{1}{45}\Gamma_b(\epsilon_s-1)^4+1\right)}+39\right)}{84\Gamma_b}+\frac{3\sqrt{\frac{3}{2}}5^{3/4}\log\left(\frac{60}{5^{3/4}\sqrt{6}\sqrt[4]{\Gamma_b}(\epsilon_s-1)+\frac{15\sqrt[4]{5}\sqrt{6}}{\sqrt[4]{\Gamma_b}(\epsilon_s-1)}-30}+1\right)}{4\Gamma_b^{3/4}}$$

$$+\frac{\sqrt[4]{5}\left(2035-1008\sqrt{5}\sqrt{\Gamma_b}\right)\tan^{-1}\left(\frac{\sqrt{\frac{2}{3}}\sqrt[4]{\Gamma_b}(\epsilon_s-1)}{\sqrt[4]{5}}+1\right)}{224\sqrt{6}\Gamma_b^{5/4}}$$

$$-\frac{\sqrt[4]{5}\left(1008\sqrt{5}\sqrt{\Gamma_b}-2035\right)\tan^{-1}\left(1-\frac{\sqrt{\frac{2}{3}}\sqrt[4]{\Gamma_b}(\epsilon_s-1)}{\sqrt[4]{5}}\right)}{224\sqrt{6}\Gamma_b^{5/4}} \tag{A.10}$$

$$+\frac{2035\sqrt[4]{5}\tanh^{-1}\left(\frac{5^{3/4}\sqrt{6}\sqrt[4]{\Gamma_b}(\epsilon_s-1)}{\sqrt{5}\sqrt{\Gamma_b}(\epsilon_s-1)^2+15}\right)}{224\sqrt{6}\Gamma_b^{5/4}}$$

and

$$B_1(\Gamma_b)=-\frac{18825(\epsilon_s-1)^3}{112\Gamma_b(\Gamma_b+\Gamma_b\epsilon_s^4-4\Gamma_b\epsilon_s^3+6\Gamma_b\epsilon_s^2-4\Gamma_b\epsilon_s+45)}-\frac{5\left(13\epsilon_s^3-39\epsilon_s^2+795\epsilon_s-769\right)}{84\Gamma_b}$$

$$-\frac{45\sqrt{\frac{3}{2}}\sqrt[4]{5}\left(112\sqrt{\Gamma_b}+101\sqrt{5}\right)\tan^{-1}\left(1-\frac{\sqrt{\frac{2}{3}}\sqrt[4]{\Gamma_b}(\epsilon_s-1)}{\sqrt[4]{5}}\right)}{224\Gamma_b^{7/4}}$$

$$+\frac{45\sqrt{\frac{3}{2}}\sqrt[4]{5}\left(112\sqrt{\Gamma_b}+101\sqrt{5}\right)\tan^{-1}\left(\frac{\sqrt{\frac{2}{3}}\sqrt[4]{\Gamma_b}(\epsilon_s-1)}{\sqrt[4]{5}}+1\right)}{224\Gamma_b^{7/4}} \tag{A.11}$$

$$+\frac{45\sqrt{\frac{3}{2}}\left(101\ 5^{3/4}-112\sqrt[4]{5}\sqrt{\Gamma_b}\right)\tanh^{-1}\left(\frac{\sqrt{\frac{2}{3}}\sqrt[4]{\Gamma_b}(1-\epsilon_s)}{\sqrt[4]{5}\left(\frac{\sqrt{\Gamma_b}(\epsilon_s-1)^2}{3\sqrt{5}}+1\right)}\right)}{224\Gamma_b^{7/4}}\ .$$

A.2.2. Contribution from Crossover Region

The contribution to $A_j(k)$ from the crossover wave vectors is

$$-\frac{\Gamma_b}{(2j+1)!}I_m^{(n_b)}(\Gamma_b)\eta_{j,m}\ , \tag{A.12}$$

where

$$\begin{aligned}\eta_{j,m} &= \int_{1-\epsilon_s}^{1+\epsilon_l} k^{2j+2}(k-\alpha)\\ &= \sum_{q=0}^{m}\frac{(-\alpha)^m m!}{(m-q)!q!}\int_{1-\epsilon_l}^{1+\epsilon_s} k^{2j+2+m-q}\\ &= \sum_{q=0}^{m}\frac{(-\alpha)^m m!}{(m-q)!q!}\left(\frac{1}{2j+m-q+3}\right)\left[(1+\epsilon_l)^{2j+m-q+3}-(1+\epsilon_s)^{2j+m-q+3}\right]\ .\end{aligned} \tag{A.13}$$

The explicit forms of the I_m coefficients as functions of Γ (for the assumed expansion point of $\alpha = 1$) are given by

$$I_0^{\infty} = \frac{0.756\Gamma_b}{0.016\Gamma_b + 1.} \ , \tag{A.14}$$

$$I_1^{\infty} = \frac{(-0.0473\Gamma_b - 0.376)\Gamma_b}{(0.016\Gamma_b + 1.)^2} \ , \tag{A.15}$$

$$I_2^{\infty} = \frac{(0.00187\Gamma_b^2 - 0.025\Gamma_b - 0.0542)\Gamma_b}{(0.016\Gamma_b + 1.)^3} \ , \tag{A.16}$$

$$I_3^{\infty} = \frac{(-0.0000595\Gamma_b^3 + 0.00431\Gamma_b^2 + 0.0204\Gamma_b + 0.0185)\Gamma_b}{(0.016\Gamma_b + 1.)^4} \ , \tag{A.17}$$

$$I_4^{\infty} = \frac{(\left(1.66 \times 10^{-6}\right)\Gamma_b^4 - 0.000298\Gamma_b^3 + 0.00148\Gamma_b^2 + 0.0173\Gamma_b - 0.0506)\Gamma_b}{(0.016\Gamma_b + 1.)^5} \ , \tag{A.18}$$

and

$$I_5^{\infty} = \frac{(\left(-4.24 \times 10^{-8}\right)\Gamma_b^5 + 0.0000147\Gamma_b^4 - 0.000399\Gamma_b^3 - 0.00281\Gamma_b^2 + 0.00375\Gamma_b + 0.0413)\Gamma_b}{(0.016\Gamma_b + 1.)^6} \ , \tag{A.19}$$

where parameter independent constants have been estimated numerically to three digits to make them compact and emphasize the dependence on the system dependent parameter, Γ_b.

A.2.3. Contributions from the Large Wave Vector Region

The integrals over the large wave vector forms can again be done purely numerically. For convenience the series is written as

$$\sum_{l=1}^{l_{max}} (-1)^{l+1} \left(\frac{a_{lj}}{\Gamma_b}\right)^{l-1} \ , \tag{A.20}$$

where

	l=1	l=2	l=3	l=4	l=5	l=6	l=7	l=8	l=9	l=10
j=0	25.11	293.1	63.65	40.22	32.89	29.59	27.81	26.74	26.04	25.58
j=1	25.79	263.	55.76	35.14	29.01	26.55	25.46	25.04	25.	25.23
j=2	14.51	161.3	45.85	31.96	27.87	26.48	26.18	26.42	26.95	27.66
j=3	6.349	86.34	37.26	29.75	27.6	27.1	27.29	27.84	28.58	29.45
j=4	2.254	37.21	26.78	25.17	25.2	25.8	26.66	27.65	28.72	29.84
j=5	0.6604	12.88	16.98	19.41	21.35	23.06	24.66	26.18	27.64	29.07
j=6	0.1634	3.676	9.67	13.85	17.	19.58	21.82	23.83	25.7	27.45
j=7	0.03484	0.8884	5.029	9.267	12.87	15.94	18.62	21.01	23.21	25.25
j=8	0.006517	0.1857	2.418	5.864	9.324	12.51	15.39	18.03	20.45	22.71
j=9	0.001085	0.03418	1.086	3.535	6.504	9.511	12.39	15.1	17.65	20.04
j=10	0.0001626	0.005611	0.4587	2.042	4.388	7.035	9.738	12.39	14.94	17.39

TABLE A.2. Numerically integrated values for the infinite multiblock large wavevector coeficients $a_{l,j}$

$$a_{l,j} = \begin{cases} \left(\int_{1+\epsilon_s}^{\infty} \frac{(Y^{bm(\infty)}(k))^2}{Z^{bm(\infty)}(k)} \right)^{\frac{1}{j-1}} \text{ if } & l \neq 1 \\ \int_{1+\epsilon_s}^{\infty} \text{ if } & l = 1 \end{cases} . \tag{A.21}$$

Values for these coeficients are given in table A.2

Figures A.1-A.4 show the numerically integrated forms of the $A_j(\Gamma_b)$ coefficients and the approximation forms given here for $\Gamma > 40$.

A.3. Infinite Multiblock Model for Low Densities/Very Small Blocks

For systems where the effective interpenetration parameter $\Gamma_b = -N_b \rho_c c_0$ is large enough for the theory to work, but relatively small ($1 << \Gamma < 40$), the asymptotic expansion used in the appendix above for the large wave vector behavior at large Γ_b diverges badly, and no longer provides a good approximation for the $A_j(\Gamma_b)$. The power series expansion for the effective potential remains convergent, however, if numerically integrated values from the exact form in Fourier space are used.

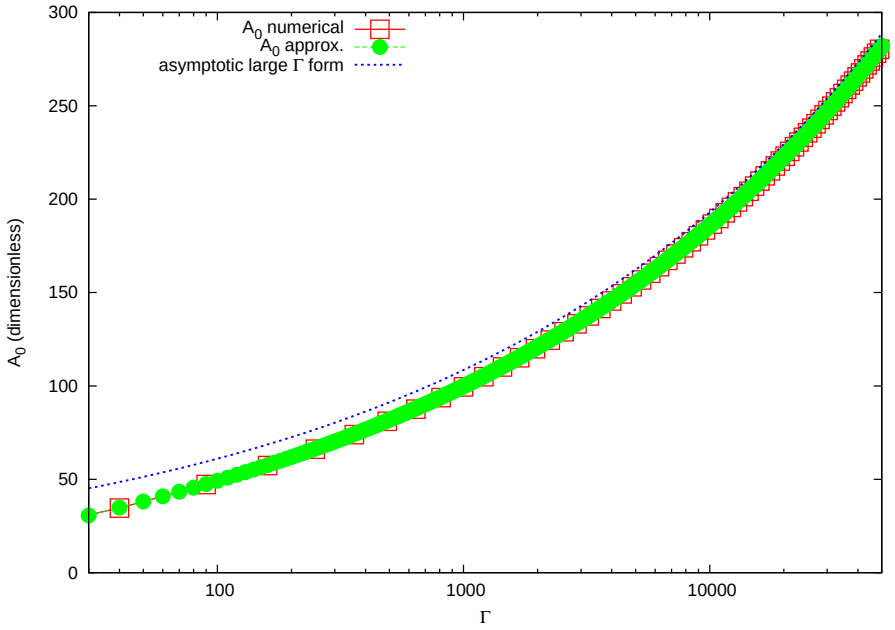

FIGURE A.1. Comparison of the three region approximations with the asymtotic expansion for large wavevector for $A_j(\Gamma_b)$ numerically integrated form for the lowest order coefficent. Comparison is shown for Γ_b>40, where these approximations are quite good. Dramatic deviations occur for Γ_b<40, especially for higher order terms

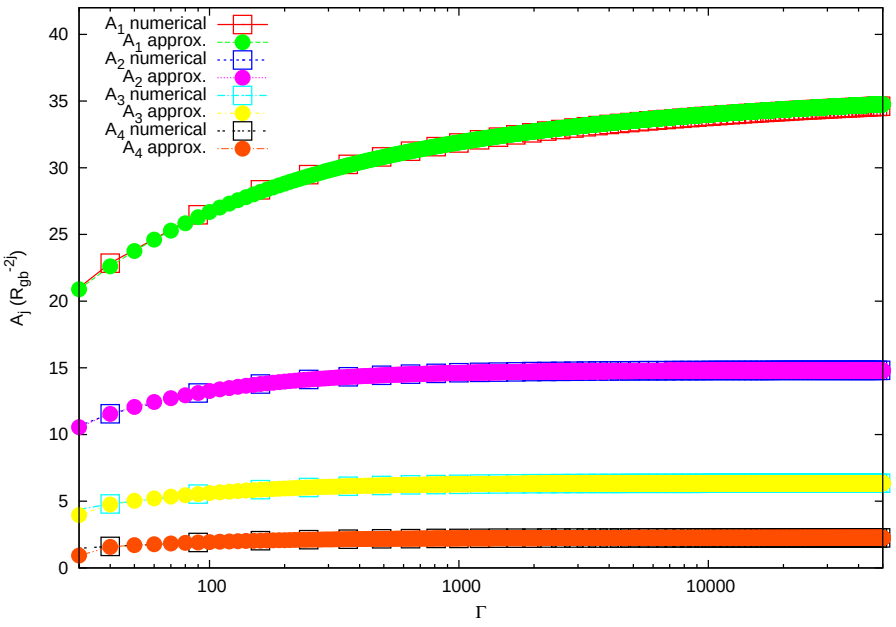

FIGURE A.2. Comparison of the three region approximations with the asymtotic expansion for large wavevector for $A_j(\Gamma_b)$ numerically integrated forms. Comparison is shown for Γ_b>40, where these approximations are quite good. Dramatic deviations occur for Γ_b<40, especially for higher order terms

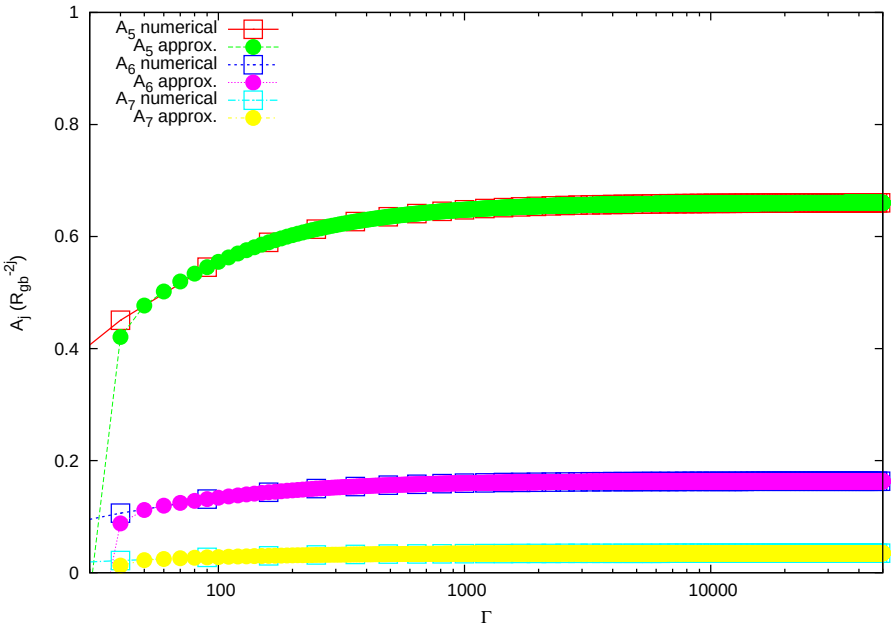

FIGURE A.3. Comparison of the three region approximations with the asymtotic expansion for large wavevector for higher order $A_j(\Gamma_b)$ numerically integrated forms. Comparison is shown for Γ_b>40, where these approximations are quite good. Dramatic deviations occur for Γ_b<40, especially for higher order terms

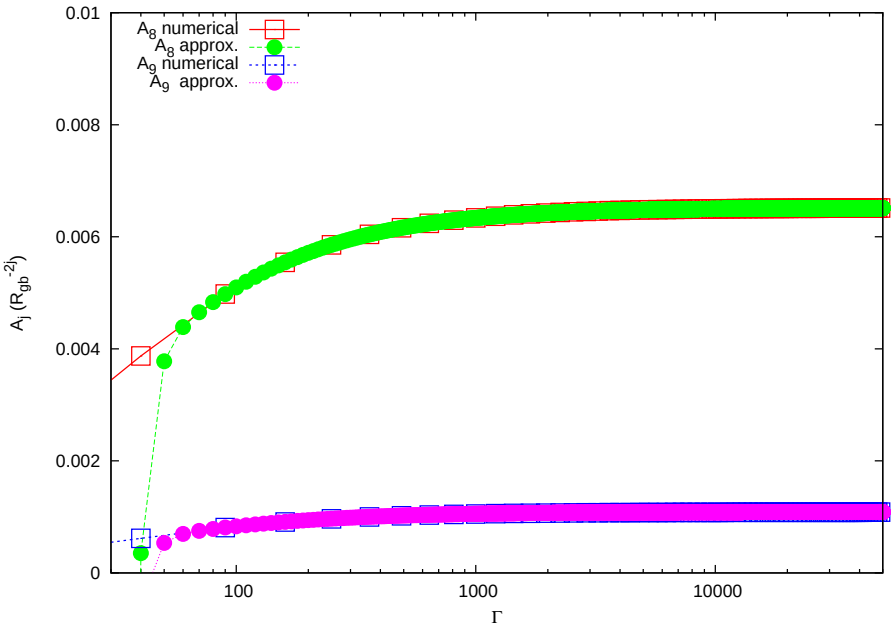

FIGURE A.4. Comparison of the three region approximations with the asymtotic expansion for large wavevector for higher order $A_j(\Gamma_b)$ numerically integrated forms. Comparison is shown for Γ_b>40, where these approximations are quite good. Dramatic deviations occur for Γ_b<40, especially for higher order terms

REFERENCES CITED

[1] L. Jacobson and V. Molinero, J. Phys. Chem. B **114**, 7302 (2010).

[2] J. J. de Pablo, Ann. Rev. Phys. Chem. **62**, 555 (2011).

[3] A. Savelyev and G. A. Papoian, Proc. Natl. Acad. Sci. USA **107**, 20345 (2010).

[4] V. A. Harmandaris, N. P. Adhikari, N. F. A. van der Vegt, and K. Kremer, Macromol. **39**, 6708 (2006).

[5] B. G. Levine, D. N. Le Bard, R. De Vane, W. Shinoda, A. Kohlmeyer, and M. L. Kein, J. Chem. Theory Comp. **7**, 4135 (2011).

[6] G. DAdamo, A. Pelissetto, and C. Pierleoni, Soft Matter **8**, 5151 (2012).

[7] de Gennes, P.-G., *Scaling Concepts in Polymer Physics* Cornell University Press, Ithaca, NY, 1979.

[8] G. Strobl, *The Physics of Polymers* (Springer, Heidelberg, 1996)

[9] J. P. Wittmer, P. Beckrich, H. Meyer, A. Cavallo, A. Johner, J. Baschnagel, Phys. Rev. E **76** 011803 (2007)

[10] P. Beckrich, A. Johner, A.N. Semenov, S.P. Obukhov, H. Benot, and J.P. Wittmer, Macromol. **40** 3805-3814 (2007)

[11] J.P. Wittmer, P. Beckrich, J. Johner, A.N. Semenov, S.P. Obukhov, H. Meyer, and J. Baschnagel, Europhys. Lett. **77** 56003 (2007)

[12] J.P. Wittmer, P. Beckrich, F. Crevel, C.C. Huang, A. Cavallo, T. Kreer, and H. Meyer, Comput. Phys. Commun. **177** 146-149 (2007)

[13] K. Kremer and G. S. Grest, J. Chem. Phys. **92**, 5057 (1990).

[14] Ji-Xuan Hou1, Carsten Svaneborg, Ralf Everaers, and Gary S. Grest, Phys. Rev. Lett. **105** 068301 (2010)

[15] T. Vettorel, G. Besold, and K. Kremer, Soft Matter **6** 22822292 (2010)

[16] M. Doi and S. F. Edwards, *The Theory of Polymer Dynamics* (Oxford University, Oxford, 1986).

[17] E. K. Watkins and W. L. Jorgensen, J. Phys. Chem. A **105** 4118 (2001).

[18] M. Putz, J. G. Curro, and G. S. Grest, J. Chem. Phys. **114** 2847 (2001).

[19] M. G. Martin and J. I. Siepmann, J. Phys. Chem. B **102** 2569 (1998).

[20] D, Heine, D. T. Wu, J. G. Curro, and G. S. Grest, J. Chem. Phys **118** 914 (2003).

[21] E. Jaramillo, D. T. Wu, G. S. Grest, and J. G. Curro, J. Chem. Phys **120** 8883 (2004).

[22] A. Uhlerr, M. Doxastakis, V.G. Mavrantzas, D. N. Theodorou, S. J. Leak, N. E Adam, and P. E. Nyberg *Europhys. Lett.* **57**, 506 (2002).

[23] N. Ch. Karayiannis, V. G. Mavrantzas, and D. N. Theodorou, Phys. Rev. Lett. **88**, 1055031 (2002).

[24] P. Carbone, H. A. Karimi Varzaneh, X.Y. Chen and F. Müller-Plathe, J. Chem. Phys. **128**, 0649041 (2008).

[25] R. L. Henderson, Phys. Lett. **49A**, 197 (1974).

[26] J. F. Rudzinski and W. G. Noid, J. Chem. Phys. 135 214101 (2011).

[27] S. Izvekov, M. Parrinello, C. J. Burnham, and G. A. Voth, J. Chem. Phys. 120, 10896 (2004)

[28] S. Izvekov and G. A. Voth J. Phys. Chem. B, 2005, 109 (7), pp 24692473

[29] T. D. Hone, S. Izvekov, and G. A. Voth, J. Chem. Phys. 122, 054105 (2005)

[30] J. T. Padding and W. J. Briels, J. Chem. Phys. **117**, 925 (2002).

[31] J.T. Padding and W.J. Briels, J. Chem. Phys. **118**, 10276 (2003).

[32] P. Kindt and W. J. Briels J. Chem. Phys. **127**, 134901 (2007)

[33] J.T. Padding and W.J. Briels, J. Phys.: Condens. Matter **23**, 233101 (2011).

[34] V. Krakoviack, J. -P. Hansen and A. A. Louis, Europhys. Lett. **58(1)** 53 (2002).

[35] C. N. Likos, A. Lang, M. Watzlawek and H. Lowen, Phys Rev. E **63**, 031206

[36] A.A. Louis, P. G. Bolhuis, J. P. Hansen, and E. J. Meijer, Phys. Rev. Lett. **85**, 2522 (2000)

[37] P. G. Bolhuis, A. A. Louis, J.-P. Hansen, and E. J. Meijer, J. Chem. Phys.**114**, 4296 (2001).

[38] G. Yatsenko, E. J. Sambriski, and M. G. Guenza, J. Chem. Phys. **122** 054907 (2005).

[39] G. Yatsenko, E. J. Sambriski, M. A. Nemirovskaya, and M. Guenza, Phys. Rev. Lett **93** 257803 (2004).

[40] A. A. Louis J. Phys.: Condens. Matter **14**, 9187 (2002)

[41] J. -P. Hansen and I. R. McDonald,*Theory of Simple Liquids* (Academic, New York) 2 Ed. (1990).

[42] L. S. Ornstein and F. Zernike, Proc. Royal Society of Sciences of Amsterdam **17** 793 (1914)

[43] D. Chandler and H.C. Anderson, J. Chem. Phys. 57, 1930 (1972)

[44] K. S. Schweizer and J. G. Curro, Chemical Physics **149**, 105 (1990)

[45] A. Yethiraj and K. S. Schweizer, J. Chem. Phys. 98, 9080 (1993)

[46] E. J. Sambriski and M. G. Guenza, Phys. Rev. E **76** 051801 (2007).

[47] J. McCarty, I. Y. Lyubimov, and M. G. Guenza, J. Phys. Chem. B **113** 11876 (2009).

[48] J. McCarty, I. Y. Lyubimov, and M. G. Guenza, Macromol. **43**, 3964 (2010).

[49] I. Y. Lyubimov, J. McCarthy, A. Clark, and M. G. Guenza, J. Chem. Phys. **132**, 2249031 (2010).

[50] I. Y. Lyubimov, and M. G. Guenza, Phys. Rev. E **84**, 031801 (2011).

[51] Lyubimov, I. Y. (2012) *Theoretical Reconstruction of the Structure And Dynamics Of Polymer Melts from their Coarse-Grained Description* Doctoral Dissertation, University of Oregon, Eugene

[52] A. J. Clark, and M. G. Guenza J. Chem. Phys. **132**, 044902 (2010).

[53] H W Diehl and E Eisenriegler 1989 J. Phys. A: Math. Gen. 22 L87

[54] A. Rakshit and R. C. Picu, J. Chem. Phys. **125** 164907 (2006)

[55] David, E. F., and K. S. Schweizer, J. Chem. Phys. **100** 7784 (1994).

[56] H. Yamakawa, *Modern Theory of Polymer Solutions* (Harper and Row, New York, 1971).

[57] Guenza, M, H. Tang, and K. S. Schweizer, J. Chem. Phys. **108** 1257 (1998).

[58] A. J. Clark, J. McCarty, I. Y. Lyubimov, and M. G. Guenza, Phys. Rev. Lett. **109**, 168301 (2012)

[59] M. P. Allen and D. J. Tildesley *Computer Simulation of Liquids* (Oxford University Press, New York, 1987).

[60] S. Plimpton J. Comput. Phys. **117**, 1 (1995).

[61] M. Laso, H. C. Ottinger and U. W. Suter J. Chem. Phys. **95** 2178 (1991).

[62] K. G. Honnell, C. K. Hall, and R. Dickman, J. Chem. Phys. 87, 664 (1987)

[63] J. McCarty, A. J. Clark, I. Y. Lyubimov, and M.G. Guenza, Macromol. **45** 8482 (2012).